2016-06-01

Dynamic Liquefied Natural Gas (LNG) Processing with Energy Storage Applications

Farhad Fazlollahi
Brigham Young University

Dynamic Liquefied Natural Gas (LNG) Processing with Energy Storage Applications

Farhad Fazlollahi

A dissertation/thesis submitted to the faculty of
Brigham Young University
in partial fulfillment of the requirements for the degree of

Doctor of Philosophy

Larry L. Baxter, Chair
John D. Hedengren
Dave Frankman
John N. Harb
W. Vincent Wilding

Department of Chemical Engineering

Brigham Young University

June 2016

ABSTRACT

Dynamic Liquefied Natural Gas (LNG) Processing with Energy Storage Applications

Farhad Fazlollahi
Department of Chemical Engineering, BYU
Doctor of Philosophy

The cryogenic carbon capture™ (CCC) process provides energy- and cost-efficient carbon capture and can be configured to provide an energy storage system using an open-loop natural gas (NG) refrigeration system, which is called energy storing cryogenic carbon capture (CCC-ES™). This investigation focuses on the transient operation and especially on the dynamic response of this energy storage system and explores its efficiency, effectiveness, design, and operation. This investigation included four tasks.

The first task explores the steady-state design of four different natural gas liquefaction processes simulated by Aspen HYSYS. These processes differ from traditional LNG process in that the CCC process vaporizes the LNG and the cold vapors return through the LNG heat exchangers, exchanging sensible heat with the incoming flows. The comparisons include costs and energy performance with individually optimized processes, each operating at three operating conditions: energy storage, energy recovery, and balanced operation.

The second task examines steady-state and transient models and optimization of natural gas liquefaction using Aspen HYSYS. Steady-state exergy and heat exchanger efficiency analyses characterize the performance of several potential systems. Transient analyses of the optimal steady-state model produced most of the results discussed here.

The third task explores transient Aspen HYSYS modeling and optimization of two natural gas liquefaction processes and identifies the rate-limiting process components during load variations. Novel flowrate variations included in this investigation drive transient responses of all units, especially compressors and heat exchangers. Model-predictive controls (MPC) effectively manages such heat exchangers and compares favorably with results using traditional controls.

The last task shows how an unprocessed natural gas (NG) pretreatment system can remove more than 90% of the CO_2 from NG with CCC technology using Aspen Plus simulations and experimental data. This task shows how CCC-based technology can treat NG streams to prepare them for LNG use. Data from an experimental bench-scale apparatus verify simulation results. Simulated results on carbon (CO_2) capture qualitatively and quantitatively agree with experimental results as a function of feedstock properties.

Keywords: natural gas liquefaction, Cryogenic carbon capture, Aspen HYSYS, optimization, transient modeling, natural gas pre treatment

ACKNOWLEDGMENTS

I would like to express my appreciation for the financial support and technical cooperation from Sustainable Energy Solutions (SES). The financial and technical support of Sustainable Energy Solutions (SES) LLC of Orem, Utah, the Advanced Research Projects Agency – Energy (ARPA-E), U.S. Department of Energy, under Award Number DE-AR0000101 is gratefully acknowledged. This project was partially funded by SES projects sponsored by Advanced Conversion Technologies Task Force in Laramie, Wyoming through the School of Energy Resources and by the Climate Change and Emissions Management Corporation (CCEMC) of Alberta, Canada CCEMC.

I am grateful of the on demand support and insightful comments from my advisor, Prof. Larry L. Baxter. I want to thank Alex Bown for his assistance on modeling and optimization. I wish to thank other members of my committee, Dr. Frankman, Prof. Hedengren, Prof. Harb and Prof. Wilding for their useful comments and guidance.

I am very grateful for the continuous encouragement of my parents and siblings who stand by my side the whole time and never deprive me of their kindness and support.

Table of Contents

List of Figures

List of Tables

Chapter 1. Background

This investigation explores the transient behavior of an innovative carbon capture and energy storage process called energy-storing cryogenic carbon capture™ (CCC ES). This process combines a modified version of traditional natural gas liquefaction with a novel version of CO_2 separation from vitiated gases to provide the combination of both energy storage and CO_2 separation in a single process. CO_2 separation from flue gases most commonly goes by the moniker of carbon capture. Some natural gas supplies require CO_2 removal either as part of natural gas processing prior to entering a pipeline or as part of preparing pipeline-quality natural gas for use in natural gas liquefaction processes. This background outlines (a) traditional natural gas liquefaction processes, (b) the cryogenic carbon capture process, and (c) CO_2 removal from natural gas processes. Each of these sections concludes with a brief description of the contributions of this investigation to the overall process.

1.1. Natural gas liquefaction process

Natural gas plays a critical role in the global energy market. In 2012, the worldwide consumption of natural gas was about 120 trillion cubic feet with projections to grow to 163 trillion cubic feet by the year 2035. Figure 1-1 shows the actual and projected world total energy consumption through 2035 [1]. In 2006, the proven reserves of natural gas were reported to be 6,183 trillion cubic feet with the majority of these reserves being in the Middle East (2,566 trillion cubic feet) and Eurasia (2,017 trillion cubic feet). In fact, Russia, Iran, and Qatar combined account for about 58 percent of the world reserves. For instance, Qatar has a proven reserve (911 trillion

cubic feet) of natural gas and, with 15% of the global production, is the world's third largest natural gas supplier [1].

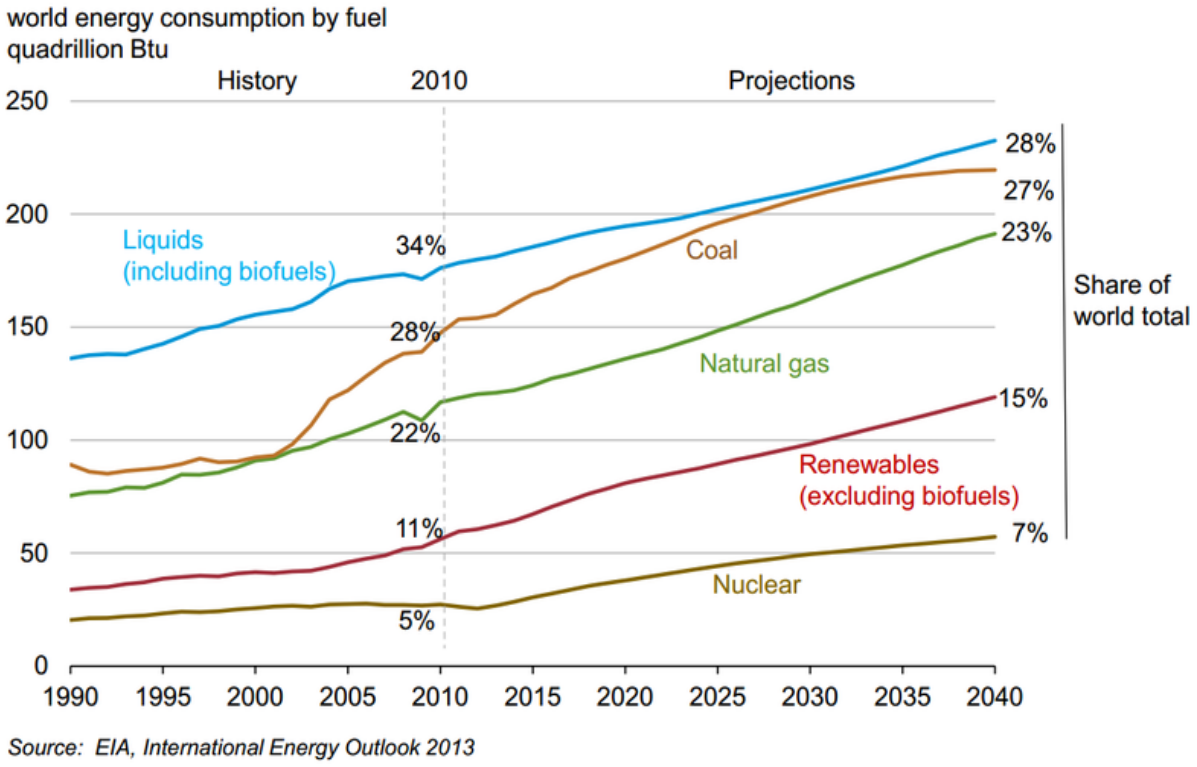

Figure 1-1. World energy consumption by fuel

Natural gas power production begins with extraction of natural gas, continues with its treatment and transport to the power plants, and ends with its combustion in boilers and turbines to generate electricity. Power plants convert gas to electricity using several methods. One method combusts the gas in a boiler to produce steam that generates electricity in a steam turbine. A more common, less expensive, and more efficient approach combusts the gas in a turbine (simple-cycle system), often extracting heat from the exhaust in a boiler (combined-cycle system). The simple-cycle system provides low-emissions and rapidly responding back-up generation for renewable sources like solar and wind and load following capabilities. The combined cycle system cannot

respond as quickly to changing demand but operates at efficiencies in the mid-to-high 50 percent range and provides low-emission baseline or somewhat load-following generation for the grid. Natural gas finishes third (quadrillion Btu) among fuels used for energy generation after petroleum and coal, but the gap between coal and natural gas is narrowing and has occasionally closed in recent months [1].

The LNG process mainly addresses transportation needs for LNG. Stranded natural gas supplies, those that exceed local market demand and have no pipeline transport options, represent good liquefaction options. LNG is usually either re-vaporized when it reaches a viable market or used as a liquid fuel in some transportation engines. There are three options currently for stranded gas exploitation and transportation to markets. They are 1) volume reduction, such as LNG, which has a history of almost 100 years [2-5], CNG (compressed natural gas) [6], and NGH (natural gas hydrate) [7, 8], 2) conversion to other products (GTL) [9,10], and 3) conversion to other energy forms such as electric power and gas to wire (GTW) [10,11]. Recently, not only has there been a proliferation of regasification plants, but also a rise in LNG production [12]. Small-scale natural gas liquefaction processes draw the attention of investors for the development of stranded gas, with advantages of low investment, simple and compact processes, start-stop convenience, strong mobility and mature technology.

The design, simulation and optimization of the natural gas liquefaction processes began in 1970. There are several licensed natural gas liquefaction processes available with varying degrees of complexities and experience. The efficiency and capital cost for these processes are competitive and the differences are typically small with regard to thermodynamics and cost. The real keys in

developing a successful liquefaction plant are equipment selection and configurations to meet a plant's capacity goals. Although reducing unit investment and operating costs is important, the primary objectives of these technological innovations are to increase the volume of LNG production gas and optimize the efficiency of the refrigeration process employed. The most thermodynamically efficient liquefaction process is the one with a refrigerant or a mixed refrigerant system that best parallels the shape of the natural gas cooling curve at operating pressure (Figure 1-2). The liquefaction process cryogenically cools natural gas to form a liquid for easier and safer storage and expands the liquefied natural gas to atmospheric conditions for reuse. A typical natural gas liquefaction process includes three zones: A precooling zone, followed by a liquefaction zone, and completed by a sub-cooling zone. These zones differ in slopes, or specific heats, along the process.

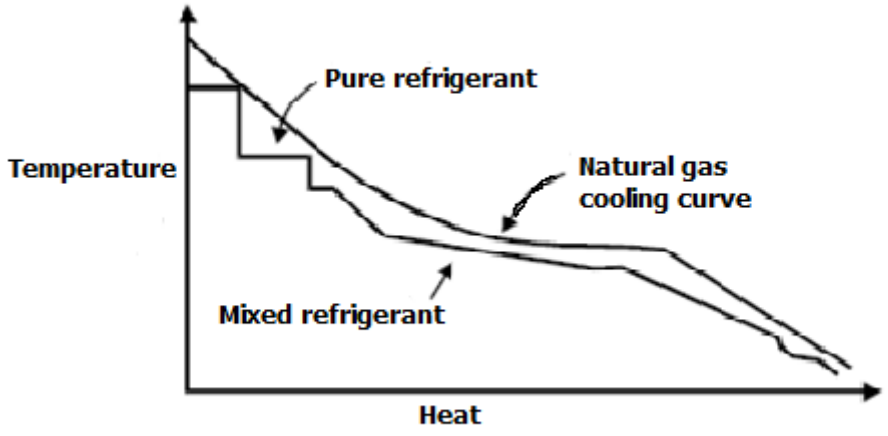

Figure 1-2. Natural gas cooling curve at operating pressure

Several processes have been reported for natural gas liquefaction, but few of them are in use (onshore plants) and many do not have industrial reference. There are mainly three types: cascade liquefaction [13, 14], mixed refrigerant liquefaction [15-17] and expander liquefaction [18, 19]. Investigators compare these liquefaction processes on the bases of energy consumption, exergy analysis, liquefaction fraction, and economic performance. Some select mixed refrigerant processes for the best choice of energy consumption consideration [20, 21], while some propose the expansion cycle [22]. Recent research has indicated that nitrogen expansion [23] is the most adaptive process when considering a combination of energy consumption, economic performance, safety, and operability.

The expansion cycle has a small footprint and high inherent safety, as no storage of hydrocarbon refrigerant is required. The major disadvantage is the relatively high power consumption. Kirillov et al. [24] introduced the vortex liquefaction technology and expansion liquefaction technology for small-scale, peak-shaving LNG plants. The liquefaction process requires significant power for compression in the refrigeration cycle so it is important to achieve energy efficiency in design and operating of refrigeration cycles [25, 26]. However, energy efficiency is not the only factor of importance, as any project must be cost effective, reliable, safe and tolerant of reasonably foreseeable feed changes. For offshore applications, it must also be easily maintained and compact [25]. To reduce input power for this process it is crucial to reduce entropy generation due to temperature differences between feed natural gas and refrigerant flow in LNG heat exchangers. Natural gas is a mixture of hydrocarbons and its specific heat capacity varies considerably during liquefaction. Therefore, liquefaction requires a variety of refrigerants [25, 27].

Academic and industrial NG liquefaction processes have a considerable literature. The processes analyzed in this project differ in important ways from these traditional processes, but they build on the both the technologies and the analytical techniques used by others. These are briefly outlined here. Adopting a pre-cooling process with propane, propylene or carbon dioxide, which is a more efficient refrigeration method in the high temperature range, can reduce energy consumption [27-30].

Carbon dioxide is a safe, non-toxic, and non-combustible refrigerant and some of these characteristics may justify some compromises in device size and capital expenditures. Compared with the hydrocarbon refrigerants used for natural gas liquefaction, carbon dioxide can achieve the same cooling effect, with the advantage of being easy to obtain, resulting in lower cost. Melaaen set up a dynamic model for the natural gas liquefaction process of a base load plant, and carried through the simulation by DASSL [23]. Shell Corporation has simulated the cascade, mixed-refrigerant and N_2 expander cycles and analyzed their advantages and disadvantages [23]. Terry adopted HYSYS software to calculate and optimize the typical liquefaction process of a peak shaving plant in 1998 [31]. Kikkawa designed the late model processes of a pre-cooling mixed-refrigerant cycle and an expander cycle by CHEMCAD software [32]. Prof. Gu An-zhong's research group of Shanghai Jiao Tong University simulated natural gas liquefaction processes [23]. Lun et al. [33] described several liquefaction processes for LNG peak-shaving based on pressure energy recovery. Lentransgaz [34] developed new natural gas liquefaction equipment that uses the pressure energy to liquefy the natural gas without an external energy source. Shirazi and Mowla [35] applied a genetic algorithm to minimize energy consumption during natural gas liquefaction in a peak-shaving plant and evaluated the exergy losses. Cao et al. [36] analyzed mixed refrigerant

cycles and the N_2-CH_4 expander cycle with HYSYS software. Small-scale natural gas liquefaction process in skid-mounted packages use these cycles. Remeljej et al. [19] compared four liquefaction processes including a single-stage mixed refrigerant cycle, a two-stage expander nitrogen cycle, and two open-loop expander processes. The single-stage mixed refrigerant cycle had the lowest exergy losses. Maunder [37] designed a process for methane gas enriched liquefaction, in which the gas was liquefied through the expander by lowering the temperature and pressure. Alabdulkarem et al. [38] optimized the mixed refrigerant cycle with propane precooling and found a new composition of mixed refrigerant that can reduce the average power consumption. Shen et al. [39] proposed a process to liquefy natural gas by utilizing the gas pipeline pressure as an energy source, but did not complete a detailed analysis and optimization. Xiong et al. [40] designed a natural gas liquefaction process that was suitable for city gates (relatively low pressure) using an expander refrigerant and heat integration technology. Gao et al. [41] designed a nitrogen expansion process with propane pre-cooling for coalbed methane liquefaction and investigated the effects of nitrogen content. A novel process for small-scale pipeline natural gas liquefaction was designed and presented by He and Ju [42]. Energy consumption of the process, as an objective function, is optimized by describing key variables of the design [37]. A low irreversibility is due to enhanced values of key parameters in the LNG heat exchangers and small-temperature differences between hot and cold composite curves. By optimizing refrigerant composition and other key variables of design, only 27% of lost work is in the LNG heat exchanger. Using a liquid expander instead of throttle valve saves 6% of the total lost work. Large temperature differences and heat exchange loads lead to exergy losses in heat exchangers and require compression with intercooling [36]. Yuan et al used Aspen HYSYS to simulate and optimize a process that liquefies 77% of the feed. The results had a unit energy consumption of 9.90 kW/kmol/h [43]. The adaptability of this process

under different pressure, temperature and compositions of feed gas was studied. He and Ju [42] also analyze exergy losses and show that their liquefaction process is suitable for use of the gas pipeline pressure due to its low unit energy consumption, simplicity and flexibility.

The CCC ES process studied in this investigation differs from all of these LNG processes in several important ways. First, the CCC ES process uses refrigerant only at the lowest temperature of the process, which allows a great deal of heat integration between the cooling and warming streams as they approach this temperature. This means that the CCC ES liquefaction always has at least a small returning stream of NG vapor, unlike any of the LNG processes discussed here. This changes the process design and generally decreases the power demand. Second, traditional LNG process designs focus on steady-state operation, whereas this investigation is focused primarily on transient operation. The success of CCC ES depends on maintaining a high process efficiency during frequent and large perturbations in total flowrate and, to a lesser extent, composition. Finally, traditional natural gas processing in preparation for LNG applications share these same characteristics, that is, they also do not have return streams and they operate at steady state. This project examines both the integrated system and its transient behavior. In addition to these differences, this investigation optimizes the processes for energy efficiency while minimizing cost. While the investigation here owes much to the traditional natural gas liquefaction community, all of the processes designed in this investigation differ in important ways from those in this traditional community. The following discussion outlines how the cryogenic carbon capture™ process works and how natural gas liquefaction enters into this process.

1.2. Energy storage of cryogenic carbon capture (CCC ES)

Energy storage represents one of the most critical needs in energy infrastructures of most nations and this need will increase as intermittent and alternative energy production increase. Energy storage (ES) is the conversion of energy from one form to a form that is more convenient and/or less expensive to store. Thereafter, the energy can be converted back to the original or to another useful form. Energy storage differs from energy sources in that the roundtrip conversion involved in energy storage at best conserves the useful energy and in practice always loses some energy or availability (if it did not, it would be an energy source). Nearly always, interest in energy storage is driven by capacity, convenience, or economic considerations that mitigate the inherent energy loss of the process. The most desirable characteristics of these energy storage systems include: sufficient capacity to affect grid dispatch schedules, rapid response to changes in demand, high round-trip efficiency, and low cost.

Recently promulgated EPA regulations under Clean Air Act Sections 111(b) and 111(d) aggressively limit CO_2 emissions from the US power industry. Under these regulations, new natural-gas- and coal-fired power plants can emit up to 500 and 635 kg of CO_2 per MWh. CO_2 emissions reductions from existing plants require about a 32% overall reduction from 2005 levels, although the regulation is not written in this way. The standard requires states or groups of states to meet specified total emission targets or, as an alternative, to meet emission rate targets. Current combined-cycle natural gas plants meet the standards for new power plants as they are about 50% below the emissions of most coal plants. Nevertheless, the regulation has specific provisions for limiting the amount of natural gas used to meet the new standards for existing power plants. Such large reductions from coal plants lie well beyond the reach of plant efficiency improvements or

other modest operational changes and threaten decommissioning of existing plants and curtailing plans for new plants. In fact, coal consumption has declined in the US and in parts of Europe for several years and there are very few new coal plants planned.

This research project focuses on energy storing cryogenic carbon capture™ (CCC ES), which addresses both of these issues. Cryogenic carbon capture™ (CCC) separates CO_2 from light gases in streams such as power plant flue gases, cement kilns, and vitiated gases from industrial processes. This innovative process could dramatically decrease the energy and economic costs of carbon capture. Some embodiments of CCC enable energy storage with similar dramatic improvements over alternative systems. This system balances daily cycles in power demand and enables more reliable renewable energy use. Most renewable energy sources are intermittent. They strain grid management systems and cause inefficiencies in base-load generation facilities. Because of this intermittency and unpredictability, power generators must provide backup systems to supply energy when the intermittent sources are not active. Therefore, adding intermittent renewable energy to a generating network does not greatly decrease the total amount of traditional energy generating capacity. Large-scale, rapidly responding energy storage can solve this problem. As renewable energy sources gain a larger portion of the energy market, the significance of rapidly responding energy storage becomes crucial to maintaining a reliable electric grid. This discussion highlights an energy storage process enabled by Cryogenic Carbon Capture™ (CCC) [44-48].

Surges in power supply and demand arise from: (1) typical daily patterns of high-energy demand during the afternoon and low demands in the night, (2) intermittent contributions from renewables such as wind or solar energy, and (3) grid instabilities. These changes in supply

typically drive changes in average energy production cost and energy price, in addition to several more complicated and region-specific issues. Such large cost swings generally change dispatch schedules and other aspects of grid management, most of which pose significant technical issues. CCC mitigates these problems, increasing grid and price stability over a period of one or several days, using an energy storage system as explained here. The CCC process can use natural gas as a refrigerant. This refrigerant provides very high-energy storage density, with the temperature-, pressure-, and phase-change energy stored in the LNG [46-48]. The energy-storing version of CCC stores surges in energy supply or periods of low energy cost by liquefying more natural gas than is needed at the time of the surge or low cost. This excess production terminates when the supply or cost returns to normal. During high-energy demand or expensive energy production periods, the cryogenic carbon capture process operates on stored liquefied natural gas, reducing its parasitic load and thereby increasing the amount of net energy produced by the power plant. Current commercial LNG storage technologies easily allow for many hours of energy storage for even the largest coal-fired power plants by this technique. In practical applications, the energy storage rate of this process typically could be up to 50% of the power plant capacity while the rate of energy release could be about 15% of the plant capacity. However, the rate of energy release could be much higher, as explained next.

The CCC system consists of two major subsystems: cryogenic carbon capture, and energy storage via natural gas liquefaction. The natural gas liquefaction is integrated into CCC as a refrigerant to cool the flue gas. The CCC process is as follows: Flue gas enters the CCC process which is a bolt-on, retrofittable system near the end of the existing process. The CCC process dries and cools the gas. After this preliminary cooling, it flows through a recuperative heat exchanger,

cooling to near its CO_2 frost point. Other pollutants, such as Hg, As, NO_2, HCl, and SO_2, condense or de-sublimate as the flue gas cools, allowing CCC ES to exceed the target removal of most criteria pollutants, mercury, and hazardous gases. The process captures large quantities of the pollutants at low temperatures. At low enough temperatures, the exhaust exiting the stack actually has less CO_2 content than the surrounding air (see Table 1-1).

Table 1-1. Common Pollutant Removal Temperatures

Temperature (ºC)	What is captured
-48	100% of the mercury in coal
-77	All of the above, plus 99% of the mercury from the atmosphere
-117	All of the above, plus 90% of the CO_2 from coal; SO_2 EPA standard met
-132	All of the above, plus 99% of the CO_2 from coal
-143	All of the above, plus 100% of the CO_2 from coal. Below this point, the exhaust exiting the stack has less CO_2 than the atmosphere.
-150	All of the above, plus 80% of the CO_2 from the atmosphere
-162	All of the above, plus 99.5% of the CO_2 from the atmosphere

Further cooling in patented de-sublimating heat exchangers [44, 45] removes CO_2 as a solid and leaves a light gas stream. A solids handling system pressurizes the solid CO_2 to at least the triple point and at most the final CO_2 product delivery pressure. A heat exchanger transfers sensible energy between the light gas streams and with the cold, solid CO_2 as it warms, melts, and further warms to room temperature (Figures 1-3, 1-4 and 1-5).

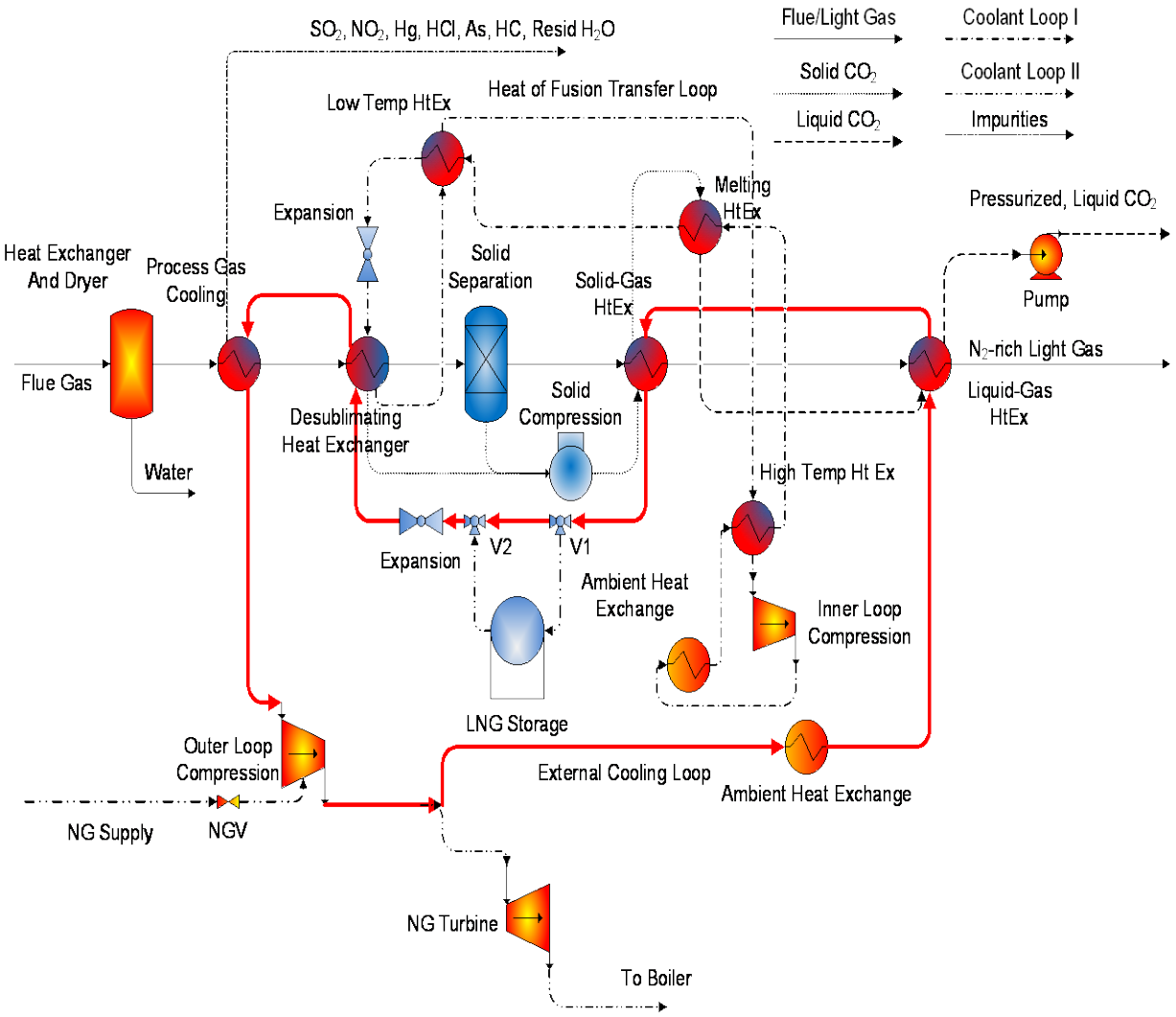

Figure 1-3. Energy storage version of CCC process under normal (neither storing nor recovering energy) operation [48]

The energy storage process, by contrast, responds rapidly to changes in demand, intermittent renewable energy sources, and other transients with widely varying time constants. Both processes involve substantial internal heat integration, but heat integration between them would destroy the ability of the LNG cooling process to respond rapidly to load changes without affecting the CO_2 capture process.

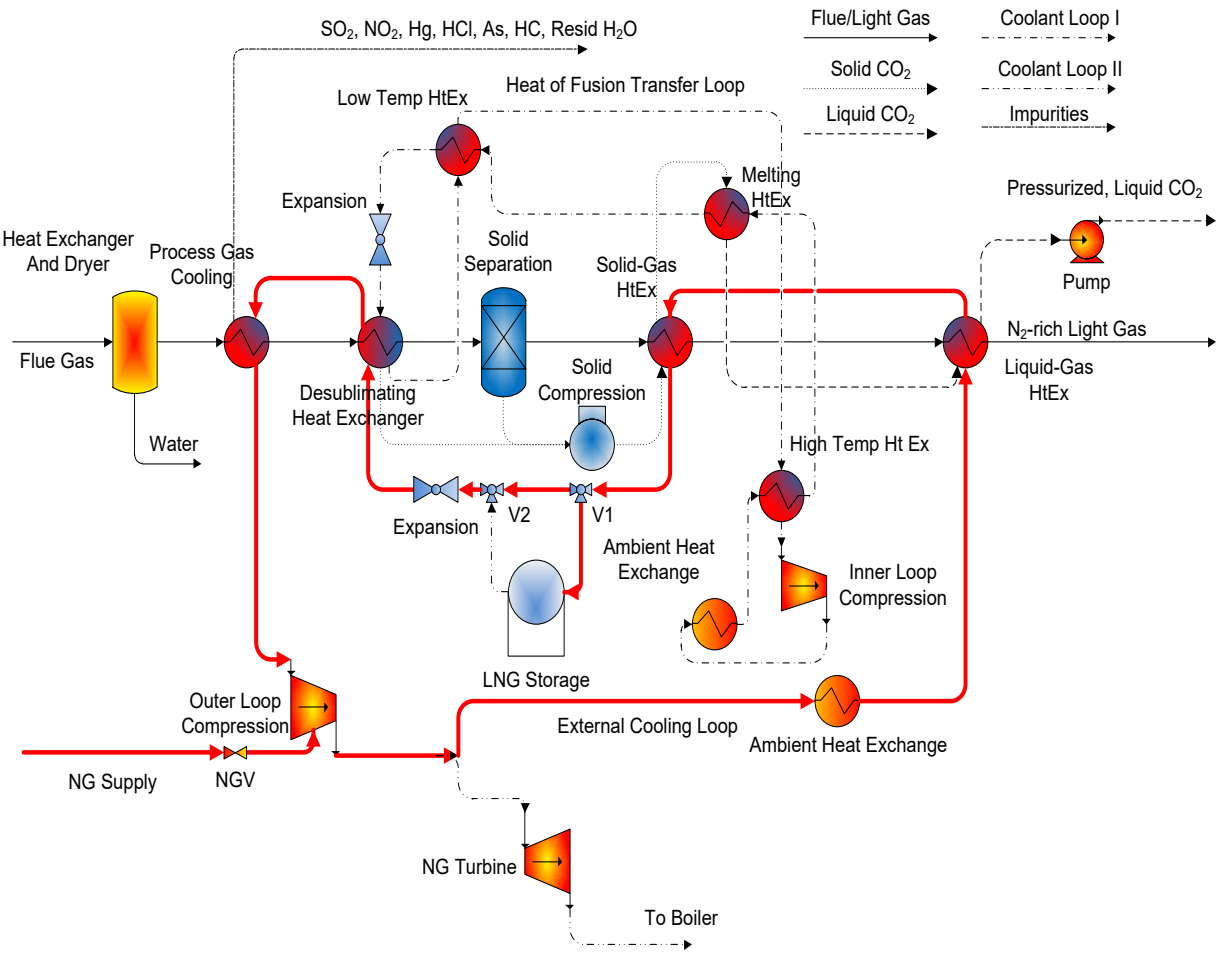

Figure 1-4. CCC process during energy storage operations. NG from the supply is pressurized and cooled prior to storage in the LNG storage at nominally -119.4 °C and 11.45 bar pressure. NG refrigerant follows the solid red/thick process lines [48]

The CCC process and the LNG-based cooling loop deliberately operate independently of one another, with essentially no heat integration aside from the LNG delivery to CCC and its return. The CCC process often couples to a power plant or some other CO_2-producing process that preferably operates at constant or very slowly varying load.

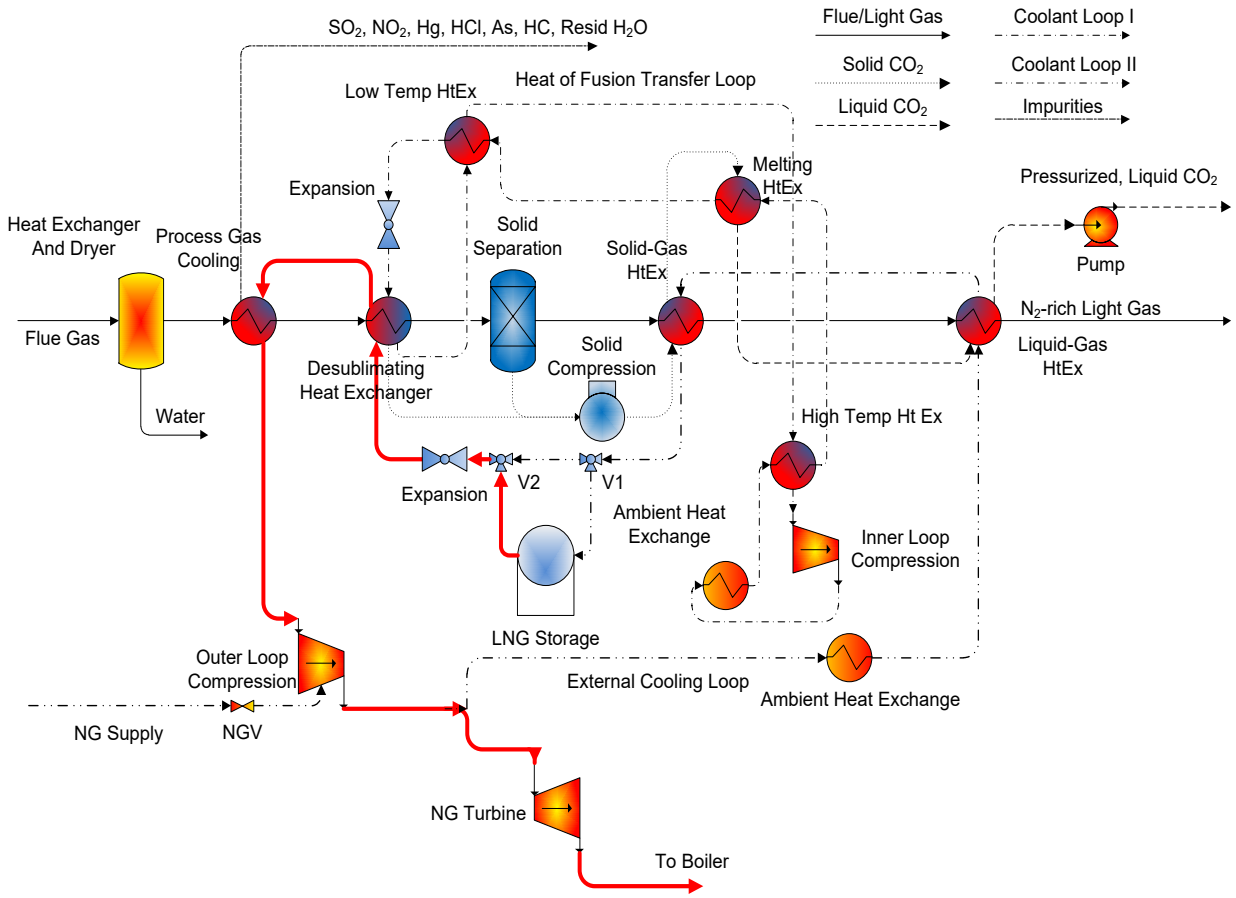

Figure 1-5. CCC process during energy recovery operations. NG from the supply is pressurized and cooled prior to storage in the LNG storage at nominally -119.4 °C and 11.45 bar pressure. NG refrigerant follows the solid red/thick process lines [48]

The distinction between the two cooling loops is elaborated in more detail here. After separating CO_2 from flue gas, the pure CO_2 solid product is well below its melting point, the latter being approximately -57 °C, depending very slightly on pressure. This pure CO_2 stream melts at essentially constant temperature, which melting involves a significant amount of the energy required in the CCC process. This is illustrated in the diagram above as Coolant Loop I or Inner Loop. A single-component cooling loop efficiently transfers the heat of CO_2 fusion from the melting point of -56.6 °C to lower temperatures by condensing at the CO_2 melting point at an elevated pressure and vaporizing at a lower temperature and pressure, in this case at the lowest

temperature in the loop. Since the CO_2 is essentially pure at this stage, this CO_2 melting/refrigerant condensation process occurs isothermally on both sides of the heat exchanger, minimizing losses. The lowest temperature at which CO_2 forms a liquid phase at any pressure is the triple point, which is -56.6 °C (at a pressure of 5.2 bar). Therefore, the inner-loop refrigerant must condense at this temperature or higher and at some reasonable pressure to provide the heat to melt the solid CO_2. It is possible to provide this heat exchange with sensible heating or with a mixed refrigerant, but neither of these options can occur at a single temperature. They would therefore create an increasing temperature difference in the heat exchanger that would lead to larger inefficiencies.

Cooling Loop II, or the outer cooling loop, transfers more heat than the inner loop in general, and unlike Cooling Loop I, this heat transfer occurs over a broad temperature range. The baseline CCC systems uses several refrigerants in this loop to optimally match the temperature profiles on both sides of the heat exchangers, that is, to maintain a constant and small temperature difference throughout the process.

The outer cooling loop uses NG as a refrigerant as indicated. During normal operation, that is, when energy is being neither stored nor recovered, there is no net NG flow to the process and no power output from the NG turbine. The overall cooling loop flow is highlighted with thick, red lines (see Figures 1-3, 1-4 and 1-5). During energy storage, NG enters the outer loop compressor from an external pipeline supply, increasing the total amount that flows through the compressor compared to normal operations and hence increasing the compressor power consumption. The excess NG flows into the LNG storage at V1 with the normal amount of NG continuing through the process, increasing the LNG level in the storage vessel. The vessel exit is closed to the process

loop, allowing the NG to accumulate. This stores the extra compressor and cooling energy in the form of LNG at cryogenic temperature and modest pressure. When the stored energy is used, the external NG supply valve closes and the external loop compressor load can decrease to near zero. Some or all of the cooling is provided by the stored NG, which flows from the vessel through the process. After returning to room temperature, the NG can either enter a NG turbine, where it is combusted, or enter a pipeline (pipeline is not shown in the figure). If it enters a turbine, the hot gases from the NG turbine vent into the convection pass of a boiler, providing NG combined cycle efficiency without having to build an additional Rankine cycle. During this phase, the power required for the largest compressor decreases, potentially to zero, and the turbine generates additional power. The additional power generated by the NG turbine is not included in the energy efficiency performance, but functionally it adds to the power plant's ability to increase power during energy recovery cycles of grid management.

Energy-storing cryogenic carbon capture (CCC ES) stores and releases 10-20% of power plant capacity in the form of cold, liquid refrigerant. This refrigerant's effective energy density greatly exceeds that of traditional thermal energy storage fluids because it includes the latent heat of phase change and the sensible heat of a large temperature change. In principle, CCC ES could use any refrigerant, but doing so requires storing cold liquid and warm vapor, the latter having a low energy density and requiring an unrealistically large storage facility for a large power plant. The warm vapor storage facility is not required if the process uses refrigerant such as liquefied natural gas (LNG) that can either generate additional power in a gas turbine or return to the pipeline. CCC ES must include an LNG process that can change load rapidly without compromising efficiency or reliability. This project develops detailed models that describe the

transient process behaviors during LNG generation and demonstrates mechanisms that allow rapid and large changes in load with minimal deleterious effects. Doing so requires a detailed understanding of fluctuations in grid power demand.

The energy-storing (ES) mode of the process generates more refrigerant than is needed for carbon capture and stores the excess refrigerant in an insulated vessel as a liquid at the low-temperature, modest-pressure point in the cycle. This normally occurs during off-peak hours or when excess power is otherwise available, such as from wind farms or other intermittent sources. During peak demand, the previously stored energy in the form of the stored, condensed refrigerant provides energy recovery (ER) by reducing the compressor load and using the stored refrigerant, eliminating nearly all of the energy required by cryogenic carbon capture for as long as the stored refrigerant lasts. The amount of refrigerant required by CCC for 3-4 hours of utility-scale power plant operation requires only a fraction of the capacity of commercially available LNG storage tanks.

Figure 1-6 illustrates the overall energy storing process. The straight line is the constant energy stream needed to capture CO_2 from a plant operating at constant load. The net plant output meets the varying demand, as indicated by the red line. The yellow line represents the NG flow into the plant. The difference between the yellow line and its average value would be the net NG outflow either into a simple cycle turbine or the NG pipeline. This investigation focuses on the LNG generation process during the transients in NG flow.

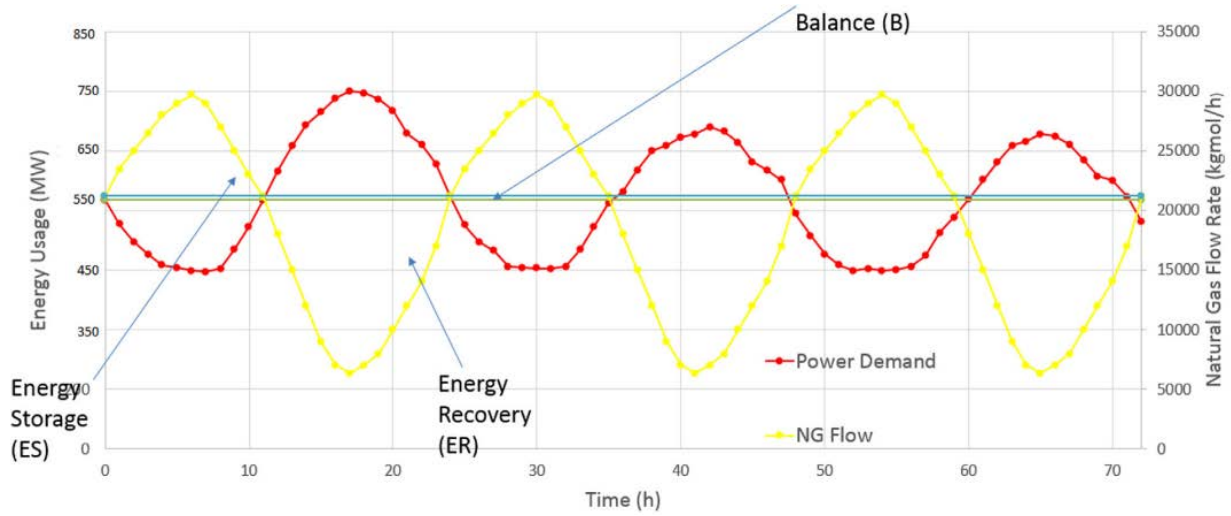

Figure 1-6. Power plant energy demand and natural gas flow rate in three cases

The energy demands for any carbon capture process are quite high – in all cases much larger than the sum of all other parasitic loads combined for commercial coal boilers, natural gas turbines, and similar power plants. The CCC ES process shifts its energy demand to periods of low power costs and high power excess capacity. This time shifting enables energy storage at very large scale that is efficient, and cost effective. Therefore, the energy storing version of CCC uses natural gas as the refrigerant. Natural gas storage as a liquid is a well-established technology, and warm natural gas can either be placed back in the pipeline or burned in a gas turbine to generate power.

Current LNG systems do not operate efficiently under such transient conditions. Optimizing a process that responds such as in Figure 1-6 is the final goal of this investigation. Aside from the return flows making these LNG processes unique compared to traditional analyses, this investigation focuses on transient modeling. The LNG process used in CCC differs from the analyses briefly reviewed in the introduction in that it always incorporates a return NG stream, similar to air separation unit (ASU) processes that incorporate substantial recuperative heat

exchange. The traditional processes produce and deliver LNG, typically with little or no return stream through the production cycle.

The CCC process uses LNG as a refrigerant and, in fact, primarily uses only refrigeration associated with LNG vaporization. Therefore, the LNG process analyzed here benefits from significant heat integration, warming low-pressure LNG vapor returning from the CCC process by cooling high-pressure LNG streams entering the process. This heat integration results in LNG production at notably lower energy and economic costs compared to traditional systems when the system operates in either energy recovery or balanced modes. Nevertheless, the process is similar enough to traditional processes that the substantial commercial experience and published analyses remain germane to this process, with some modification. This investigation applies the results of the previous investigations to this somewhat different process to analyze a system that has aspects in common with traditional LNG and ASU processes.

Factors that determine the best NG liquefaction models include energy consumption, capital cost, efficiency and exergy loss. The CCC ES system switches from energy storing to energy recovery at rates comparable to intermittent renewable power generation changes (minutes) and stores energy for smoothing base-load energy production while removing CO_2 emissions from the base-load energy production. The CCC ES process stores energy efficiently and changes load rapidly over a significant fraction of a power plant capacity. SES has demonstrated CCC ES at skid scale (about 1 tonne of CO_2 capture per day) and detailed process models describing it have been developed and optimized. However, detailed transient analyses of the process have not been completed.

This project determines the feasibility of CCC ES, which includes detailed transient energy and cost analyses along with lab demonstrations of critical process components. Included as a subsystem of CCC ES, natural gas will be prepared for liquefaction by removing water, mercury, and sour gases (CO_2 and H_2S) by natural gas cryogenic carbon capture (NG-CCC). The specific goals are (1) that the process can provide energy storage with 95+ % roundtrip efficiency, (2) that the incremental cost is less than 600 $/kW of energy storage, and (3) that NG-CCC can be performed to remove water, mercury, and sour gases from raw natural gas in preparation for natural gas liquefaction to support CCC ES. This requires optimizing the processes of natural gas liquefaction and combustion with CO_2 separation to support a large dynamic power demand. Managing this transient energy demand requires quantitative understanding of process design and operational requirements and careful optimization.

This investigation explores optimal ways to use the natural gas liquefaction process to match dynamic power demands while satisfying the mostly steady-state demand for refrigerant. Turbomachinery such as compressors adapt to such load changes relatively easily, but heat exchangers do not. This integration requires detailed transient analyses of the process, with a focus on heat exchanger and overall process performance. This investigation shows how dynamic heat exchanger concepts developed by SES provide efficient liquefaction operation even in the presence of dynamic demands while supplying steady supplies of coolant to the CCC process. Other grid-level [46] and equipment-level [51] analyses complement this plant-level analysis of these dynamics.

1.3. CO_2 removal from natural gas and operating conditions

The core concept in producing LNG is the condensation of natural gas. Other processing steps involve the elimination of undesirable impurities and separation of byproducts. Natural gas consists primarily of methane (CH_4), ethane (C_2H_6), propane (C_3H_8), small quantities of heavier hydrocarbons, nitrogen (N_2), oxygen (O_2), carbon dioxide (CO_2), water (H_2O), and sulfur compounds. Although the above-mentioned compounds may exist at low or high levels; CH_4 is the main constituent.

Natural gas is liquefied to increase its energy content (heating value) per unit volume, and facilitate energy transport in large quantities. Typically, LNG is stored and delivered at atmospheric pressure and -160 °C (-256°F), though storage can be at pressures as high as 6 bar and temperatures as high as -140 °C. It is kept in specially designed containers and transported by special cryogenic sea vessels and road tankers. The density of LNG depends on its temperature, pressure, and composition. However, a typical density is about 500 kg/m^3. LNG is odorless, colorless, noncorrosive, and non-toxic. When vaporized in air, LNG burns in the composition range of 5% to 15%. Neither LNG, nor its pure vapor, can explode in an unconfined or confined environment.

Natural gas entering a liquefaction plant must be pre-treated to remove impurities such as water, acid gases (e.g. CO_2 and H_2S) and mercury to prevent these from freezing, corroding, or depositing on process equipment and to control heating value in the final product. Nitrogen is removed at the end through flash vaporization while heavy hydrocarbons may be removed at a pre-cooling stage because of their values as natural gas liquids (NGL), liquefied petroleum gas

(LPG) and for refrigerant makeup. The compositions of natural gas suitable for liquefaction process include a mixture of methane (about 85-95%), lighter hydrocarbons and a small fraction of nitrogen [14]. The heavier carbon-containing compounds commonly form natural gas liquids (NGL) that have high market value and may be separated from natural gas during LNG production. Accordingly, methane is an even more dominant constituent of LNG than of natural gas.

Inlet receiving units are designed primarily for the initial gas-liquid separation. Additionally, condensed water, hydrocarbon liquids, and solids are removed. The other units are gas treating, dehydration, compression, and liquefaction. Gas treating involves reduction of the "acid gases" carbon dioxide (CO_2) and hydrogen sulfide (H_2S), to levels as low as 50 ppmv and 5 ppmv, respectively, to meet pipeline specifications. Dehydration removes water and dries the gas to avoid hydrate formation as well as corrosion.

This investigation shows how reducing CO_2 contents of typical pipeline-quality natural gas using cryogenic means can produce LNG-quality natural gas. This technology is important both for the immediate use of some natural gas supplies in the CCC ES process and separately as a natural gas treatment process for traditional LNG applications.

1.4. Objectives

The objectives of this research are to (a) develop steady-state models of the refrigerant generation portion of the cryogenic carbon capture™ process using commercial process simulation software and refrigeration schemes based on those used for traditional liquefied natural gas generation, (b) optimize and compare the merits of the process schemes in steady operation, (c) develop dynamic models of the most promising process schemes, (d) optimize the dynamic performance of the process and analyze the

performance, (e) implement dynamic heat exchangers in the dynamic schemes, (f) analyze the performance of the dynamic system, (g) apply the results to natural gas processing, and (h) collect experimental data from a lab-scale system and compare the predicted behaviors for natural gas processing.

Chapter 2. Steady state simulation and optimization

This section analyzes four different liquefaction models in Aspen HYSYS and optimizes them using the Visual Basic for Applications (VBA) optimizer (see the Appendix). These processes are: propane-precooled mixed refrigerant (C3-MR) cycle, a modified dual mixed refrigerant (MDMR) cycle and two single mixed refrigerant (SMR) cycles.

The model simulations include flow and thermal transients and the consequent responses of all processing steps. The transient flows are a non-trivial contribution in the energy performance and their analysis and inclusion is a distinguishing characteristic of these simulations. The Aspen Energy Sensitivity model further optimized the best models (SMR cycles). The discussion includes comparisons with available literature. However, the comparisons of these four processes discussed in this investigation use the same assumptions, the same thermodynamics and process models, and are optimized using the same techniques as one another and therefore provide a more reliable comparison to one another than is possible in comparing to independent literature results. This analysis also includes comparisons during balanced operation and during intentionally imbalanced operation, unlike most literature investigations.

2.1. Process design

Among the many publications on design and optimization of LNG processes, only a few include transient or dynamic simulations. A dynamic process simulator estimates transients and dynamics and examines and verifies control schemes. Turbo machinery and most equipment other than heat exchangers adapt relatively easily to the transients.

The heat exchangers, however, become significantly imbalanced during these transients, leading to large thermal stresses and inefficiencies associated with large local changes in temperature and temperature differences. These imbalances prematurely age equipment, lead to equipment failures, and cause the process to miss specifications and perhaps fail completely. This investigation evaluates design modifications and capture cases using dynamic simulation and quantifies the effects of flowrate changes on efficiency and other process figures of merit.

2.1.1 Feed gas parameters

The simulations discussed here require several specifications, as summarized in Table 2-1. A feed gas flow rate of 21200 kgmol/h provides the amount of natural gas refrigerant required for the steady operation of CCC on a 550 MW power plant. During energy storage and recovery, the rates change to 29680 kgmol/h and 6360 kgmol/h, respectively. These flow rates represent a 40% increase and a 70% decrease in coolant flow. The context here is that the amount of cooling provided to the CCC process at the power plant is constant (base-loaded plant) while the demand on power for the LNG production process could change +40% to – 70% based on grid variations. In reality, the off-peak period commonly lasts much longer than the peak period, but this simple approach illustrates how the system works and is a worst-case scenario from a controls standpoint. All other parameters mentioned in Table 2-2 remain constant. The liquefaction rate is 100% after the main heat exchanger, but to satisfy the CCC process, that is, to avoid temperature cross over in CCC's heat exchanger, the output temperature from the LNG plant should be around -120 °C. Therefore, the LNG partially vaporizes (27%) after the main heat exchanger. The streams labeled "From CCC" and "Water" return to the liquefaction process from the CCC process. Water can be used to reduce heat load but, as will be shown in the transient analysis, a separate heat exchanger for water is more robust.

Table 2-1. Process parameters for the four processes

Parameters	Value		Notes
Feed gas pressure	3700 kPa		
Feed gas temperature	21 °C		
Feed gas flow rate	21200 kgmol/h		
Feed gas mole fraction components	CH_4	0.95	
	C_2H_6	0.03	
	C_3H_8	0.02	
LNG storage pressure	1145 kPa		
LNG temperature before expansion	-94 °C		
Liquefaction rate before expansion	100%		
NG temperature after expansion	-119.4 °C		
Liquefaction rate after expansion	73%		
Pressure drop in heat exchanger	5 kPa		To simplify the process
Pressure drop in water cooler	1 kPa		
Temperature after water cooler	21 °C		
The adiabatic efficiency of compressor	90%		[47]
The adiabatic efficiency of turbine	92%		[47]
Pressure ratio of each compressor	1-3		
Water's temperature from CCC	1.0561 °C		
From CCC's temperature	-98.5 °C		
From CCC's flow rate	21200 kgmol/h		
The minimum approach temperature of heat exchanger	1-3 °C		

Table 2-2. Specifications of NG common to all four models

Conditions	From pipeline	To CCC (final conditions)
Vapor / Phase Fraction	1	0.27
Temperature [°C]	21	-119.4
Pressure [kPa]	3700	1145

2.1.2. Liquefaction process

Based on characteristics of commercial, full-scale LNG plants, this investigation explores three typical liquefaction processes for analysis and comparison. These are included in four different models simulated using Aspen HYSYS: Two different single mixed refrigerant cycles (SMR), one modified dual mixed refrigerant (MDMR), and one propane-pre-cooled mixed refrigerant (C3-MR) cycle. These are simulated and optimized to choose the best model with regard to energy input requirements, exergy loss, cost, and heat exchanger efficiencies.

2.1.2.1. Single Mixed Refrigerant cycle (SMR)

The SMR is the simplest NG liquefaction process. The Single MR Cycle uses only one MR loop for pre-cooling, liquefaction, and sub-cooling (Figures 2-1a and 2-1b).

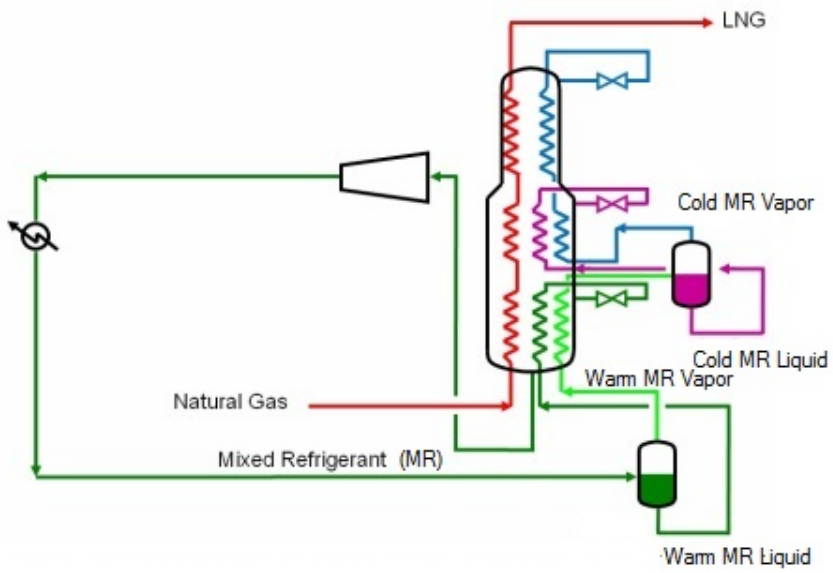

a)

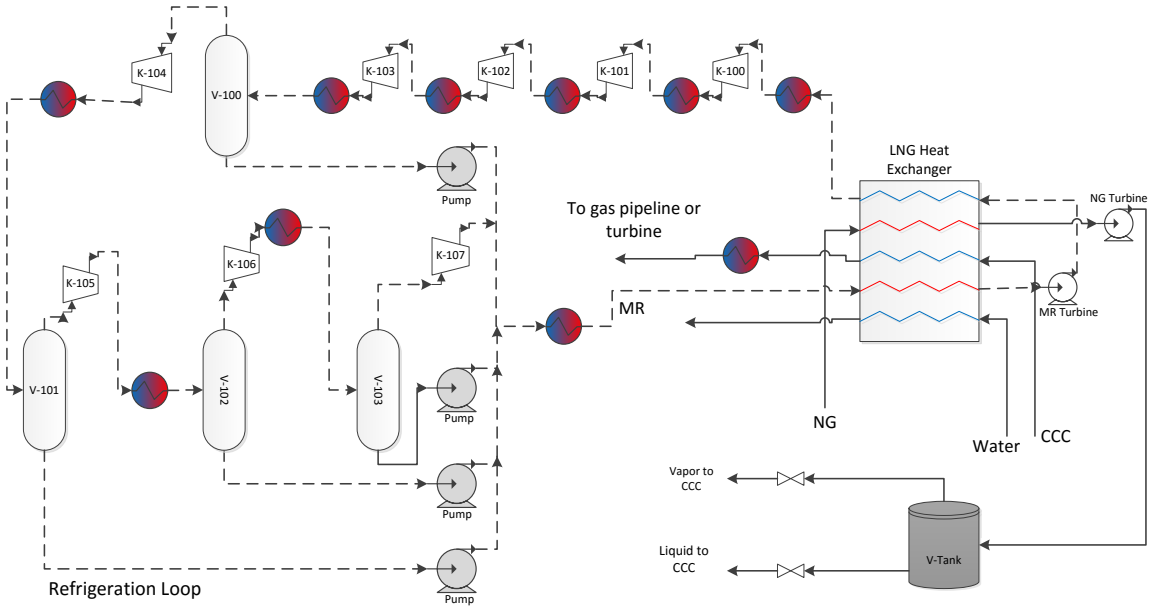

b)

Figure 2-1. a) Flow sheet of SMR model b) HYSYS simulation of SMR

The cycle compresses and cools the refrigerant until liquid is formed, and then vaporizes the refrigerant in the LNG exchanger. The refrigerant cools -condenses the natural gas, NG, to

liquefied natural gas, LNG. The refrigerant composition is optimized such that the net warm- and net cold-stream temperature profiles in the heat exchangers are as close and parallel as possible.

The simulation flow sheet of the SMR process (Figure 2-1a and 2-1b) uses an eight-stage compressor with inter-stage cooling. Phase separators separate the mixed refrigerant into gas and liquid phases in each cooler. Pumps pressurize the liquid after the phase separator.

A single LNG heat exchanger liquefies and cools the natural gas to the required LNG storage condition of about -119.4 °C and 11.45 bar pressure. Subsequent expansion prepares the LNG for the CCC process. The LNG can optionally cool further and be stored at lower pressure, with less evaporation prior to entering the CCC process, but the conditions here provide a sufficient basis to illustrate the dynamic responses of the system. The return natural gas (now all vapor) stream and a stream of water condensed from the flue gas return from the CCC process to the LNG process. Water reduces heat load.

Table 2-3 summarizes the optimized mixed refrigerant composition and key parameters, where ER, B and ES represent energy storing, balanced, and energy recovery respectively, that is, conditions when LNG is accumulating for future use by the CCC process, when LNG demand from the CCC process is balanced with its production rate, and when stored LNG levels are dropping.

Table 2-3. a) Key parameters and b) mixed refrigerant conditions for three cases

a)

	Entrance			Loop		
Conditions	**ER**	**B**	**ES**	**ER**	**B**	**ES**
Vapor / Phase Fraction	0.43	0.023	0.00	0.23	0.086	0.10
Temperature [°C]	30.00	20.5	16.12	-87.99	-93.191	-92.05
Pressure [kPa]	3704.65	3704.65	3704.65	108.4	108.394	108.40

b)

Component	Mole fraction
Methane	0.0418
Ethane	0.8461
Propane	0.0017
n-Butane	0.0053
n-Pentane	0.1051

2.1.2.2. Modified Dual Mixed Refrigerant (MDMR)

In the modified Dual MR cycle, a high boiling point Warm Mixed Refrigerant (WMR) containing methane, ethane and propane replaces the pre-cooling propane refrigerant in the C3-MR process. This significantly reduces the propane inventory in the process. The MDMR process achieves efficiencies comparable to C3-MR (discussed later) and has been used successfully in

land-based LNG [13]. The MDMR design balances refrigeration loads across the two similar refrigerant compressors, reducing overall power requirements. This increases the applicable range for the most efficient centrifugal compressor operation and reduces spare parts costs. The WMR forms a single liquid phase after compression, cools in the main heat exchangers pre-cooler, and flashes to a single pressure level to provide pre-cooling refrigeration. The process can therefore be configured and optimized to meet the project requirements in Table 2-2. Figure 2-2 includes the simulation flow sheet of the MDMR process.

This process adds a second loop to the SMR design, which increases the cost relative to the SMR even though the two loops require smaller compressors than the SMR. This additional loop controls the flow rate and temperature, resulting in the most efficient heat exchanger among these processes. Other options to avoid the methane loop are not practical like using ethane instead of methane. The minimum temperature approach is unrealistically less than 1 ºC.

The process can therefore be configured and optimized to meet the project requirements. Table 2-4 and Table 2-5 indicated the mixed refrigerant conditions and key parameters for the warm and the cold loops, respectively.

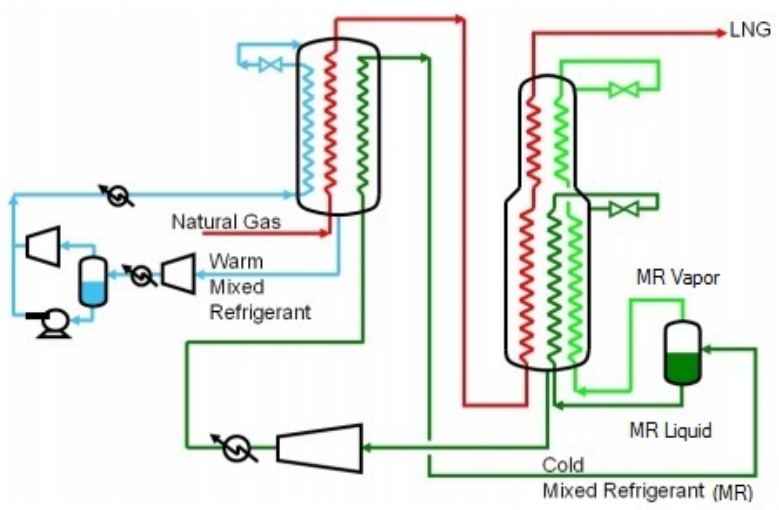

a)

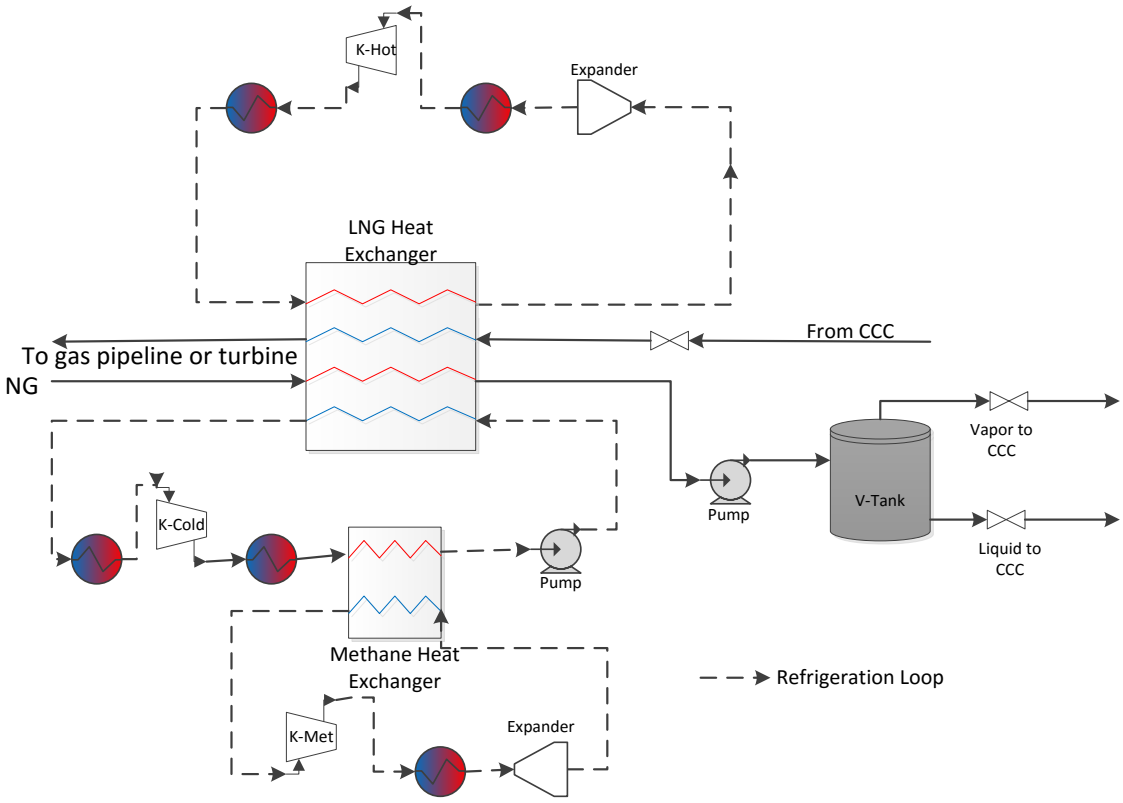

b)

Figure 2-2. a) Flow sheet of MDMR model b) HYSYS simulation of MDMR

Table 2-4. a) Key parameters and b) warm mixed refrigerant composition for MDMR

a)

	Entrance			Loop		
Conditions	**ER**	**B**	**ES**	**ER**	**B**	**ES**
Vapor / Phase Fraction	1	1	1	1	1	1
Temperature [°C]	24.97	16.90	10.83	-37.48	-17.85	1.244
Pressure [kPa]	194.1	194.1	194.1	189.1	189.1	189.1

b)

Component	**Mole fraction**
Methane	0.335
Ethane	0.255
Propane	0.410

Table 2-5. a) Key parameters and b) cold mixed refrigerant composition for MDMR

a)

	Entrance			Loop		
Conditions	**ER**	**B**	**ES**	**ER**	**B**	**ES**
Vapor / Phase Fraction	0.11	0.1028	0.1028	0.79	1	1
Temperature [°C]	-95.86	-96.52	-96.52	-82.15	-18.34	15.72
Pressure [kPa]	107.9	107.9	107.9	102.9	102.9	102.9

b)

Component	**Mole fraction**
Methane	0.064
Ethane	0.830
Propane	0.106

2.1.2.3. Propane-pre-cooled mixed refrigerant cycle (C3-MR)

The C3-MR process produces over 80% of the world's LNG. This process combines a propane-based refrigeration loop for the initial cooling to around -30 °C with a mixed refrigerant for cooling to the final conditions (Figure 2-3). Natural gas liquefies at high pressures (20-50 bar) and condensation temperatures at or near the critical temperature (about -83 °C). The propane also pre-cools the compressed, mixed refrigerant. After pre-cooling, the partially condensed mixed refrigerant separates into liquid and vapor phases. As the mixed refrigerant vaporizes and flows

downward on the shell side of the main heat exchanger, it cools and condenses the natural gas. The vaporized mixed refrigerant returns to the compressor to complete the loop. The single-component pre-cooling fluid provides an efficient, easy to control pre-cooling step. The mixed refrigerant permits phase change over a temperature range that matches the range of condensation temperatures of the NG, leading to high efficiency. Consequently, the C3-MR cycle minimizes the number of equipment items and leads to easier operation, and high reliability.

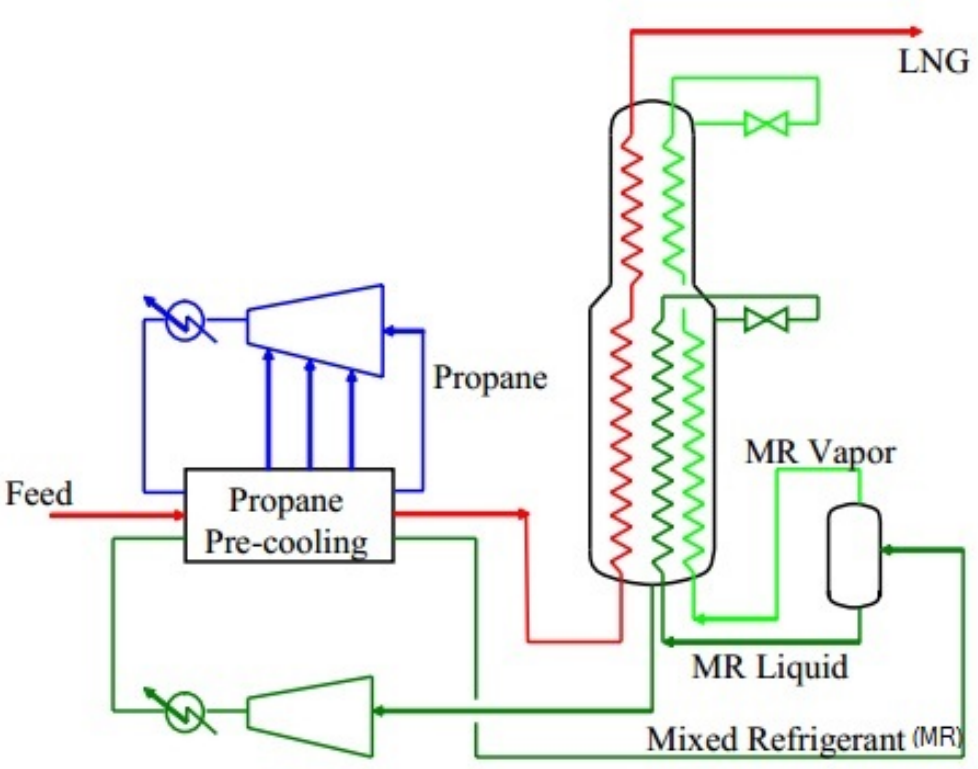

a)

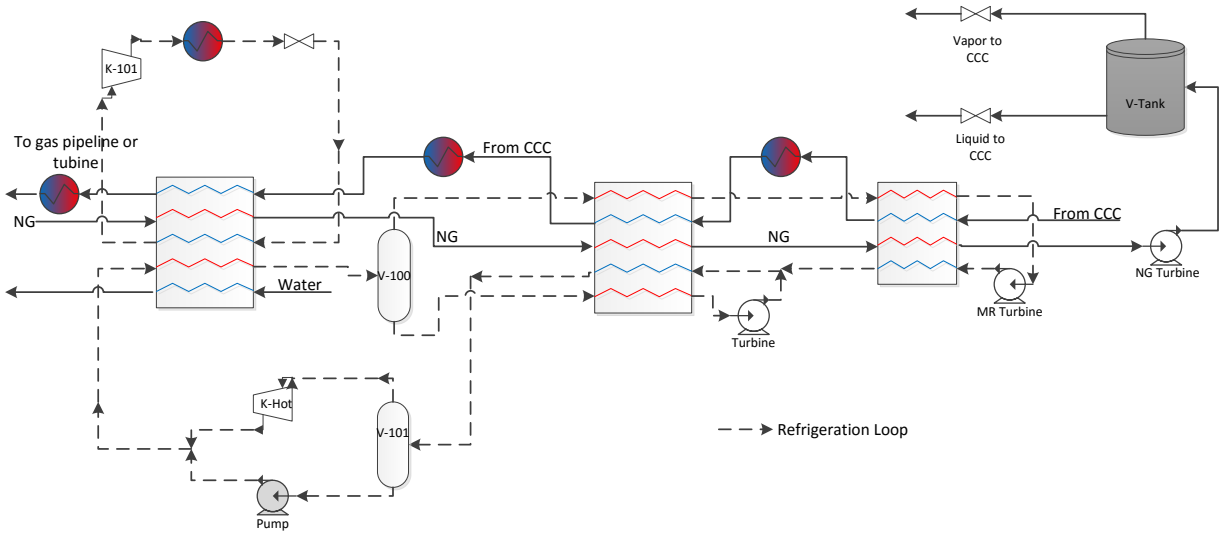

b)

Figure 2-3. a) Flow sheet of C3-MR model b) HYSYS simulation of C3-MR

Table 2-6 and Table 2-7 provide mixed refrigerant conditions and propane precooled conditions, respectively.

Table 2-6. a) Key parameters and b) mixed refrigerant composition for C3-MR

a)

	Entrance			Loop		
Conditions	**ER**	**B**	**ES**	**ER**	**B**	**ES**
Vapor / Phase Fraction	1	0.84	0.90	0.08	0.00	0.00
Temperature [°C]	30.07	11.02	14.98	-102.8	-94.54	-95.18
Pressure [kPa]	2561	2561	2561	995.7	1398	1326

b)

Component	Mole fraction
Methane	0.3330
Ethane	0.4340
Propane	0.2050
n-Butane	0.0224
n-Pentane	0.0056

Table 2-7. Propane-precooled conditions

	Entrance			Loop		
Conditions	**ER**	**B**	**ES**	**ER**	**B**	**ES**
Vapor / Phase Fraction	0.99	0.99	0.90	0.16	0.16	0.15
Temperature [°C]	-3.18	-2.10	-0.19	-2.81	-1.74	0.15
Pressure [kPa]	429.14	443.85	470.71	434.14	448.85	475.71

2.2. Phase equilibrium equations

Phase equilibrium provides the quantitative basis for much of the process simulation. The Peng-Robinson equation is used in this investigation and is a cubic equation of state:

$$P = \frac{RT}{v-b} - \frac{a}{v(v+b)+b(v-b)}$$

Where, for a binary system,

$$a = \sum_i \sum_j z_i z_j (a_i a_j)^{\frac{1}{2}} (1 - k_{ij})$$

$$b = \sum$$

$$b = \sum z_i b_j$$

The PR equation can also be expressed in the form of a compressibility factor, in which form its classification as a cubic equation of state is more evident (cubic in compressibility):

$$Z^3 - (1 - B)Z^2 + (A - 3B^2 - 2B)Z - (AB - B^2 - B^3) = 0$$

Where

$$Z = \frac{PV}{RT}$$

$$A = \frac{aP}{(RT)^2}$$

$$B = \frac{bP}{RT}$$

2.3. Process optimization

The C3-MR, MDMR, and a version of the SMR system called SMR 2 models developed in Aspen HYSYS provided energy requirements, cost and exergy utilization rate, and the three factors were taken as figures of merit for natural gas liquefaction. This investigation minimized energy input requirements by changing mixed refrigerant composition, pressure, temperature, and flow rate, subject to several constraints and compared the exergy and cost of these optimized processes. The work done per unit of LNG production formed the objective function:

$$f(X) = \min\left(\frac{W_{net}}{q_{LNG}}\right)$$

Where

$$W_{net} = \sum W_{compressor} - \sum W_{expanders}$$

and q_{LNG} represents the mass flow of the produced LNG. The constraints for this optimization include:

1) A minimum internal temperature approach (MITA) ≥1 °C
2) No condensates in compressors (100% vapor flow)
3) A single liquid phase in turbines and pumps (100% liquid flow)
4) The sum of mixed refrigerant mole/mass fraction is 1

The optimization indicates that a SMR process generally produces the best results. The version of SMR being used in the steady-state process analyses using Aspen Plus is called SMR 1 and was developed by previous investigators [49]. This investigation re-optimized the SMR process using Aspen HYSYS and Visual Basic, producing a slightly altered alternative optimized process called SMR 2. The optimization indicates that SMR 2 consumes marginally less energy in energy storage and balanced modes and more energy in energy recovery mode (Figure 10), with the overall energy consumption slightly higher in a typical cycle. The SMR 1 conditions and refrigerant compositions are in Table 2-8 while the SMR 2 compositions and conditions were presented earlier in Table 2-3. The two different simulators and optimization approaches produced very similar optimized conditions. The remainder of this investigation uses SMR 1 conditions in Aspen HYSYS.

Table 2-8. a) Key parameters b) mixed refrigerant composition for SMR 1

a)

	Entrance			Loop		
Conditions	**ER**	**B**	**ES**	**ER**	**B**	**ES**
Vapor / Phase Fraction	0.00	0.00	0.00	0.06	0.08	0.09
Temperature [°C]	22.13	21	16.15	-96.04	-93.19	-92.99
Pressure [kPa]	4500	4500	4500	108	108	108

b)

Component	**Mole fraction**
Methane	0.0423
Ethane	0.8451
Propane	0.0000
n-Butane	0.02813
n-Pentane	0.08447

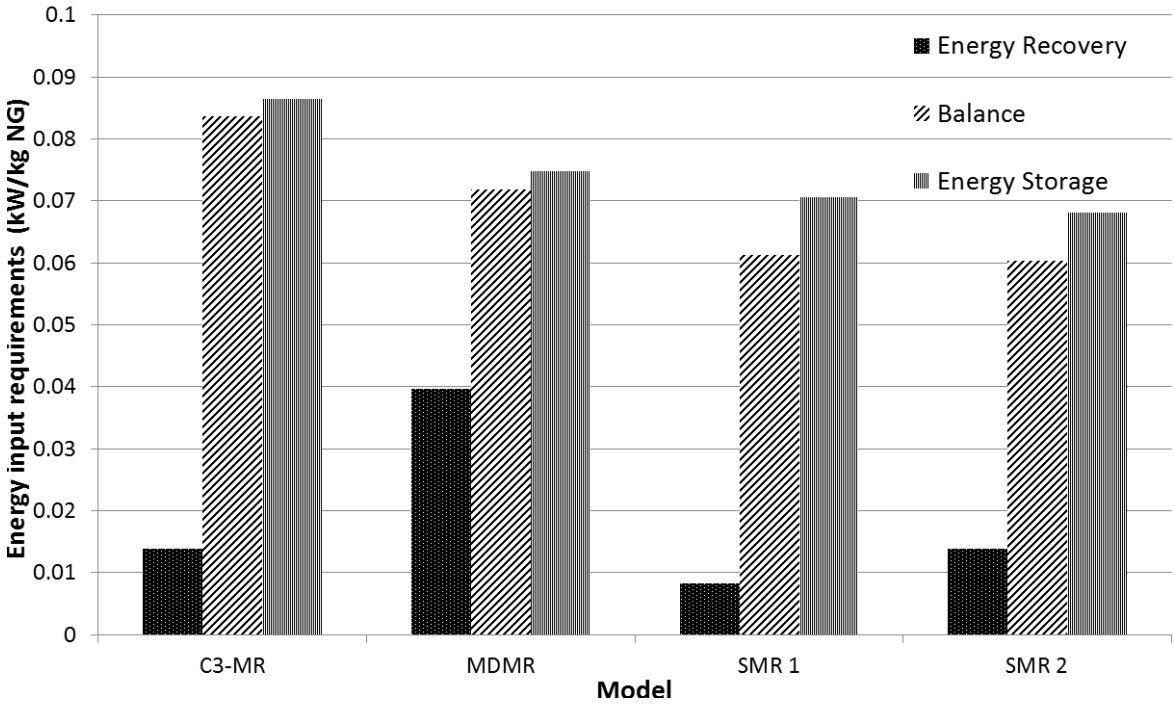

Figure 2-4. Energy input requirements for four models

This investigation also showed that the C3-MR is the worst process for energy input requirements in both Balanced and ES cases and the MDMR process performs slightly worse in energy storage and balanced modes and significantly worse in energy recovery mode compared to either of the SMR cases.

Additional figures of merit beyond energy efficiency for these processes include exergy loss, heat exchanger efficiency, and both capital and operating costs. Each of these is discussed in the sections below.

2.4. Exergy theory and Exergy analysis of equipment

Exergy is closely related to availability and efficiency and measures the irreversible losses in a process, typically in the form of lost capacity to do work. For a system operating at the same

temperature as the heat rejection temperature, exergy and Gibbs energy are identical. If the system is operating at other temperatures, the definition of exergy is very similar to Gibbs energy, namely

$$E(T,P) = (H_1(T) - H_0(T)) - T_0(S_1(T,P) - S_0(T,P))$$

Where H_0 and S_0 are the enthalpy and entropy at the standard state, normally considered as the ambient temperature and pressure. This represents the maximum amount of useful work that can be produced (or the minimum work that needs to be supplied) as a system changes from its current state to an equilibrium state. The exergy consumed by each component in a process quantifies its inefficiency. This exergy analysis provides one of the quantitative measures of system performance at both steady and transient conditions. The equipment, including the heat exchanger, compressor, expander, water cooler, pumps and valves, causes irreversibility of the process leading to exergy losses.

Li et al. [50] have introduced the exergy loss equations for the equipment, as is shown in Table 2-9, where ΔE_x represents the exergy losses of the equipment, E_{in} is the inlet exergy of the equipment, E_{out} the outlet exergy of the equipment, T_0 the ambient temperature, S_{in} the inlet entropy of the equipment, S_{out} the outlet entropy of the equipment, H_{in} the inlet enthalpy of the equipment, H_{out} the outlet enthalpy of the equipment, W_c the power consumption of the compressor, W_e the work of the expander, Q the exchanged heat flow of the water cooler, ΔT the water temperature difference of the cooler, Tw_{in} the temperature of water into the water cooler, Tw_{out} the temperature of water out of the water cooler.

Table 2-9. Exergy change expressions for differing types of equipment

Equipment	Exergy loss equation
Compressor	$\Delta E_x = E_{in} - E_{out} + W_c$
Expander	$\Delta E_x = E_{in} - E_{out} - W_c$
LNG heat exchanger	$\Delta E_x = \sum E_{in} - \sum E_{out}$
Water cooler	$\Delta E_x = E_{in} - E_{out}$
Valve	$\Delta E_x = T_0(S_{out} - S_{in})$

Table 2-10 summarizes the exergy changes associated with these processes. In a normal liquefaction process, the exergy losses of the water cooler are large because the outlet temperature of the compressor is high; therefore, the exchangers destroy large amounts of exergy when the gas cools to a low temperature.

Table 2-10. The exergy analytical results as a percent of total exergy loss for major equipment

	C3-MR			MDMR			SMR 1			SMR 2		
	ER	**B**	**ES**	**ER**	**B**	**ES**	**ER**	**B**	**ES**	**ER**	**B**	**ES**
LNG	24.91	9.26	5.85	5.25	0.72	0.51	12.67	0.91	1.74	9.32	1.00	1.62
Valves	5.25	0.40	0.35	0.01	0.01	0.00	0.04	0.01	0.01	0.03	0.01	0.01
Compressors	41.02	29.64	27.44	24.58	24.05	20.28	14.66	17.49	17.26	15.56	16.84	16.57
Water Coolers	15.92	58.20	64.34	66.35	68.76	72.78	66.61	79.75	79.50	69.91	80.37	80.32
Turbines	12.87	2.40	1.96	0.47	1.06	0.95	6.01	1.83	1.47	5.16	1.76	1.48
Pumps	0.04	0.12	0.08	0.00	0.01	0.01	0.03	0.03	0.03	0.02	0.03	0.02
Expanders	0.00	0.00	0.00	3.35	5.40	5.49	0.00	0.00	0.00	0.00	0.00	0.00

For C3-MR, the compression ratios for compressors are the highest (2.6) and contribute to highest exergy losses. The compressors contribute small exergy losses [42, 51] in all four processes because compression ratios are generally small. These losses can be further decreased by high efficiency, multi-stage, intercooled compression. The valves contribute less than 0.1% to the total exergy loss for SMR 1, MDMR and SMR 2. For C3-MR they contribute almost 5.5% of the total exergy losses. Pump and expander exergy losses are negligible for all four models and three cases. Turbine exergy losses for all models except C3-MR are less than 6 percent.

All four models produced exergy losses in the heat exchangers well below those reported in the literature [35, 42, 51]. This is in part because this process involves refrigerant return streams that do not exist in traditional processes and in part because of careful attention to heat exchanger design. The temperature profiles discussed later illustrate the effectiveness of the heat exchanger design.

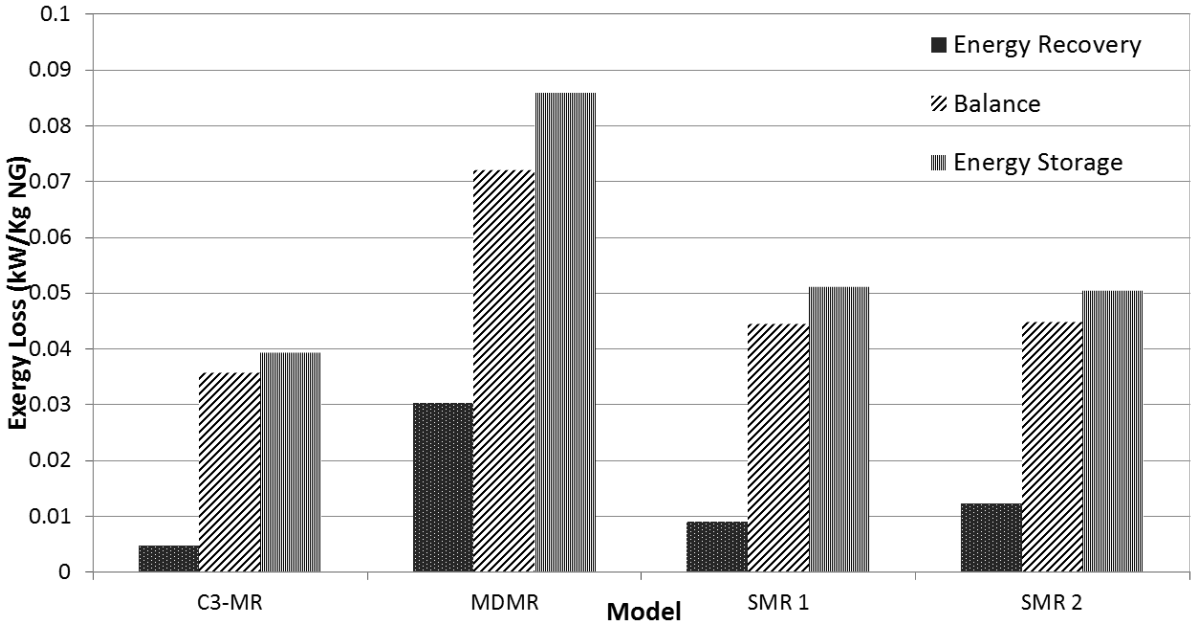

Figure 2-5. Exergy loss comparison for four models

Figure 2-5 illustrates the overall exergy loss for all four models. The MDMR model has the highest exergy loss for all three cases, consistent with its highest energy input requirements. In all cases, exergy loss is greatest during energy storage, consistent with the higher total energy demand, and lowest – approaching zero – during energy recovery, again consistent with a very low energy demand.

2.5. Heat exchanger efficiency

The technical literature does not unambiguously define a heat exchanger efficiency and sometimes confused efficiency with effectiveness. This document suggests a useful efficiency definition. Insulated heat exchangers conserve enthalpy, so a first-law definition is problematic. That is, the enthalpy flowing out of the system equals that flowing in. Heat exchangers do not involve shaft work, so a second-law definition (work over heat) does not naturally come to mind. Nevertheless, this document proposes a second-law definition for heat exchanger efficiency that is both useful and simple [48, 52, 53].

Conceptually, this efficiency describes the consequence of heat exchange on the flow streams' (a) ability to do work (availability or exergy) or, equivalently, (b) entropy. Quantitatively, the heat exchanger efficiency is one minus the difference in exergy between the streams exiting and entering a heat exchanger normalized by the largest achievable difference in such exergy. The largest achievable difference with respect to heat exchange occurs if all the streams come to the same temperature, or thermal equilibrium. Significantly, the definition does not involve total equilibrium (vapor-liquid and composition) among streams, just thermal equilibrium. These analyses and this definition assume no heat transfer between the exchanger and its surroundings.

Therefore, the difference in exergy is proportional to a difference in entropy, with the ambient temperature as a proportionality constant.

$$\eta = 1 - \frac{\sum_{outlet} m_i \hat{b}_i - \sum_{inlet} m_i \hat{b}_i}{\sum_{eq} m_i \hat{b}_i - \sum_{inlet} m_i \hat{b}_i} = 1 - \frac{\Delta_{obs} m_i \hat{s}_i}{\Delta_{eq} m_i \hat{s}_i} = \frac{\sum_{eq} m_i \hat{s}_i - \sum_{outlet} m_i \hat{s}_i}{\sum_{eq} m_i \hat{s}_i - \sum_{inlet} m_i \hat{s}_i}$$

Where $\hat{b}_i = \hat{h}_i - T_0 \hat{s}_i$ represents the specific exergy of stream i and $\Delta_{eq} m_i \hat{s}_i$ is the difference between the entropy in all the streams at equilibrium temperature and entropy of the streams at the inlet temperature. The temperature T_0 represents the temperature of the ambient environment and, since it drops out of the equation, is irrelevant to the exchanger efficiency. This ambient temperature should not affect a well-posited efficiency definition for reasons discussed below. The middle form of the equation results from the sum of the inlet enthalpy flows equaling the sum of the outlet enthalpy flows.

This investigation makes frequent reference to this efficiency in the context of functioning processes. Nonfunctioning processes can lead to results that illustrate a distinction between efficiency and effectiveness. The efficiency by this definition would be unity in the extreme case of a completely dysfunctional exchanger that transfers no heat among streams. However, the effectiveness would in this case would be zero.

This efficiency becomes unity if the total exergy of the outlet streams equals that of the inlet streams, which can only occur in the limit of the hot and cold streams transferring heat with no temperature difference at any given point along the exchanger (ideal heat exchanger). The efficiency is zero if all outlet streams approach the same temperature, which represents the poorest possible heat exchanger performance from an efficiency or entropy standpoint. An efficiency of

50% indicates that heat exchanger generates half of much entropy it would generate if all streams come to the same temperature.

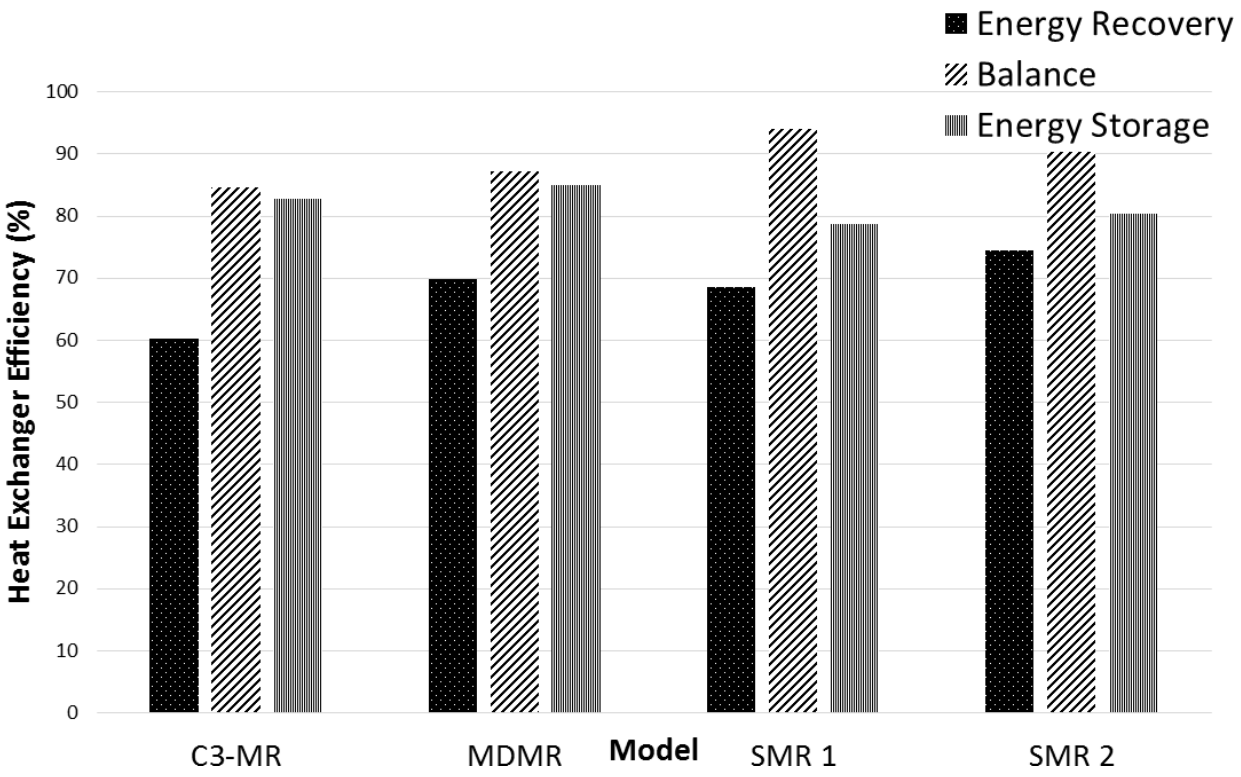

Figure 2-6. Heat exchangers efficiencies for four models

Figure 2-6 summarizes the heat exchanger efficiencies for all four models. SMR 1 and SMR 2 have the highest efficiencies. For the balanced case, SMR 1 is better but for energy storage and energy recovery cases, SMR 2 is better.

There are three heat exchangers involved in the C3-MR process (the third one is the main heat exchanger summarized in the graph) and their efficiencies are as follows:

Table 2-11. C3-MR heat exchangers efficiencies

Heat exchanger	Efficiency (%)		
	Energy Recovery	Balanced	Energy Storage
1st heat exchanger	77.28%	13.27%	96.65%
2nd heat exchanger	20.58%	35.21%	42.14%

2.6. Heat exchange load and temperature distribution

The main energy loss of a natural gas liquefaction process occurs in compressors and heat exchangers. The comparison of heating and cooling curves in MDMR, C3-MR, SMR 1, and SMR 2 illustrate the temperature and heat transfer profiles for the exchangers. Individual heating and cooling curves for ER, ES, and Balanced (Figure 2-7) indicate where the major inefficiencies for each exchanger occur as the distance between the cold and hot stream temperature at each point. This type of pinch analysis is common in heat exchanger design [54] and is adopted in the LNG heat exchangers discussed here.

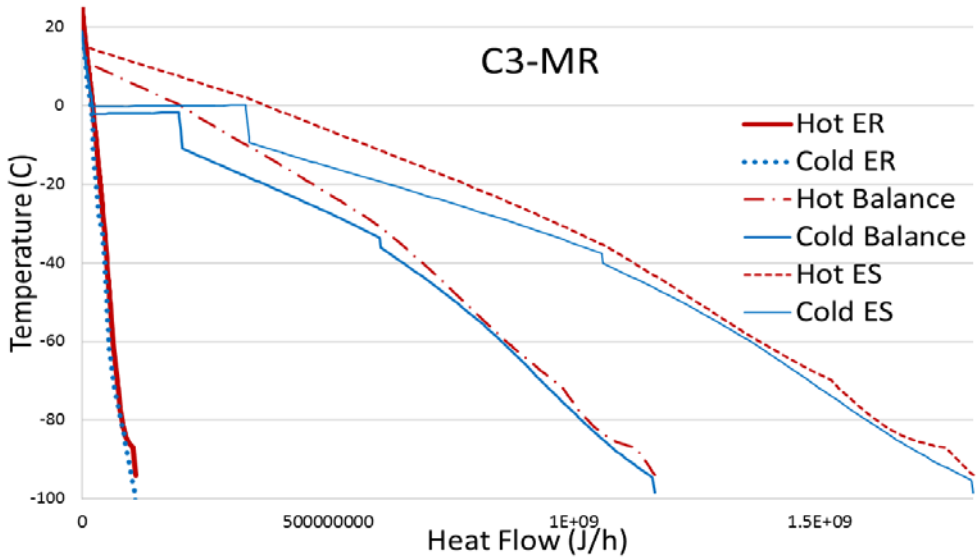

a)

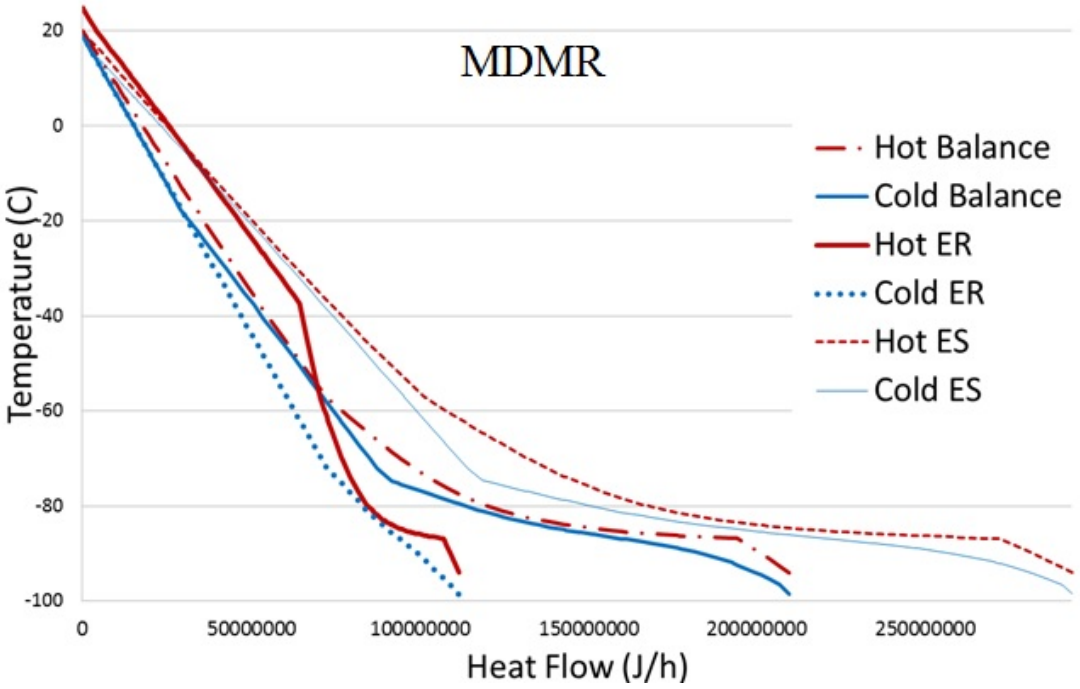

b)

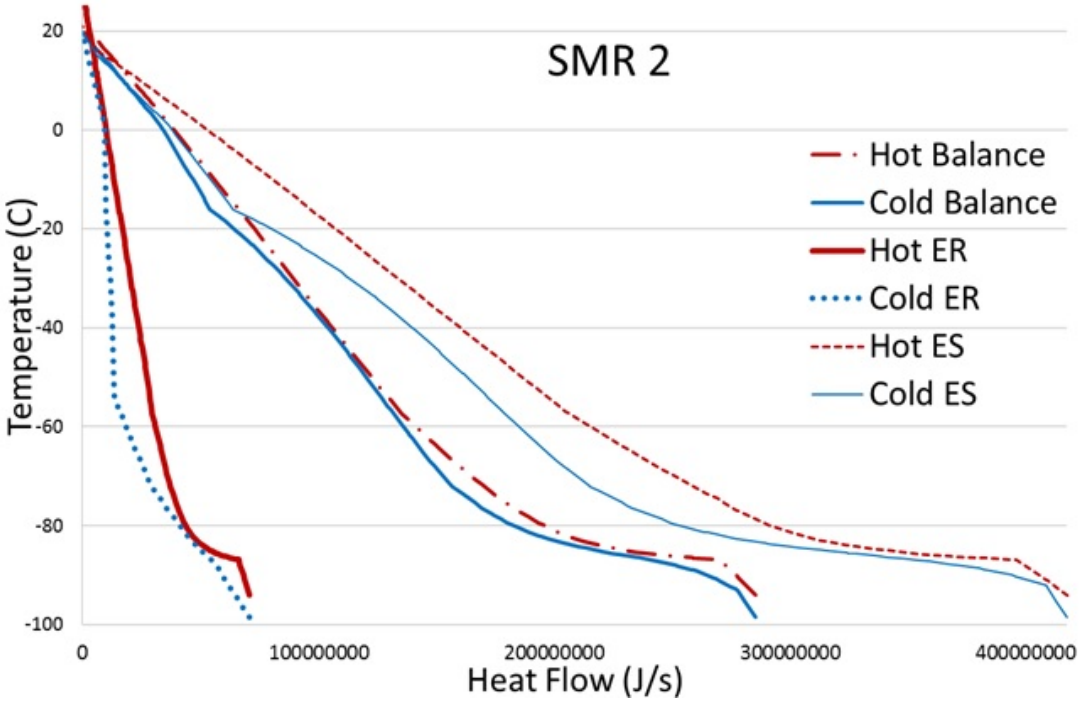

c)

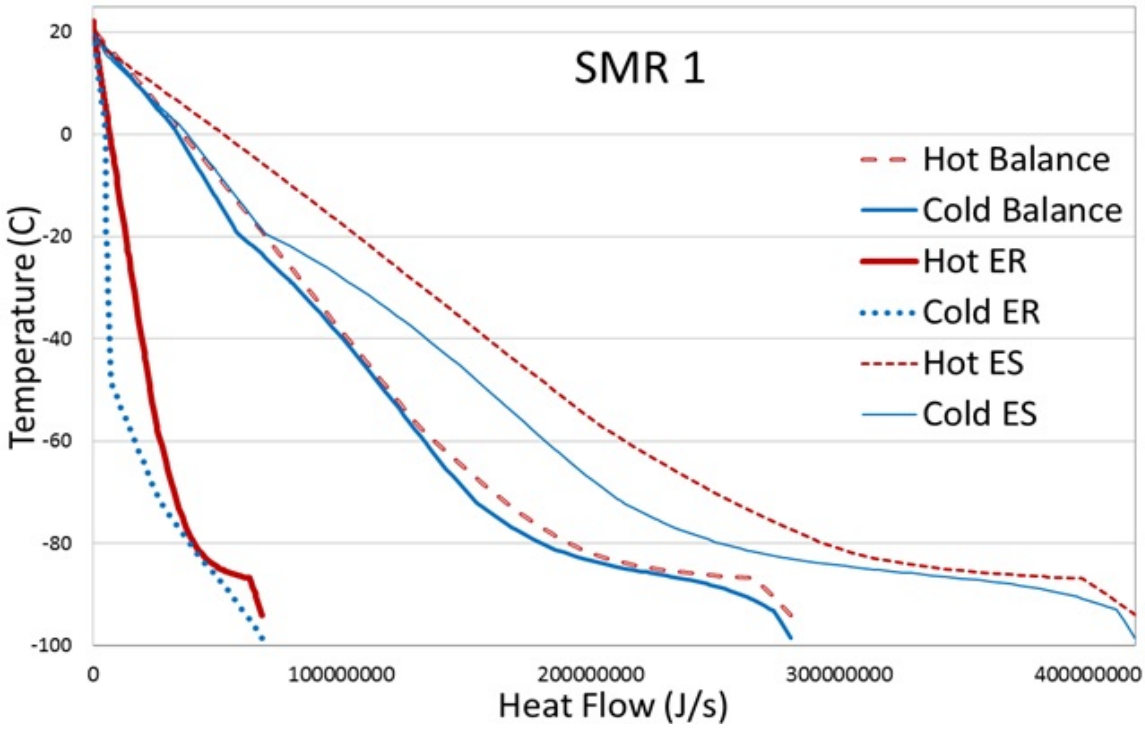

d)

Figure 2-7. Temperature profiles for a) C3-MR; b) MDMR; c) SMR 2 and d) SMR 1, each operating at the three process conditions

The temperature difference and heat exchange load in heat transfer contribute to the exergy loss, so large temperature difference and heat exchange load primarily contribute to exergy loss in heat exchangers. If the hot composite curve matches the cold curve well, the resulting exergy loss is small. The MDMR model has the lowest temperature difference hence it has the lowest heat exchanger exergy loss. The results for exergy loss and heat exchanger efficiency agree with the temperature profiles.

2.7. Costing

Capital and operating costs represent the final figure of merit investigated here. Capital and operating costs of all systems depend as much or more on market demands and raw materials costs as on equipment size and type. These market-based fluctuations cannot be accurately anticipated.

The approach used here relies on a consistent method to predict costs and to compare them across designs, with full recognition that actual costs may vary substantially based on unforeseen market shifts. The largest equipment size required by any one operating regime determines equipment costs. The largest size generally corresponds to energy storage. Heat exchangers, compressors and expanders are the most expensive units. Since HYSYS does not include a multi-stage compressor, several single-stage compressors with inter-stage cooling appear in the Aspen HYSYS process flow diagram. The costs, however, are based on a system modeled in Aspen Plus (which does have multi-stage compressors). A single-stage compressor with high pressure ratio is both costlier and less efficient. Total capital costs for C3-MR are the lowest (Figure 2-8) due to lower-pressure-ratio compressors. The SMR 1, SMR 2 and MDMR processes divide compression into a series of single-stage compressors. Operating costs in terms of electricity and water costs follow (Figure 2-9 and Figure 2-10).

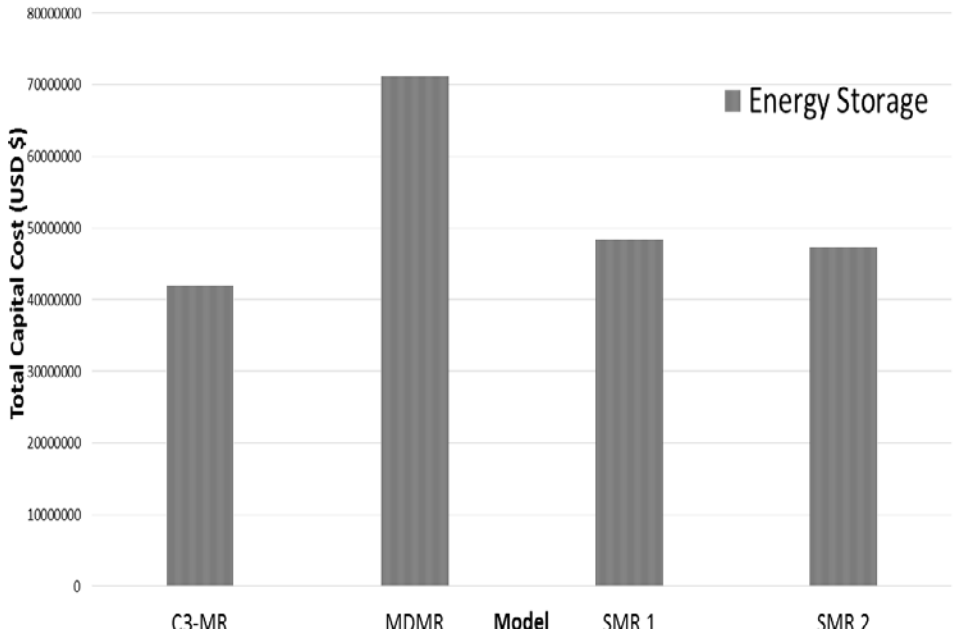

Figure 2-8. Total capital cost for four models

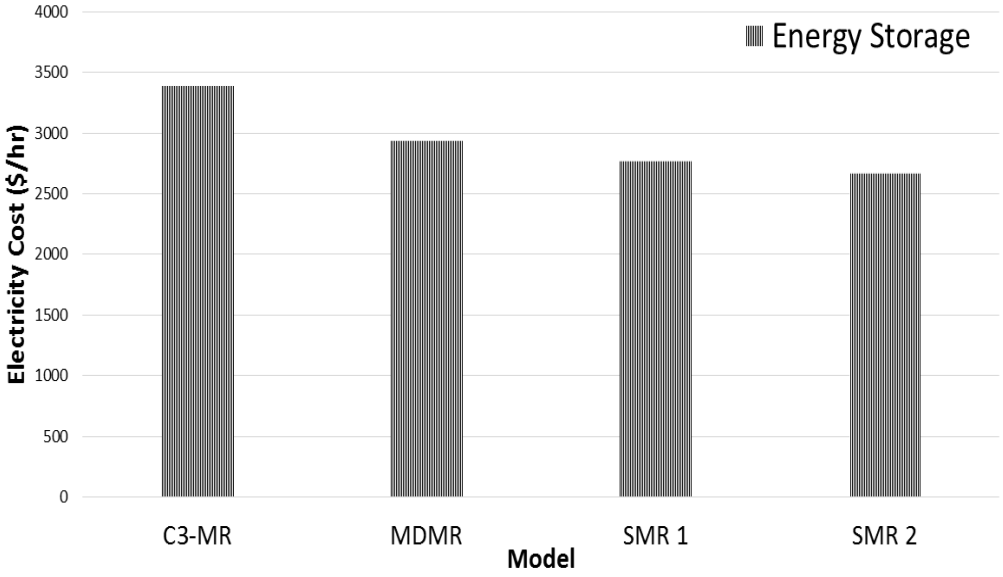

Figure 2-9. Electricity cost for each model

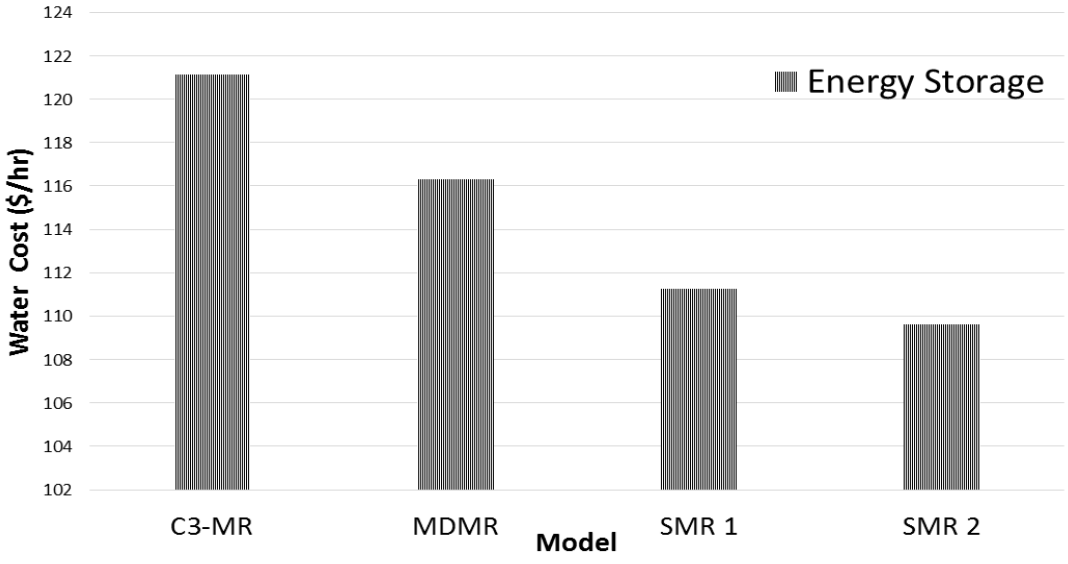

Figure 2-10. Water cost for each model

Chapter 3. Dynamic modeling and transient responses

This investigation applies the results of the previous investigation to analyze a system that has aspects in common with traditional LNG and Air Separation Unit processes. However, the transient analysis developed here has very little precedent in the literature. It is crucial to reduce entropy generation due to the temperature difference between the feed natural gas and return refrigerant flows in the LNG heat exchangers. Large temperature differences and heat exchange load are the primary reasons of exergy loss in heat exchangers. Additionally, the LNG process here uses staged compression with intercooling [47, 48].

In this investigation, Aspen HYSYS Dynamics develops the transient modeling of LNG production for the best model from the previous section (SMR model). The controllers regulate temperatures, pressures and other operating conditions. K-value and U value techniques provide control mechanisms for heat exchangers as described shortly. Mixed refrigerant and natural gas flowrates vary with time. Process and heat exchanger efficiency graphs summarize temporal process responses to changing flows.

3.1. Process design

The simulation flow sheet of the SMR process (Figure 3-1) uses an eight-stage compressor with inter-stage cooling. Phase separators separate the mixed refrigerant into gas and liquid phases in each cooler. Pumps compress the liquid after the phase separator.

Table 2-8 summarizes the optimized mixed refrigerant composition and key parameters, where ER, B and ES represent energy storing, balanced, and energy recovery, respectively. (Refer to Section 2.1.1 for a more complete description).

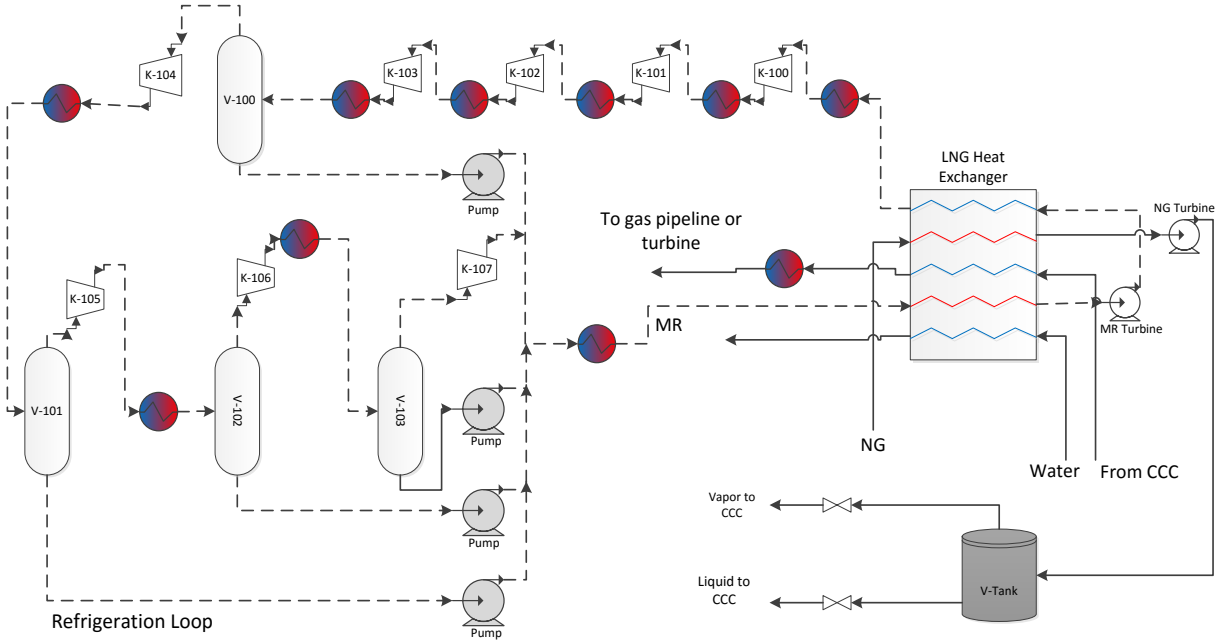

Figure 3-1. HYSYS simulation of SMR

3.2. Transient modeling

3.2.1. Dynamic heat exchanger modeling

Developing a dynamic model of the heat exchanger represents arguably the most critical aspect of this dissertation. Dynamic plant simulation requires accurate equipment sizing, proper pressure or flow rate specifications as boundary conditions and specifying resistance of unit operations. Geometry information is important since transient behaviors are influenced by volume of equipment. Rating of a multi-stream brazed plate heat exchanger includes:

a) Length and width of the exchanger

b) Layer configuration

c) Zone configuration

d) Heat transfer configuration.

3.2.1.1. Length and width of the exchanger

The total surface area calculations result from the number of zones, the surface area for each zone and layer can be calculated.

3.2.1.2. Layer configurations

The configuration of heat exchanger streams affects the total heat load distribution. The optimal configuration used here alternates cold and hot layers in a countercurrent flow pattern.

3.2.1.3. Zone configuration

In a pressure-flow dynamic model, the heat exchanger determines flowrates using resistance equations. Each zone features a stacking pattern with one feed and one product connected to each representative layer in the pattern. The resistance equation modeled after the turbulent flow equation is:

$$F = k\sqrt{\rho\,\Delta\,P}$$

Where

k = pressure flow coefficient, $\frac{kg}{h}\times\sqrt{\frac{\frac{kg}{m^3}}{kPa}}$

ρ = density of fluid, $\frac{kg}{m^3}$

ΔP = total pressure drop, kPa

The resistance equation calculates flowrates from the pressure differences of the surrounding nodes using pre-specified k-values.

Dynamic heat exchangers require k-values. However, temperature and pressure drops for each zone are not known a priori; thus, exact k-values cannot be specified. Specified temperature and pressure drops on the dynamic tab, in Aspen HYSYS, allow the process to calculate K's. K-value set up is one of the most important steps for heat exchangers' design in dynamic mode and errors in this step might lead to pressure and temperature imbalances and even reverse flows during the transient estimates.

3.2.1.4. Heat transfer configuration

Aspen HYSYS provides UA values for each stream; hence, surface area determines U for each layer. Aspen Economic Analysis sizes and costs the equipment, including heat exchangers' surface area (A). Equal UA-values remain constant for a layer in each zone. Steady state UA values provide initial estimates.

3.3. Process optimization

This optimization is a non-automated version of the genetic algorithm. Several variables appear in the optimization objective function for the mixed refrigerant stream including pressure, composition, and flow rate along with the pressure exiting the expansion turbine. The algorithm changes multiple parameters including pressure, composition, and flow rate of the mixed refrigerant stream as well as the exit pressure of the turbine. The individual components of the mixed refrigerant stream, C1-C5 n- hydrocarbons, varied instead of composition and overall flow-rate. This reduces the number of optimization parameters to seven. All of these parameters vary

continuously and there is no reason to expect that any of them generate discontinuities in either the objective function or its partial derivatives. Each variable had three to five values specified, including mid-, low-, and high-values. The decision to include additional higher and/or lower values depends on the previous set of variables. Aspen's sensitivity analysis tool calculates the total power required by the cooling loop and the conditions that led to that result. A subset of the best solutions combines pairwise to form a set of new input test values through cross-over or recombination algorithms, which are generally linear combinations of the parameters of the parent solutions. Many algorithms also employ mutation searches in which one or more new parameters assumes values that differ from genetic or linear combinations of the previous solutions. No mutation searches appeared necessary in this problem. The process repeats until the optimal solution repeats several times with adjustments to input values. The specific algorithm tuning parameters (weighting of properties of the parents in creating new parameter sets, probabilities of parents being selected and paired, and conditions for defining optimum) affected the time required to find the optimum but did not lead to different optima. These optimal conditions appeared to be robust with respect to initial conditions and optimization tuning parameters and this investigation did not explore further details of varying parameters in this algorithm.

Genetic algorithms have advantages for objective functions that are discontinuous, non-differentiable, stochastic, or highly nonlinear or that have multiple local minima. The objective functions used here should be continuous, deterministic, and in principle differentiable. However, they can be highly nonlinear and may have multiple local minima.

The model assumed:

1) A minimum of 1 °C approach temperature was necessary in brazed plate heat exchangers,

2) Compressors operate at 92% isentropic efficiencies,
3) Inter- and after-coolers are capable of cooling the gases to 20 °C
4) No condensates formed in the compressors (100% vapor flow)
5) A single liquid phase forms in the turbines and pumps (100% liquid flow)
6) The sum of mixed refrigerant mole/mass fraction is 1
7) The expansion valves operate adiabatically

After applying the genetic algorithm approach, it appears that derivative-based approaches may have been as good or better as there were no clearly defined local minima and the nonlinearities could probably have been adequately addressed with other techniques. The optimized model yielded energy input requirements is illustrated by Table 3-1. As mentioned previously, these numbers are lower than and not directly comparable to industrial LNG operations because this process always has a return stream of cold, vaporized NG that helps with sensible cooling of the incoming stream whereas industrial LNG production has no similar returning stream.

Table 3-1. Optimized energy input requirements for each case

	ER	B	ES
Energy input requirements (kW/kg NG)	0.0083	0.0613	0.0706

3.4. Exergy results and efficiency

In a normal liquefaction process, the exergy losses of the water coolers are very large because the outlet temperature of the compressor is high; therefore, it loses large amounts of exergy

when the gas is cooled to a low temperature. Figures 3-2a, 3-2b and 3-2c particularly show the exergy losses for major equipment in three cases.

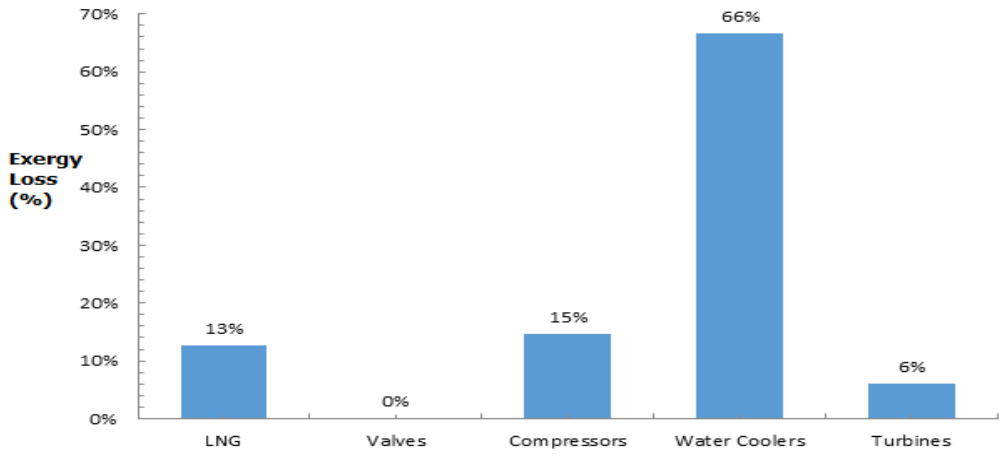

a)

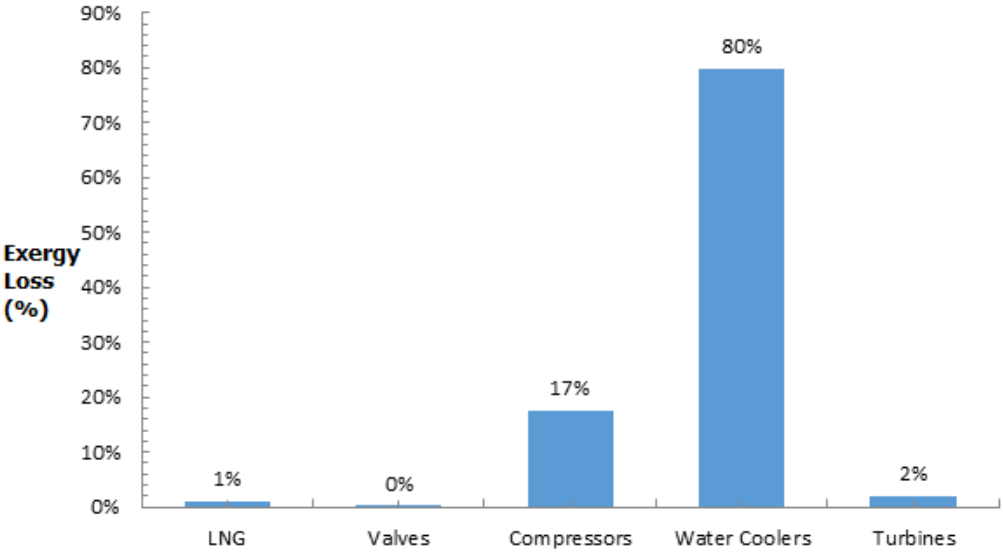

b)

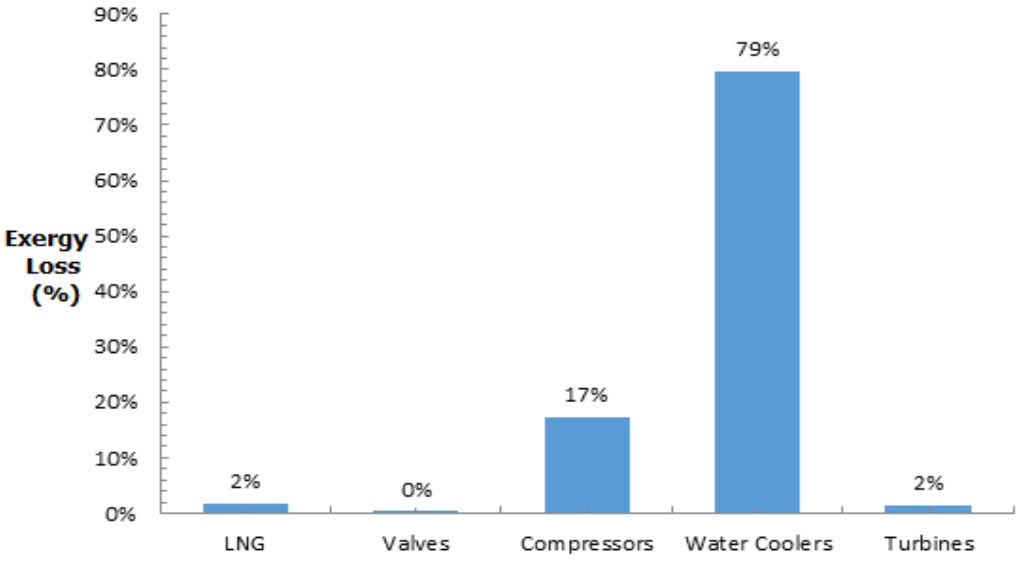

c)

Figure 3-2. Major equipment exergy losses in a) ER, b) B and c) ES

And the total exergy loss is given in Table 3-2:

Table 3-2. Total exergy loss for three cases

	ER	B	ES
Exergy loss (kW/kg NG)	0.0089	0.0444	0.0511

Heat exchanger efficiency is given in Table 3-3.

Table 3-3. Heat exchanger efficiency for each case

	ER (%)	B (%)	ES (%)
Heat exchanger efficiency	74.35	93.86	80.21

This investigation maintains transient heat exchanger efficiency high and stable, similar to steady-state values.

3.5. Transient modeling of natural gas liquefaction process

Figure 3-3 shows the process flow diagram for a natural gas liquefaction process using a mixed refrigerant.

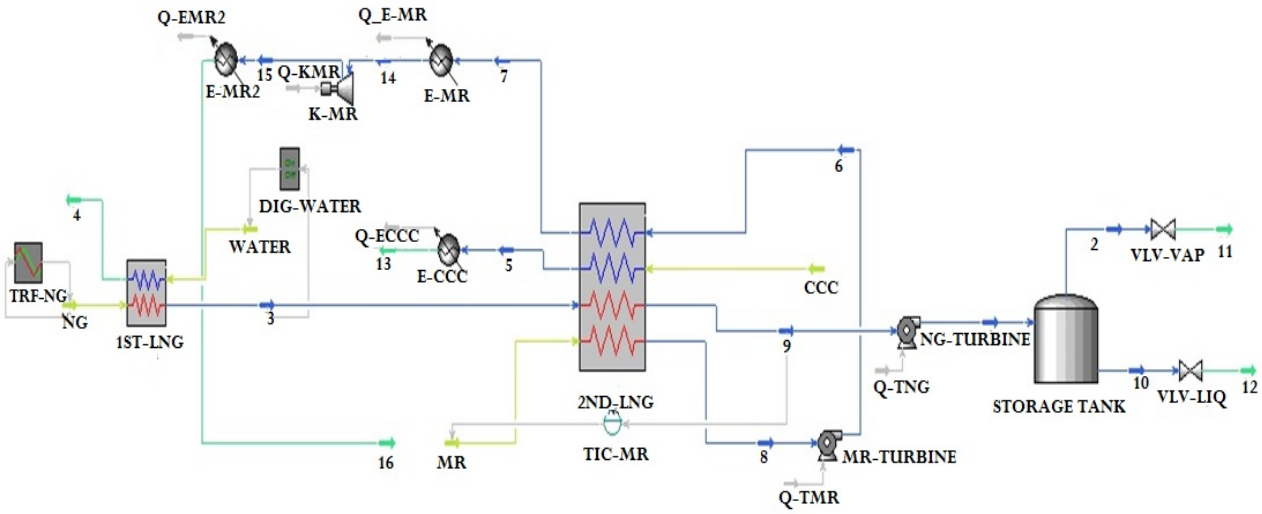

Figure 3-3. Transient modeling of SMR liquefaction process

Aspen HYSYS simulates dynamic modeling of this process, which required several modifications relative to the steady-state model. Some of the most important include:

1) Changing mixed refrigerant flow rates in Traditional Heat Exchanger Design (THED) control the output temperature using a PID controller.
2) Digital on/off controllers regulate cooling water flow rate. Specifically, when natural gas flow rate is below its average value, the water flow turns on and when the natural gas is above its average, water flow turns off.

3) Transfer functions have two important impacts in Aspen modeling. One is used to break the closed loop, which greatly increases the convergence speed. Transfer functions force the input of an open loop to equal the output, making an open loop function like a closed loop. Transfer functions also provide the values of the ramping flow rates in the simulation.

4) As shown in Figures 3-4a, 3-4b and 3-4c, in all three case PID controllers reaches the set point and satisfy the output temperature. The blue line illustrates how robust the simulation is. For example, for the first graph, results are 98.4% accurate. It takes 2-8 minutes for a PID to reach the set point in three cases. The set point temperature is -94 ºC before NG expansion.

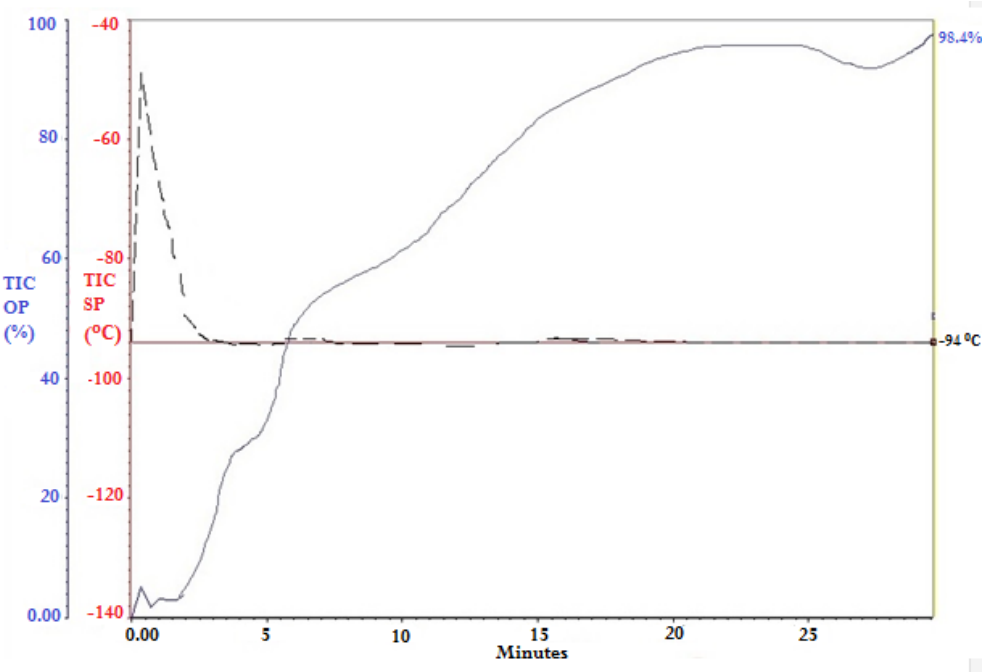

a)

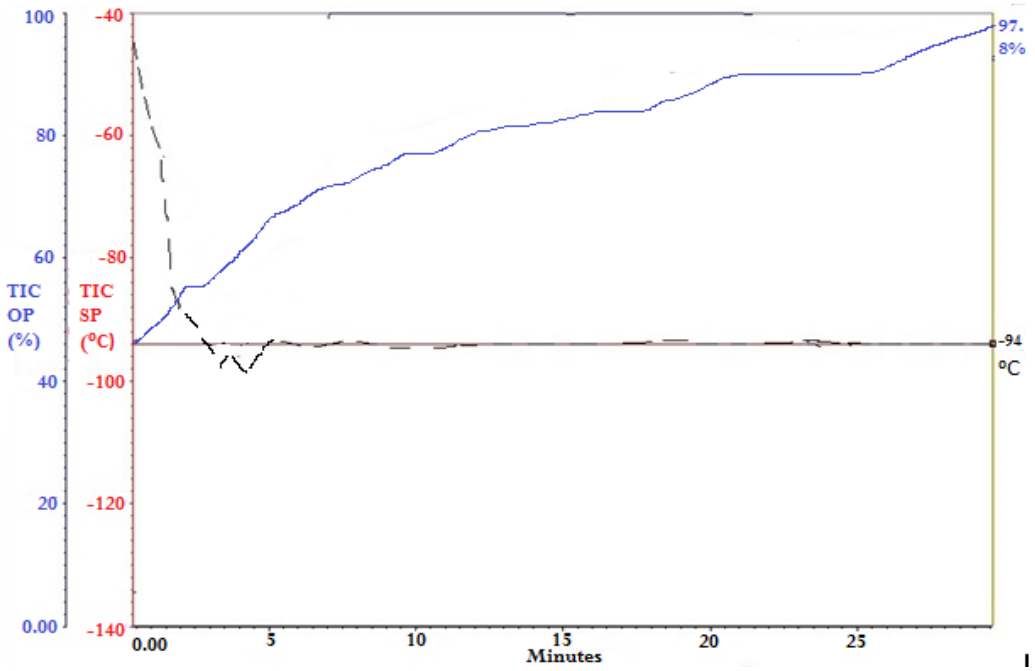

b)

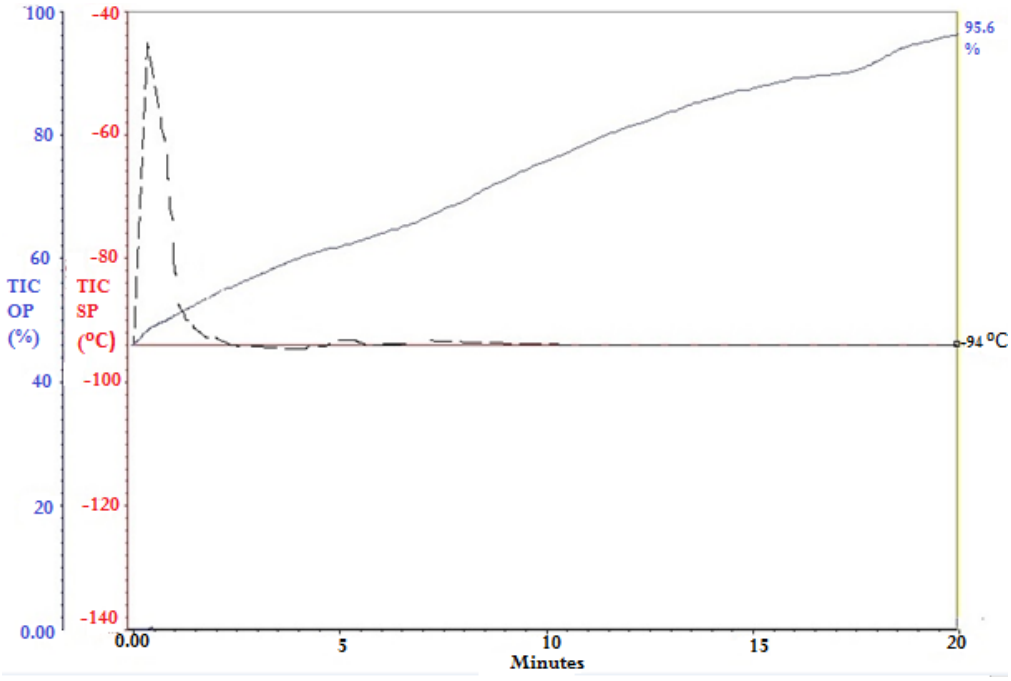

c)

Figure 3-4. PID controller in the a) B b) ES and c) ER cases, solid red line= set point °C; dashed black line= temperature °C

The output temperatures for LNG and MR and NG flowrates appear in Figure 3-5a and 3-5b. Changing the NG flowrate (decreasing or increasing) leads to changes in the MR flow rate to maintain a constant set point temperature.

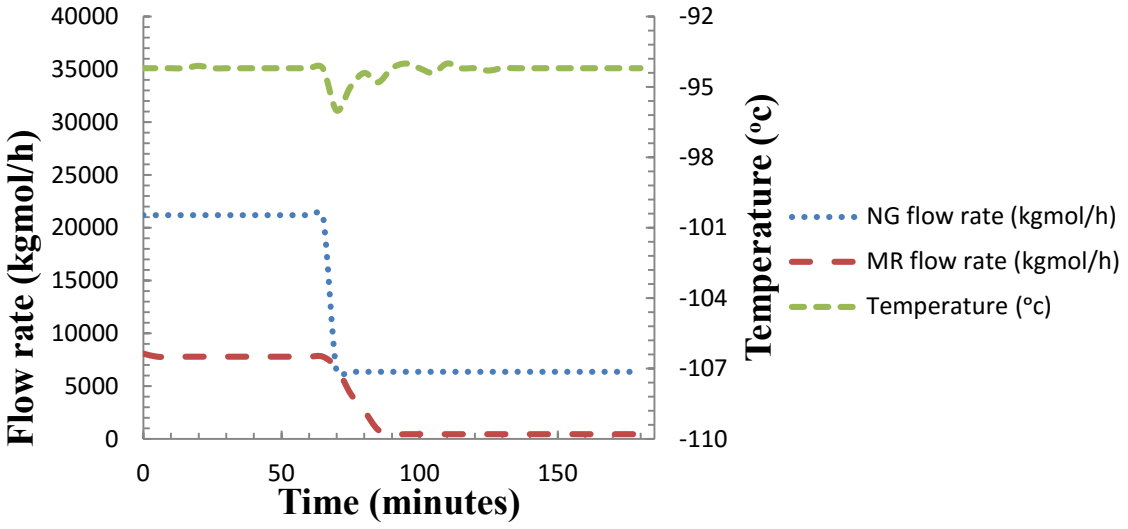

a)

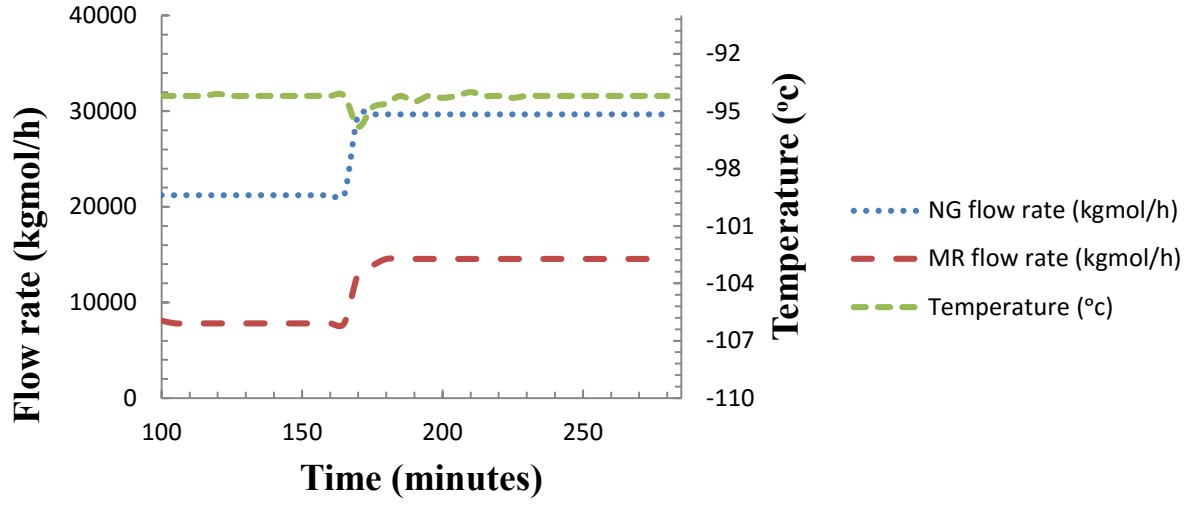

b)

Figure 3-5. Output LNG temperature and NG and MR flow rates in a) B-ER b) B- ES

The model explores responses to both step changes and ramping changes in flow rate. During a step change, the natural gas flow rate varies among three specific values, one each for energy storing, balanced, and energy recovery. This discussion focuses on four main transient responses during these changes, including total energy usage, NG turbine production, MR turbine production and NG flow rate (Figures 3-6a, 3-6b, 3-7a and 3-7b). These responses adequately provide the behavior required to balance changing power availability (Figure 1-6).

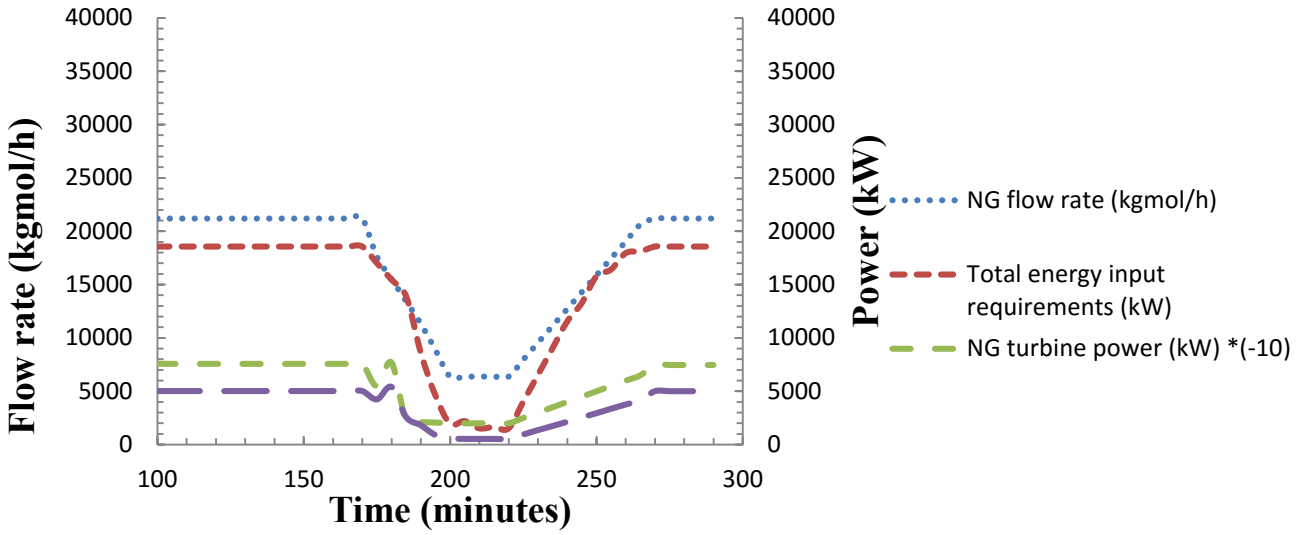

a)

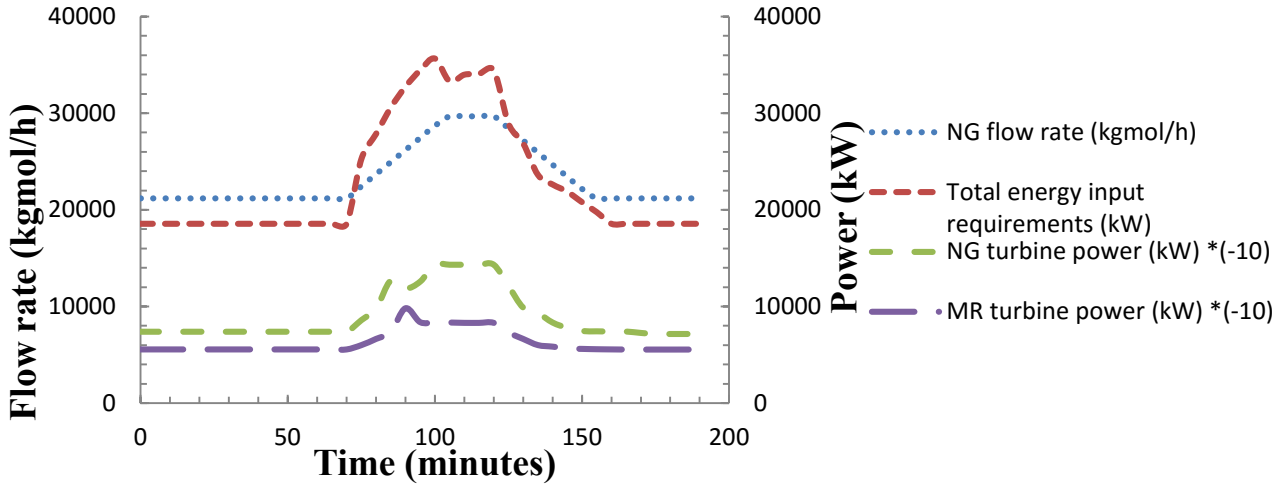

b)

Figure 3-6. Ramping a) B-ER-B and b) B-ES-B performances

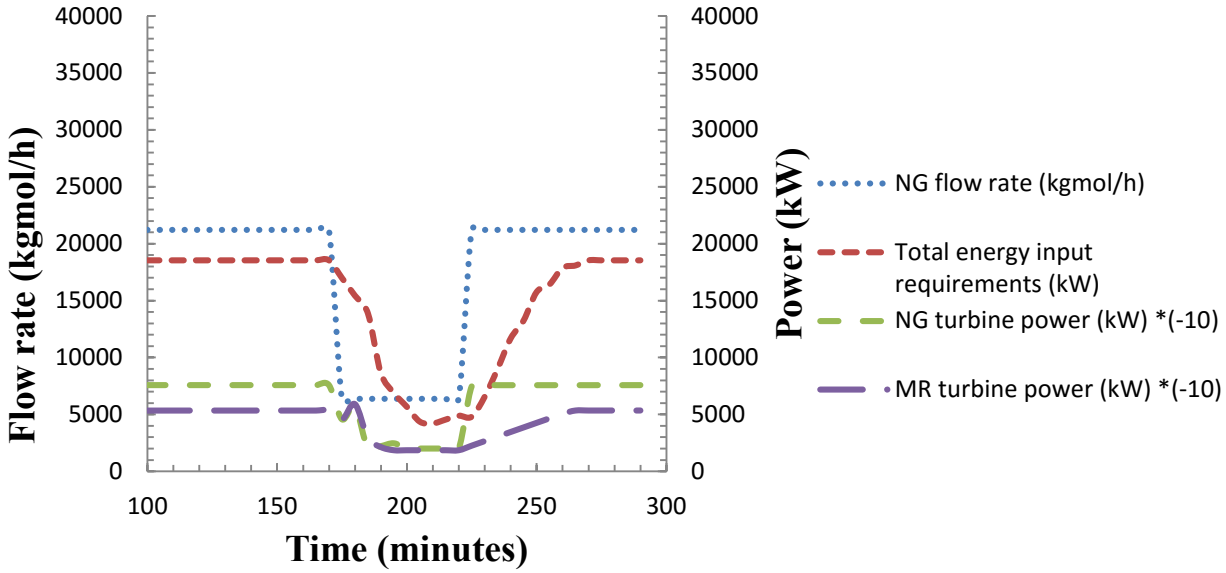

a)

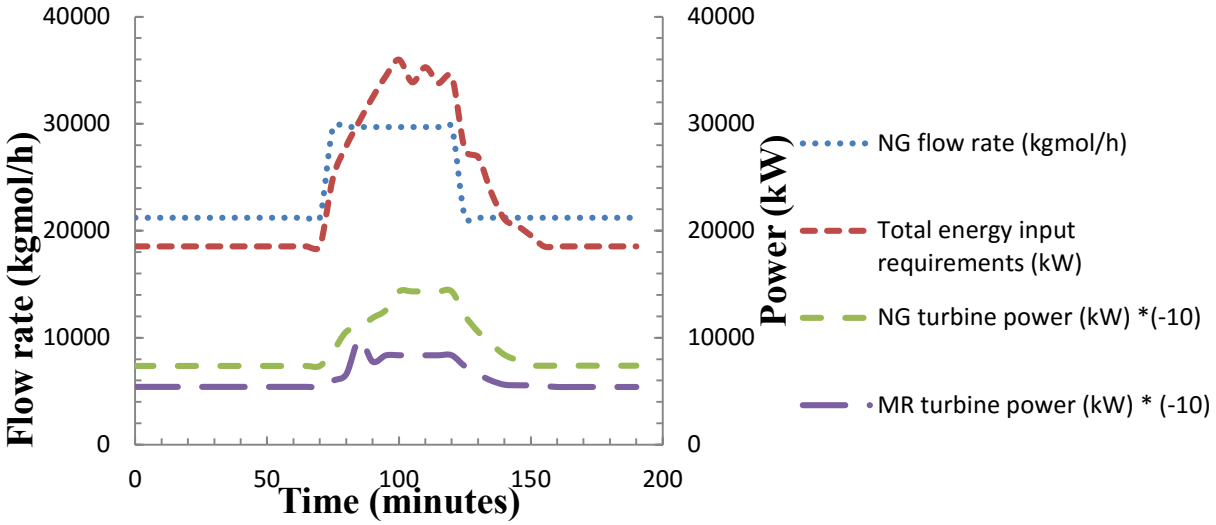

b)

Figure 3-7. Step changing a) B-ER-B and b) B-ES-B performance

These simulations show that the heat exchangers require about 30 minutes to equilibrate to new conditions after a step change in flow. As will be shown later, portions of the heat exchangers undergo temperature changes of 85 degrees. Industry practice generally limits the maximum rate of temperature change during a transient in cryogenic heat exchangers to 1 degree per minute to avoid damage from thermal stress. This constraint would extend the transient response time from about 30 to about 85 minutes. As illustrated in the rapid response discussion later, it requires even more time (up to 120 minutes) for the LNG production to equilibrate with the NG input during these transients. The potential for equipment damage and the significant impacts on productivity and quality during these transients represent two of the major reasons that traditional LNG production systems change conditions very slowly. However, the process investigated here must respond very rapidly to provide energy storage that is compatible with the sometimes rapid changes in grid demand. Total energy usage decreases as the NG flow decreases and vice versa. Energy production by the NG and MR turbines increases as NG flow decreases. The changes in

flow rate versus total energy consumption appear in Figures 3-8a, 3-8b, 3-9a and 3-9b. NG and total energy input requirements decrease and increase together because the process MR requirements scale approximately with NG flow rate, with some variation due to changes in process equipment temperature profiles.

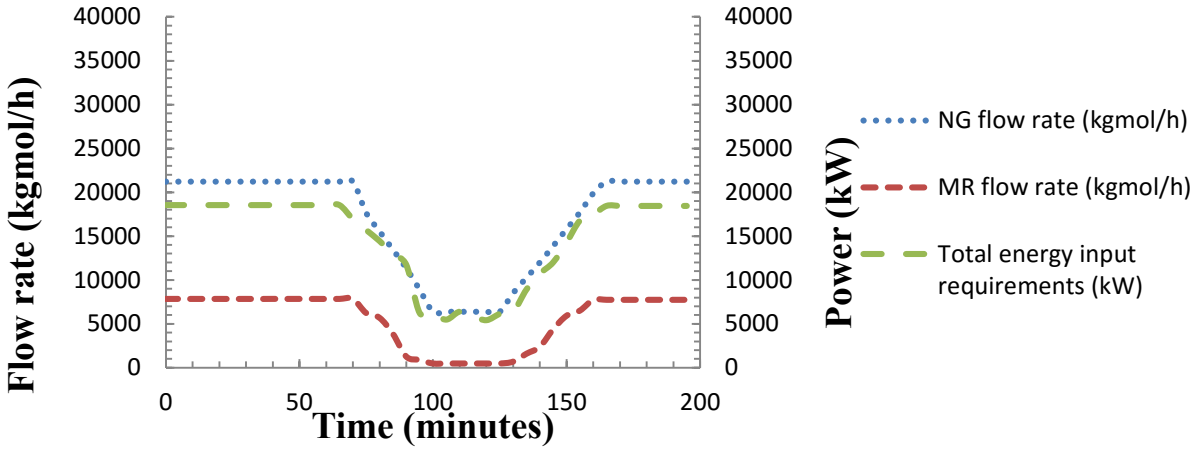

a)

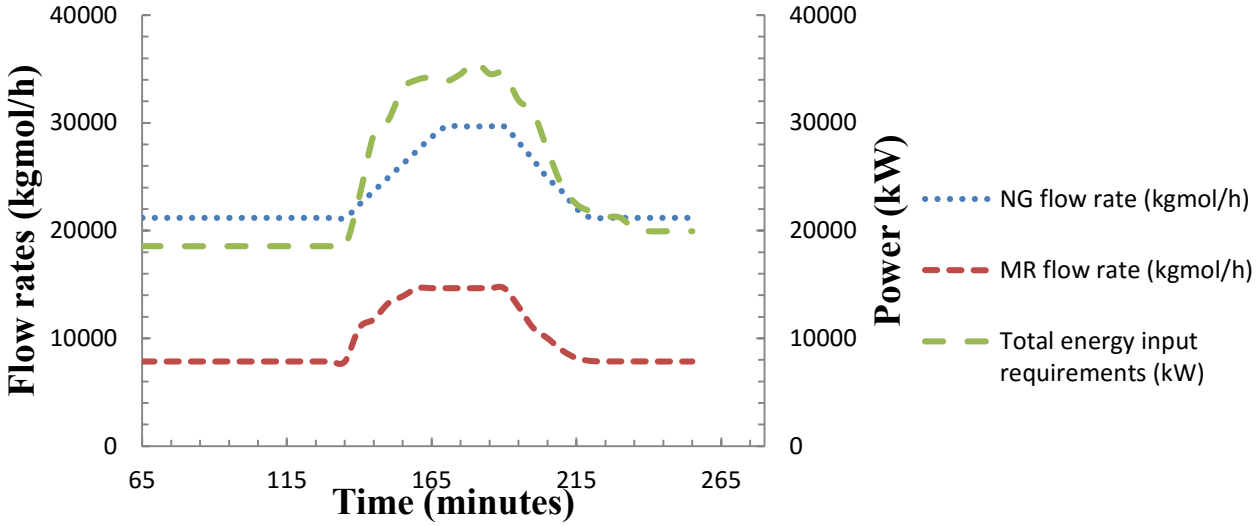

b)

Figure 3-8. Change of MR and NG flow rates versus total energy input requirements with ramping a) B-ER-B and b) B-ES-B

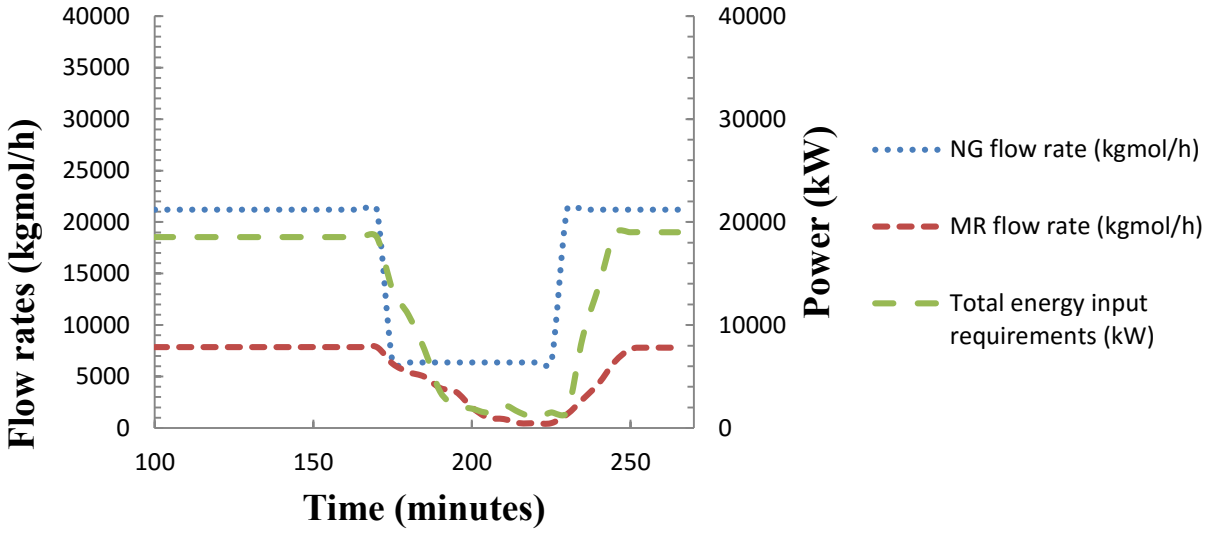

a)

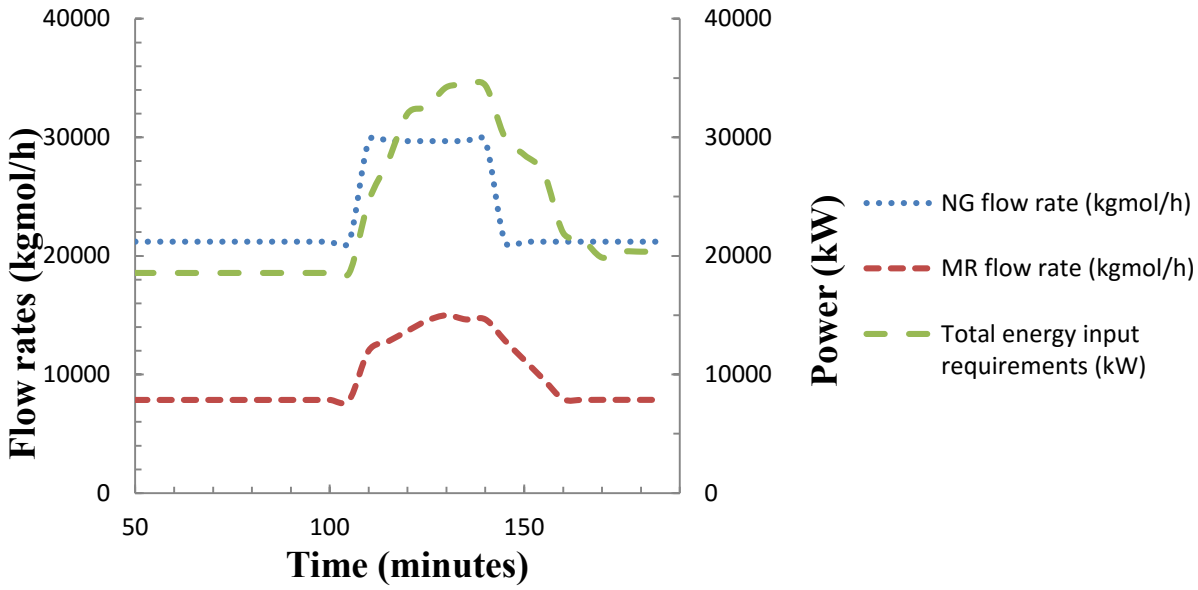

b)

Figure 3-9. Change of MR and NG flow rates versus total energy input requirements with step size change a) B-ER-B and b) B-ES-B

Heat exchanger temperature profiles represent the most critical component of these simulations, both because of entropy generation and because of thermal stresses. The previous graphs provide some idea of the temporal variation as the transients in these graphs largely arise from changes in the heat exchanger profiles. The end-point spatial variations in the heat exchanger temperatures appear in Figures 3-10a, 3-10b and 3-10c, all of which are computed as the final profile after the step change in flow rate. As indicated, all of the heat exchangers come to their optimal condition of small and approximately constant temperature differences between the hot and cold streams even though the profiles are far from linear. However, the temperature changes at any one location as the process moves between ER, B, and ES modes can be large enough to cause significant thermal stresses if the rate of these changes is not carefully managed.

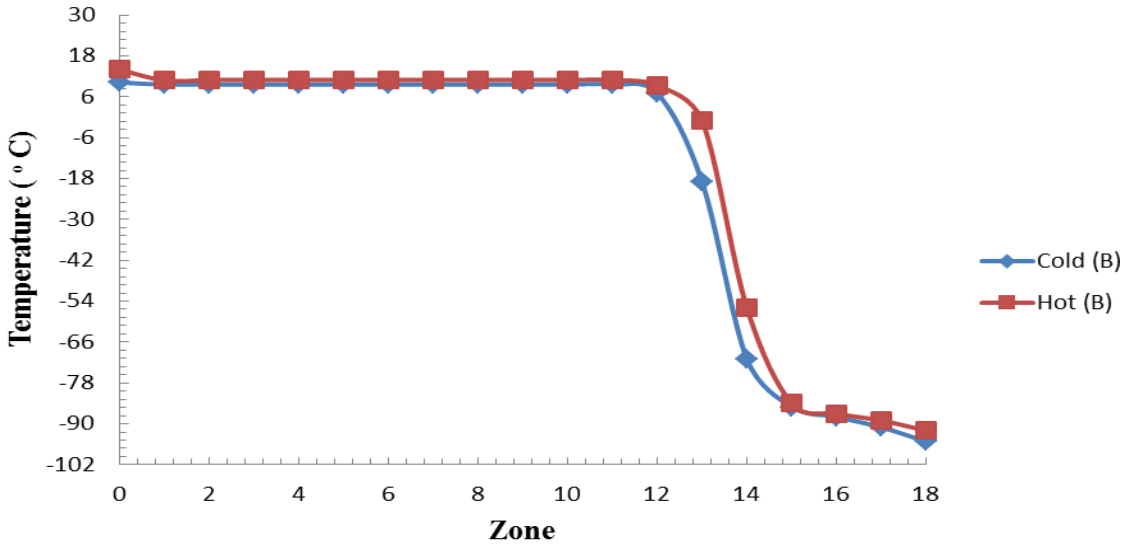

a)

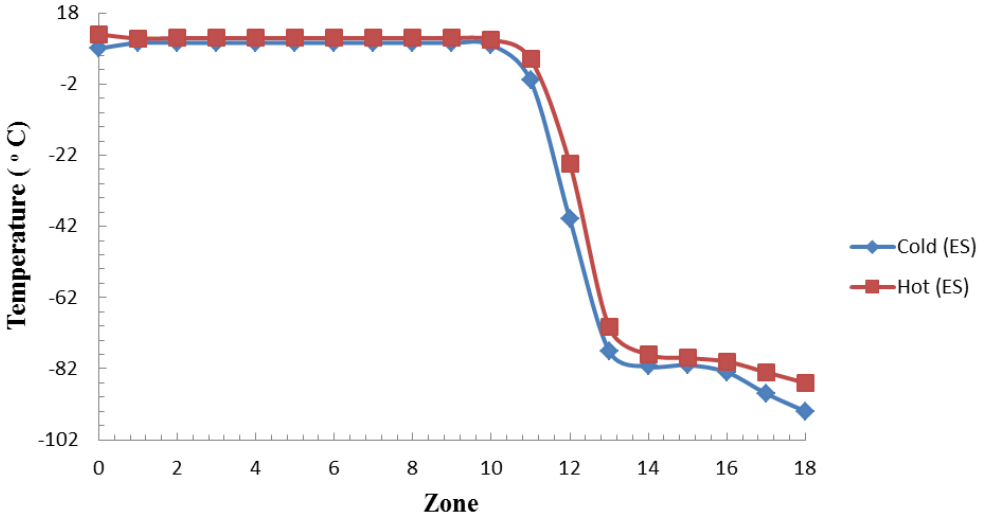

b)

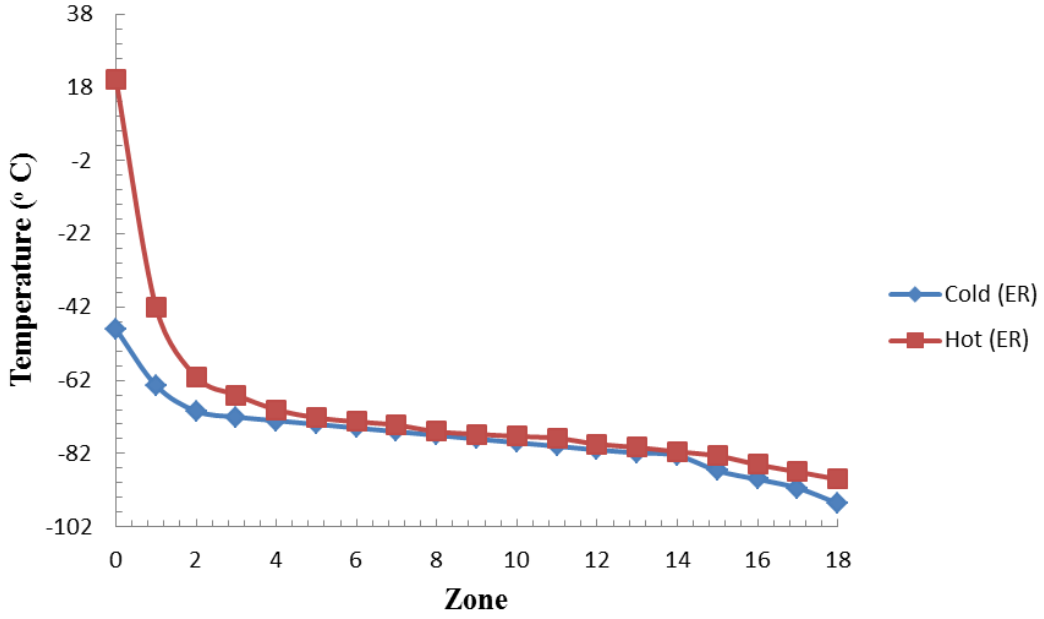

c)

Figure 3-10. Temperature profiles for a) B, b) ES and c) ER cases

These transient temperature profiles created in moving from B to ER modes, ES to ER modes, and B to ES conditions appear in Figures 3-11, 3-12 and 3-13, respectively. As illustrated,

in moving through these transitions, the internal temperatures change over a large range in a short amount of time. Depending on heat exchanger construction and operation details, these changes could exceed the allowable temperature stress limits of the heat exchangers. Recent technological innovations provide means of greatly reducing or eliminating these stresses. However, in traditional designs, these stresses can limit the response times of the entire system.

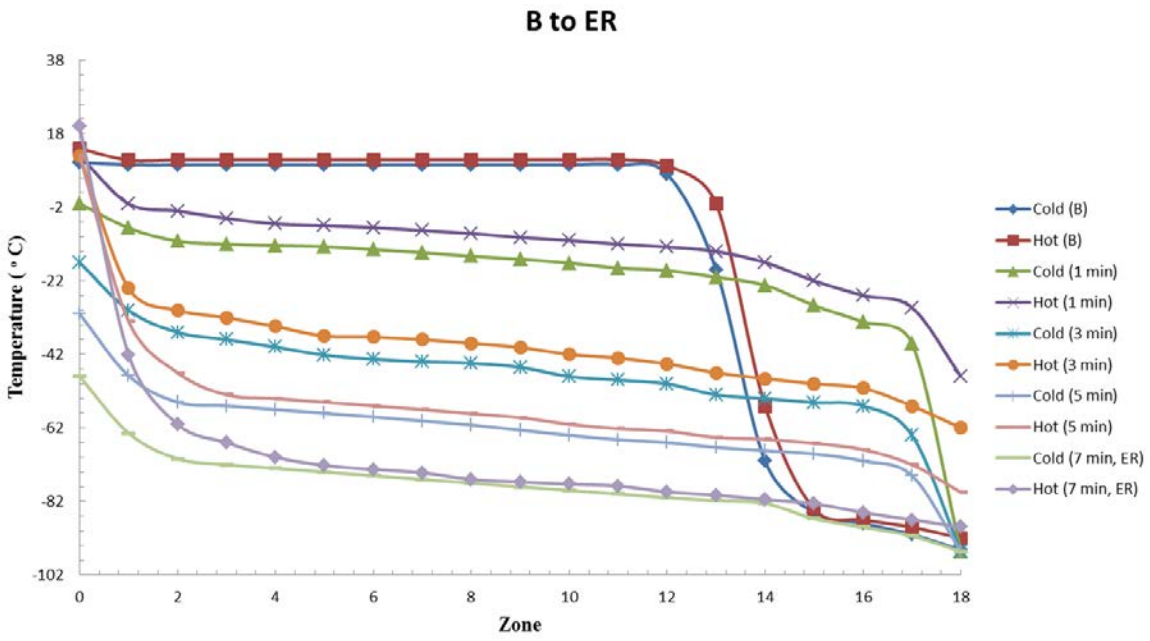

Figure 3-11. Transient temperature profiles in moving from the B to the ER condition. After 7 minutes, the transition is essentially complete

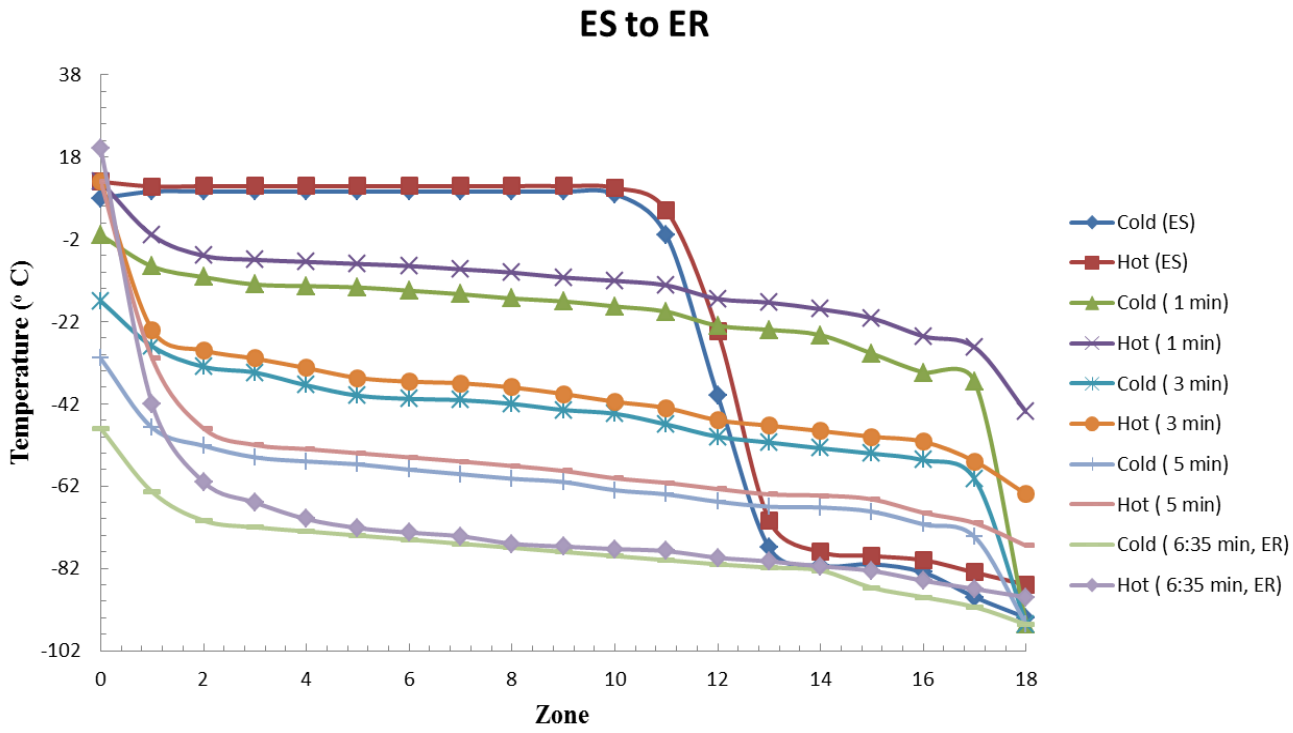

Figure 3-12. Transient heat exchanger temperature profiles in moving from the ES to the ER condition. After 6 minutes and 35 seconds, the transition is essentially complete

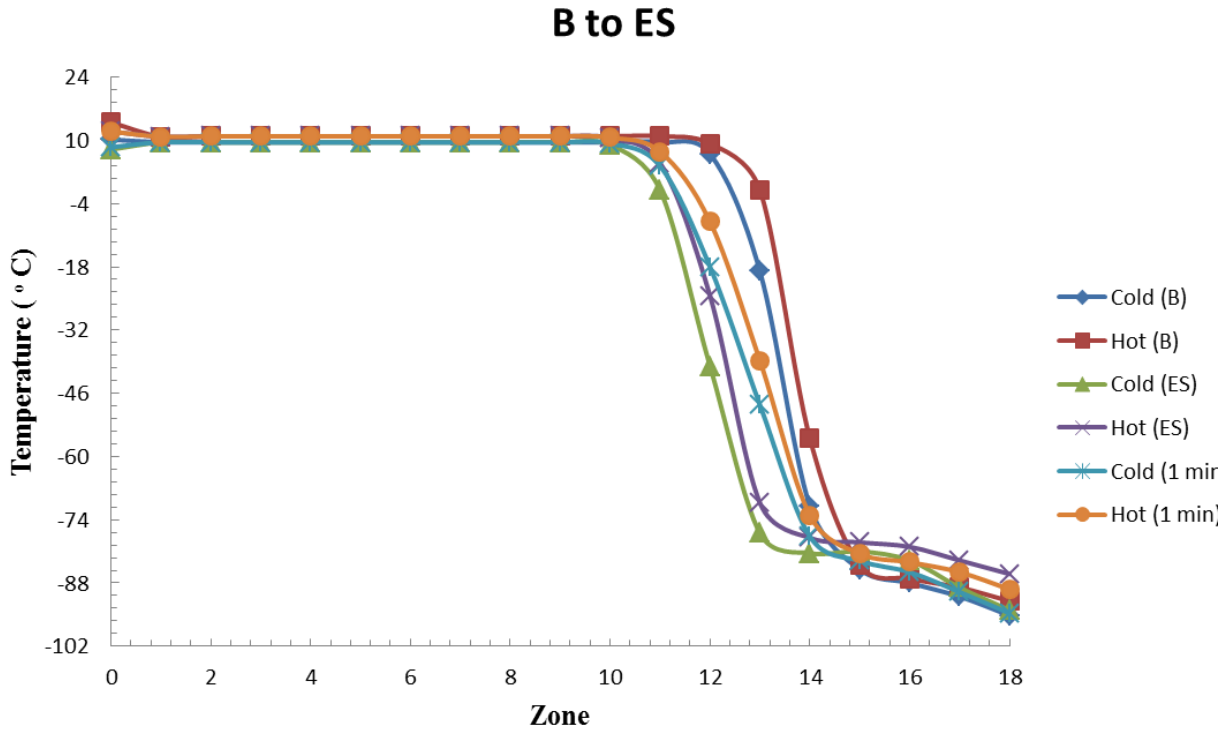

Figure 3-13. Transient heat exchanger temperature profiles in moving from B to the ES conditions. After 2 minutes and 54 seconds, the transition is essentially complete

3.6. Transient efficiency

The transient heat exchanger efficiency decreases as temperature differences between streams increase. While the previous results show that these differences can be small once the heat exchangers adjust to their new temperature profiles, it is not possible to maintain these narrow temperature differences as profiles change. The thermal heat transfer efficiency conceptually represents the Gibbs energy/entropy/exergy change in the system, as explained in Section 3.4. Grid power demands for a given plant commonly change in 5-10 minutes both because of changes in demand and, increasingly, because of very rapidly changing generation rates from intermittent renewable sources such as wind and solar. As illustrated in the previous sections, LNG production using traditional heat exchangers cannot match these time constants without significant damage to both equipment and efficiency. This section analyzes the behavior of a single heat exchanger.

Figure 3-14 indicates that a single heat exchanger reaches a new quasi-steady value in about 3 minutes. However, these computed response times are limited only by the transient heating of heat exchangers. In practice, the limit of temperature change rates in heat exchangers is about 1 °C per minute to avoid excessive thermal stresses. At this rate, these transients would require about 20-30 minutes in each heat exchanger to adjust to the new conditions, and there are many heat exchangers in series. The effect on instantaneous heat exchanger efficiency is also severe during the changes, with average efficiency dropping by about 10% over a typical cycle. Efficiencies greater than 100% indicate that the heat exchanger structural elements are helping to change a fluid temperature in addition to the counter-flowing fluid.

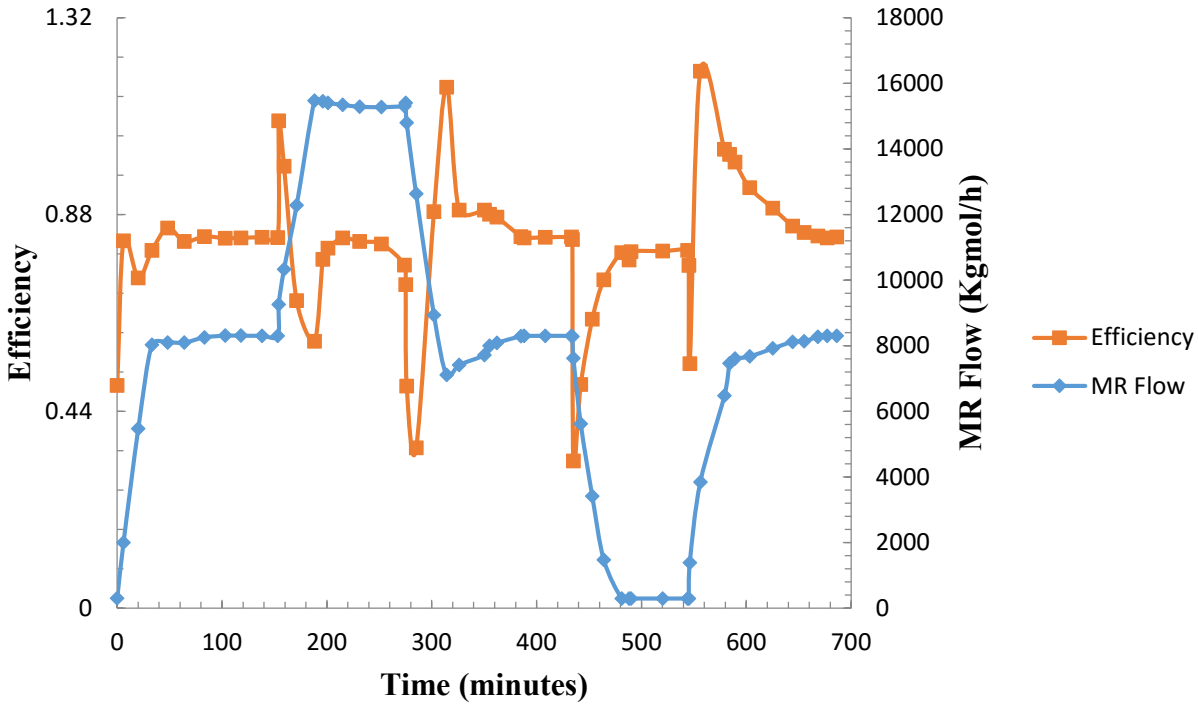

a)

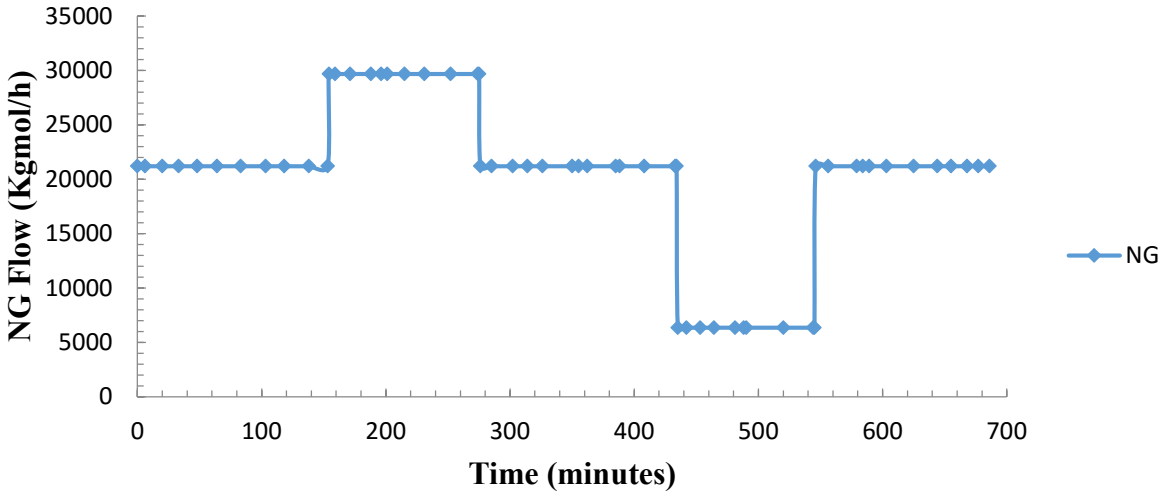

b)

Figure 3-14. Transient efficiency with respect to a) MR and b) NG flow rates

Chapter 4. Dynamic modeling comparison and transient responses

This section outlines models for transient natural gas liquefaction in two ways using Aspen HYSYS Dynamics: traditional heat exchanger design (THED) and dynamic heat exchanger design (DHED). In THED, Aspen HYSYS dynamics optimizes a single mixed refrigerant (SMR) process. In DHED, patent-pending dynamic heat exchangers use two methanol streams in addition to the traditional streams to regulate flow rate and heat exchanger temperature profiles during transients. Operating conditions, MR compositions and the nominal heat exchanger size are the same for both designs. K-value and U-value techniques manage heat exchanger flow rates and temperature profiles. All cases involve LNG and NG transients. Heat exchanger temperature profiles and efficiency depend on operating conditions, as discussed below.

4.1. Process design

The single mixed refrigerant (SMR) is the simplest and the most efficient NG liquefaction process [51]. The single MR cycle uses only one MR loop for pre-cooling, liquefaction, and sub-cooling (Figure 4-1). The cycle compresses and cools the refrigerant until liquid forms, and then vaporizes the refrigerant in the LNG exchanger. The refrigerant cools -condenses the natural gas, NG, to liquefied natural gas, LNG. The refrigerant composition is optimized such that the temperature profiles in the heat exchangers are as close and parallel as possible. Table 2-8 summarizes the optimized mixed refrigerant composition and key parameters, where ER, B and ES represent energy storing, balanced, and energy recovery respectively.

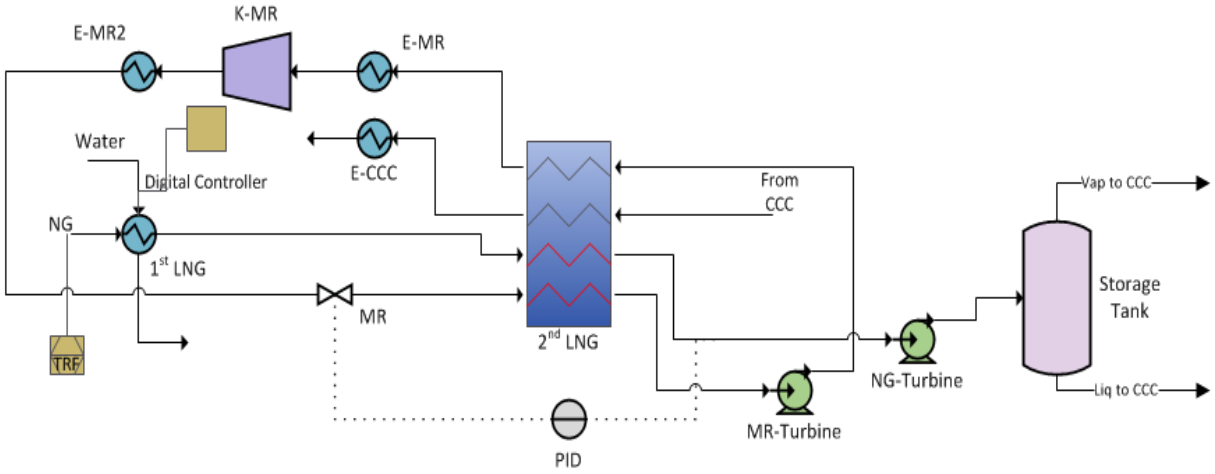

Figure 4-1. Aspen HYSYS simulation of SMR for THED

There are two dynamic heat exchanger configurations. The first configuration involves the THED process shown in Figure 4-1 and the second configuration introduces two additional methanol streams, as shown in Figure 4-2. The dynamic heat exchangers are patented new innovations that maintain internal heat exchanger temperature profiles near their balanced conditions. They do so by filling or emptying local hot or cold storage tanks to maintain a net balanced flow in the exchanger. These dynamic heat exchangers benefit the process in several ways. In their absence, natural gas flow rate changes create temperature profile changes in the heat exchanger. PID controllers try to compensate by adjusting refrigerant flow rate, but refrigerant flow rate changes alone cannot completely restore the optimized temperature profile. Large temperature changes in the heat exchanger cause thermal stresses as well as efficiency losses. The dynamic system can solve these issues. If an upset or transient changes one of the cold or hot flows, the dynamic system compensates by adjusting the balancing stream through filling one tank by emptying the other tank such that the heat exchanger functions at its highest efficiency. A future

transient or upset in the opposite direction allows the system to return to its baseline condition, including the original levels of stored material in the tank. Therefore, the system levels the periodic changes in flow, random transients, and other dynamics. The dynamic systems cannot fully compensate for a permanent shift in flow rates, but they can nearly perfectly compensate for temporary changes around some average [52].

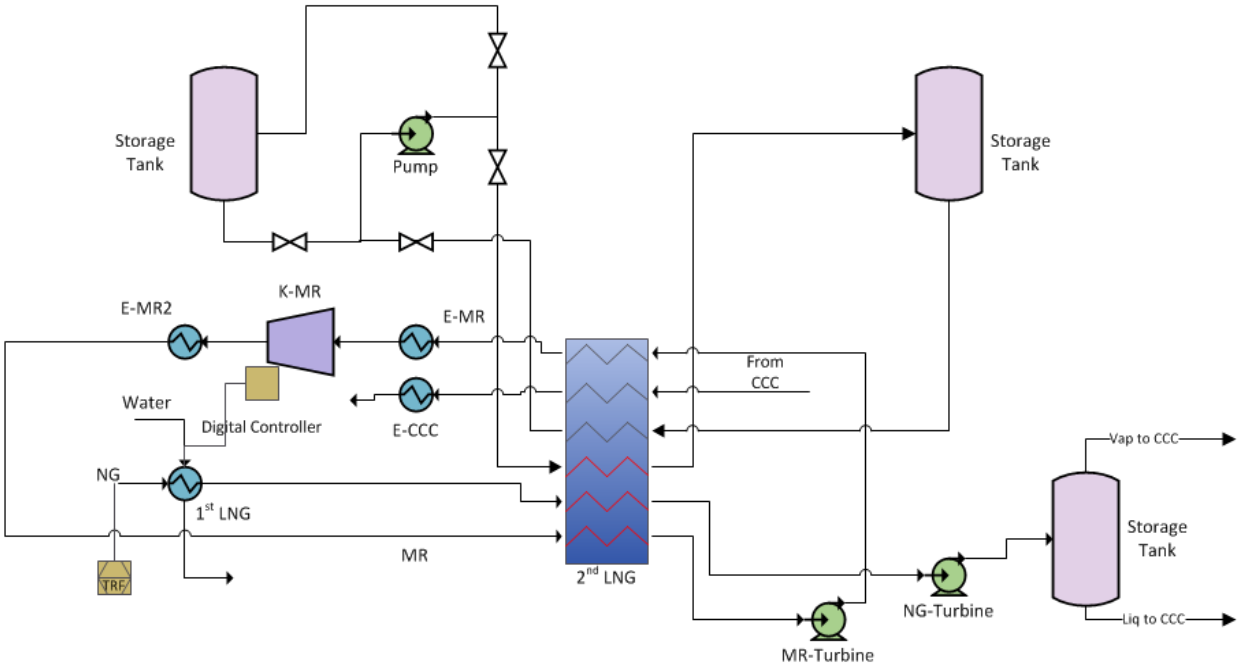

Figure 4-2. Aspen HYSYS simulation of SMR for DHED

The dynamic heat exchangers in this configuration can use essentially any fluid in the channels that connect the two tanks. An ideal fluid has a low melting point, a high boiling point, and a high volumetric heat capacity; that is, it should be a liquid with the ability to absorb as much heat as possible with minimal change in temperature. These simulations use methanol.

4.2. Process optimization

Earlier discussions described optimization using traditional heat exchanger design (THED). The following discussion involved dynamic heat exchanger design (DHED). DHED uses all the optimized conditions from THED. In addition, it optimizes two methanol streams' conditions to obtain optimum pressure, temperatures and flow rates in the heat exchanger. The thermodynamic properties of methanol determine the temperatures and pressures. This investigation optimizes flow rates using model predictive control schemes.

Model predictive control (MPC) provides the heat exchanger control for this model (see the Appendix part D). MPC requires solutions at multiple natural gas flow rates. A base case determines a baseline heat exchanger ΔT by doing an enthalpy balance on both sides of the heat exchanger. Mixed refrigerant and methanol flow rates restore the baseline ΔT during optimization.

Generally, optimization would follow this procedure for many natural gas flow rates. Visual Basic for Application (VBA) code in Excel saves time and simplifies the process. The code first links VBA to HYSYS. Once it links, VBA calculates the current ΔT of the heat exchanger and the difference in the ΔT's of the heat exchanger using the base case as a reference.

The built-in Excel solver minimizes the difference in ΔT's by changing the mixed refrigerant and methanol flow rates. Once it converges, it records the flow rates needed to converge. It then changes the natural gas flow rate to a new value and restarts the entire process.

These data provide a list of methanol flow rates versus natural gas flow rate. Empirical equations fit the data for the mixed refrigerant and methanol flow rates. Aspen verifies the validity of these empirical results and the validated correlations accelerate the optimization procedure by avoiding lengthy Aspen calculations.

Energy input requirements for both THED and DHED are given in Table 4-1:

Table 4-1. Optimized energy input requirements in DHED for each case

Energy input requirements	ER (kW/kg NG)	B (kW/kg NG)	ES (kW/kg NG)
THED	0.00831	0.06126	0.07065
DHED	0.00486	0.06132	0.05092

Table 4-1 indicates that DHED requires less energy compared to THED in both the energy recovery and energy storage modes and only slightly more energy in the balanced mode.

The reason for the slight increase in the balanced mode is explored after the following discussion on efficiency. On average, the DHED system requires significantly less energy than the THED.

4.3. Comparison of heat exchanger efficiency

Heat exchanger efficiencies at steady state for both THED and DHED appear in Table 4-2. Table 4-2 indicates DHED efficiencies are close in the three cases of balanced, energy recovery, and energy storing modes.

Table 4-2. Heat exchanger efficiency in DHED each case

Heat exchanger efficiency	ER (%)	B (%)	ES (%)
THED	74.35	93.86	80.21
DHED	91.43	91.92	91.80

The two-tank system leads to a stable efficiency that is close to the balanced case in DHED. This investigation shows that DHED heat exchanger efficiencies are on average higher and more constant compared to THED, as discussed shortly. In DHED, the heat exchanger temperature profiles are the same in all three cases (storing, recovery, and balanced), eliminating thermal stress and minimizing the required size of the heat exchangers.

The reason for the slightly higher energy requirement and slightly lower efficiency of the DHED system compared to the THED system in balanced mode is that the heat exchanger total surface area (and therefore cost) are the same in both systems. However, the DHED system includes two additional streams in the heat exchanger which, in the balanced mode, will have flowrates of zero. Therefore, these stagnant streams decrease overall efficiency with a commensurate increase in energy demand in balanced mode. In all other modes, these streams more than compensate for the compromise in balanced mode. These differences in efficiency and energy demand could be eliminated by increasing the heat exchanger surface area to compensate for the effect of the stagnant stream.

This investigation chooses not to do this to illustrate the advantage of the DHED process for transient flows. That is, larger heat exchangers can always decrease energy demand somewhat,

but in the case of transient flows, the DHED system can save energy even though it slightly compromises the balanced behavior. A second version of the dynamic heat exchanger, the retrofit version, could eliminate the disadvantage of the configuration shown here in balanced mode and actually slightly improve on the performance in energy storing and energy recovery mode, but it is not well suited to heat exchangers with gaseous streams.

4.4. Transient modeling of THED and DHED

Dynamic steps are the same for both THED and DHED, but since the DHED balanced case includes two zero flow rates in the methanol streams and, for ER and ES cases, one methanol stream zero flow rate, proper K values and U values are important. Both THED and DHED use the same sizing. The highest flow rates use K-values and the balanced case uses U-values. Aspen HYSYS automatically scales these K values and U values with respect to flow rates passing through each stream.

Both step changes and ramping inlet conditions illustrate the performance of the process. Step changes move instantaneously from one flowrate to the next while ramping changes occur over time. Four parameters quantify the dynamic system response to these changes: total energy usage, NG turbine production, MR turbine production and NG flow rate. The performance for DHED is given in Figures 4-3, 4-4, 4-5 and 4-6.

Reducing NG flow rate also reduces total energy usage. This means that the MR and NG turbines provide more energy. In the energy storage case, increasing the flow rate increases total energy consumption by compressors. Figures 4-3 to 4-6 indicate robustness of the DHED compared to THED during flow rate variation.

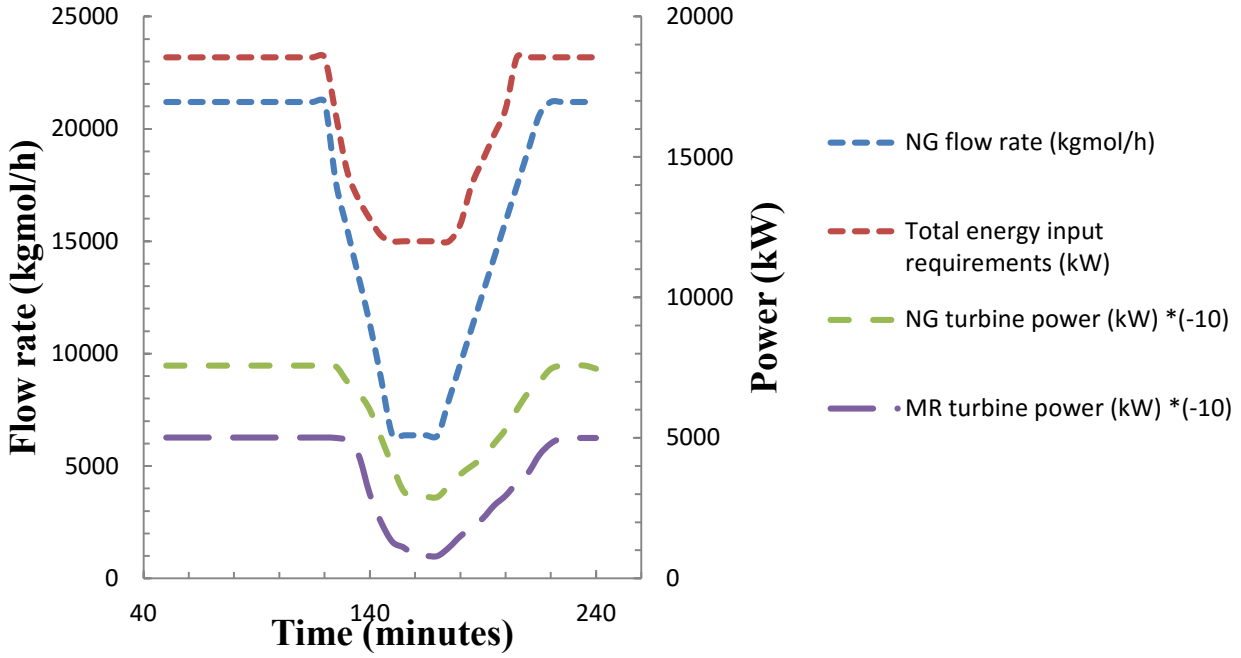

Figure 4-3. Ramping and B-ER-B performance

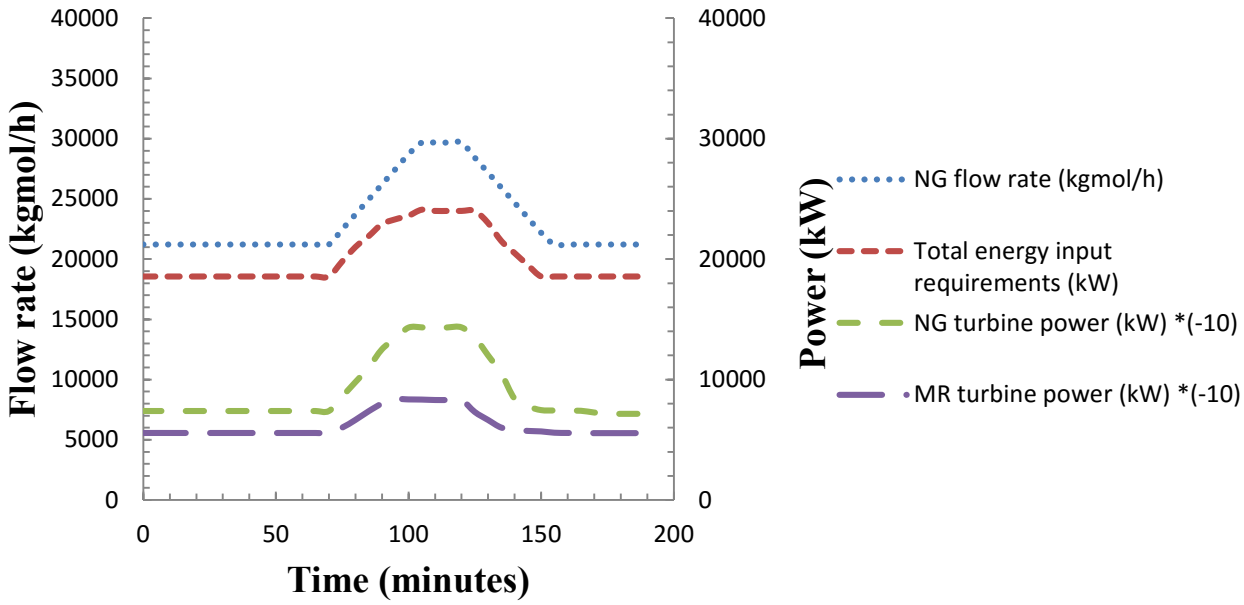

Figure 4-4. Ramping and B-ES-B performance

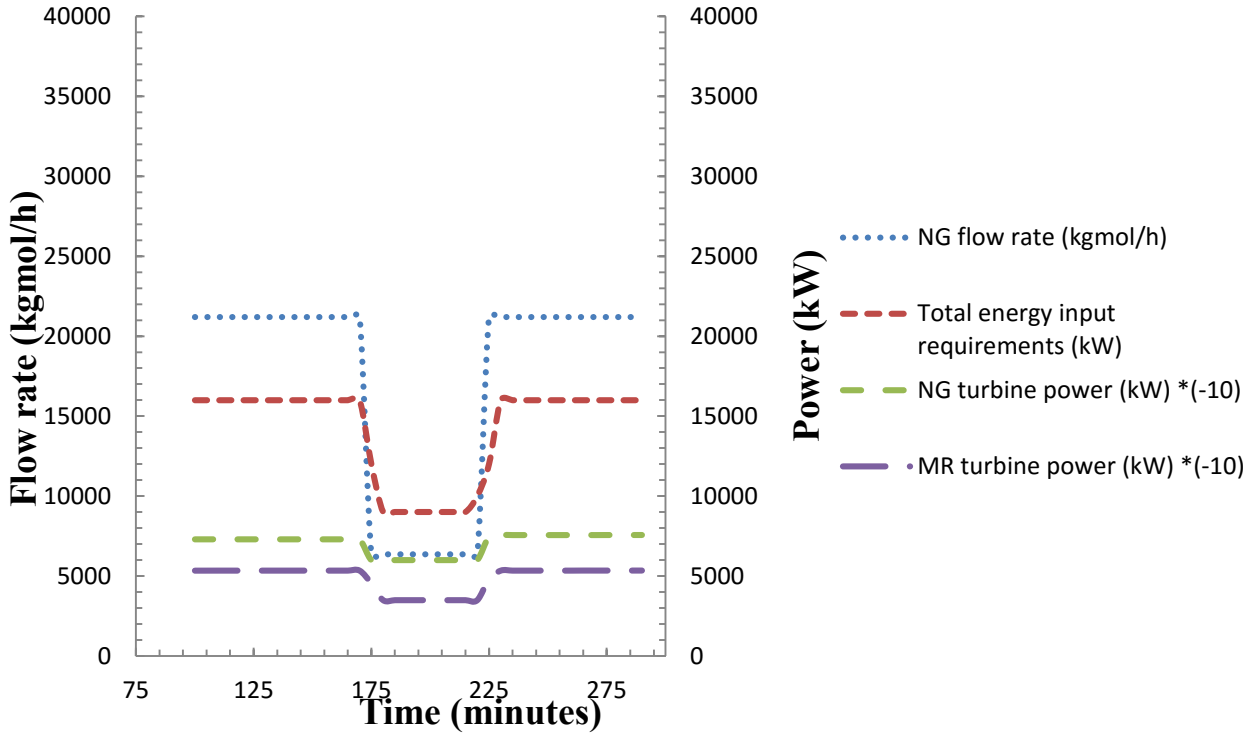

Figure 4-5. Step changing and B-ER-B performance

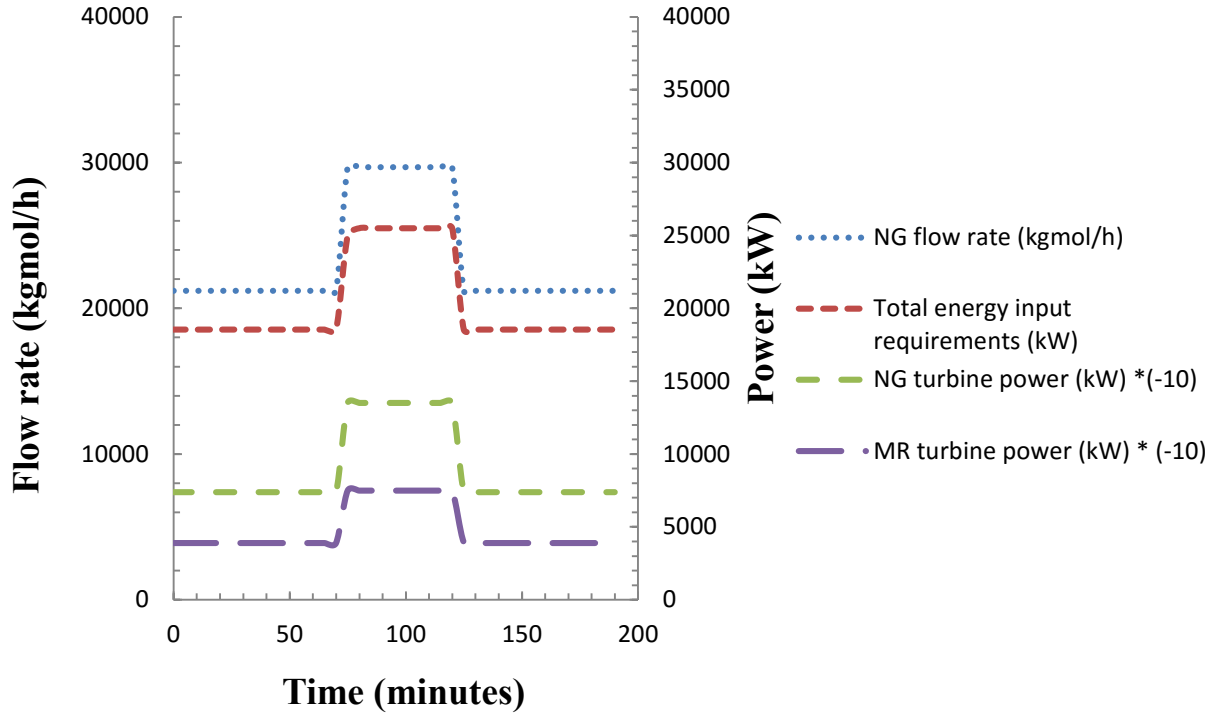

Figure 4-6. Step changing and B-ES-B performance

Heat exchanger temperature profiles provide some of the most important information on efficiency and effectiveness. The temperature profiles for THED are given before (Figures 3-10a, 3-10b and 3-10c).

As previously mentioned, one of the most important goals for DHED is to have one temperature profile for all three cases. This technology achieves this goal. The temperature profile for DHED is as follows:

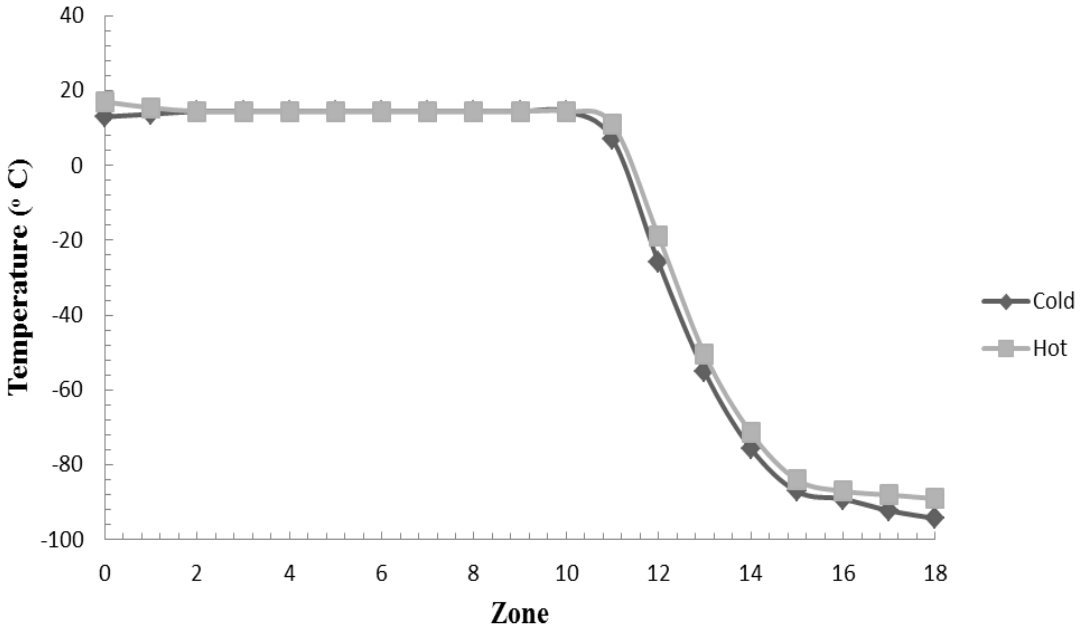

Figure 4-7. Temperature profile for DHED

The temperature difference and heat exchange load in heat transfer contribute to the exergy loss, so large temperature difference and heat exchange load primarily contribute to exergy loss in heat exchangers. If the hot composite curve matches the cold curve well, the resulting exergy loss is small.

4.5. Transient efficiency

The transient spikes seen in the THED data can be virtually eliminated by DHED. Even though the process goes through a relatively large transient – the same transient indicated in Figure 3-13 – the heat exchanger maintains nearly constant conditions. This reduces energy input requirements for whole system and exergy losses for heat exchanger. The efficiency for DHED exceeds that of the THED as shown in Figures 4-8 and 4-9, where efficiencies are higher, constant, and even during transients have almost no spikes.

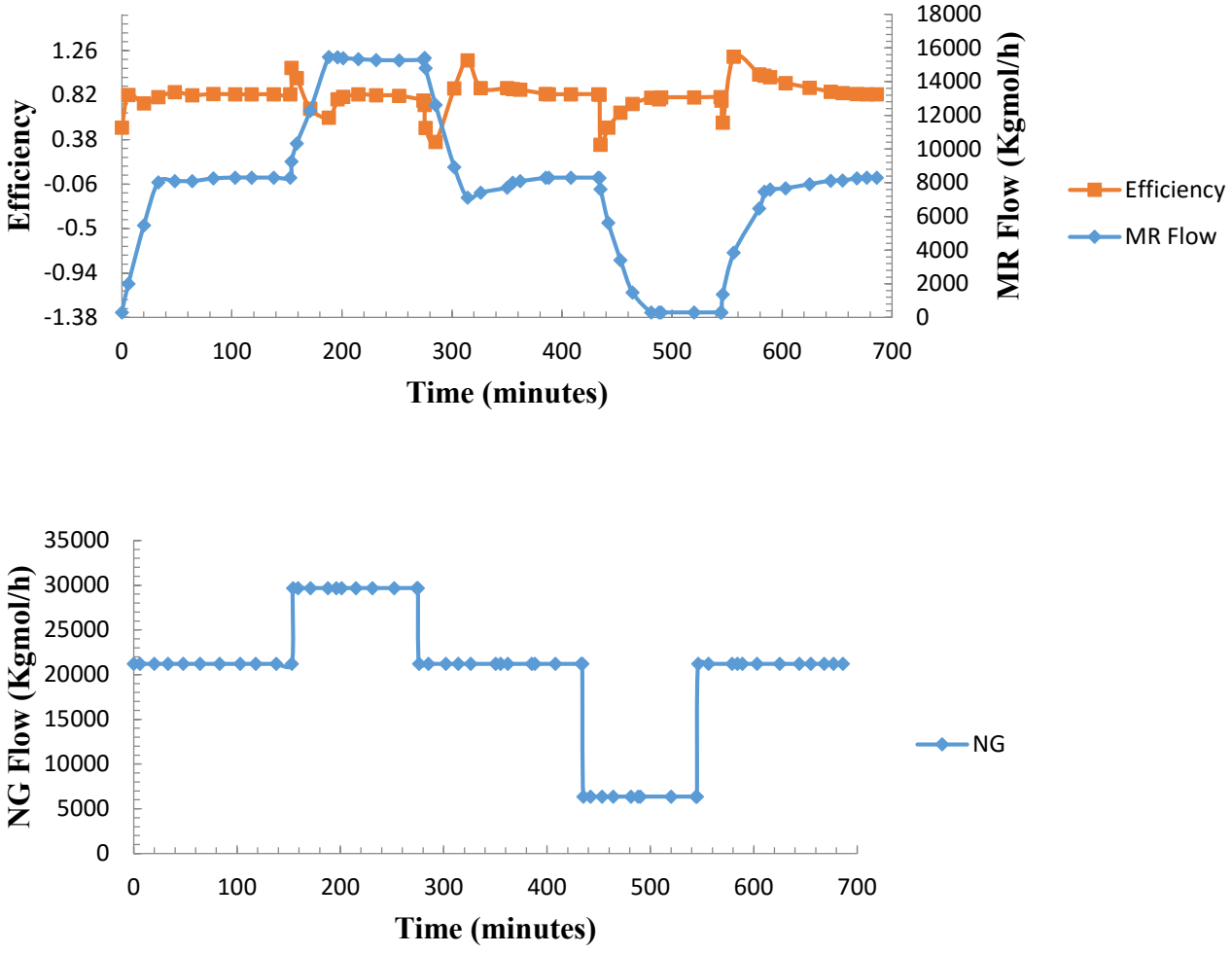

Figure 4-8. Transient flow rates and efficiencies for THED with respect to MR and NG flow rates (Automatically tuned PID)

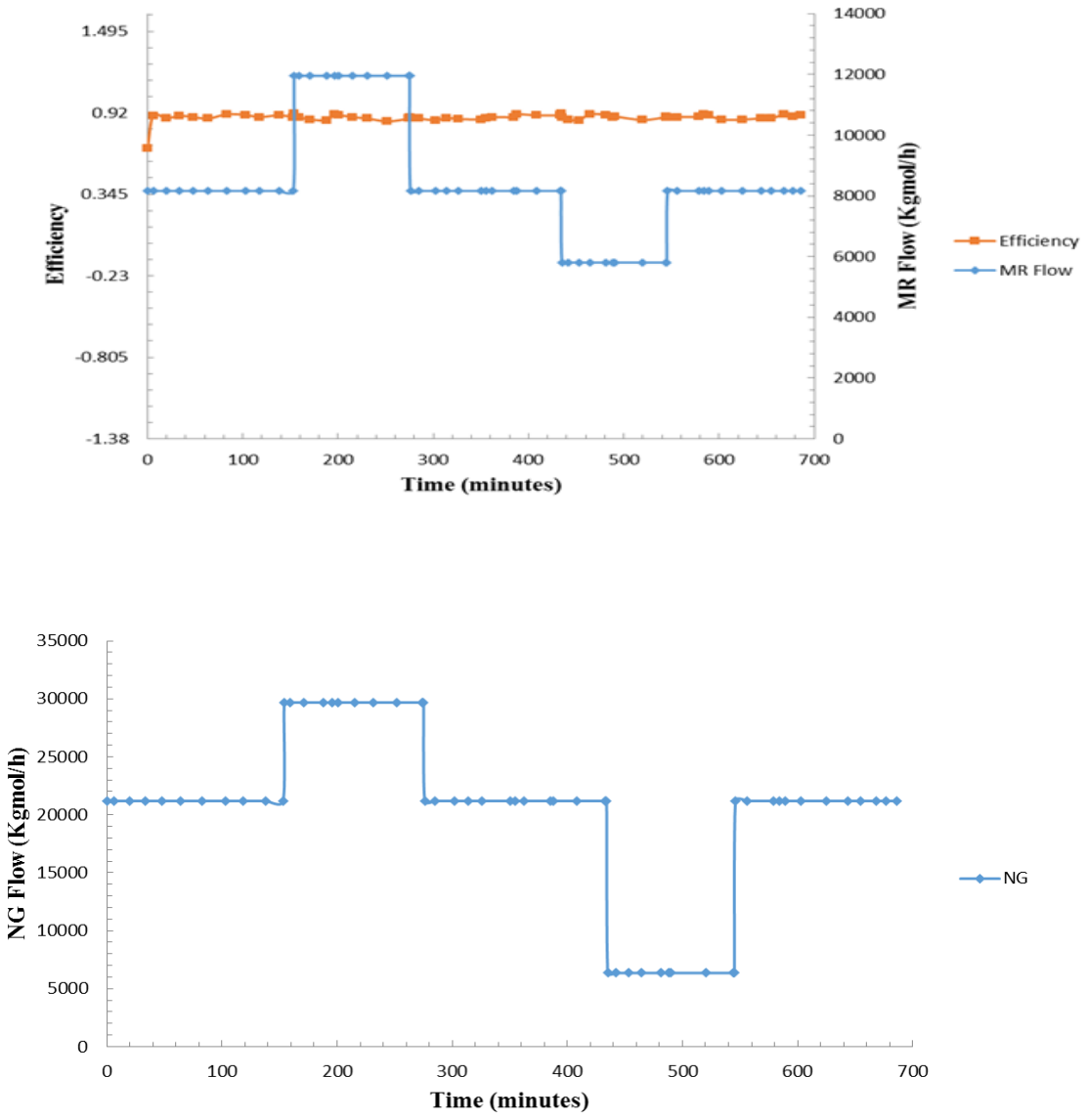

Figure 4-9. Transient flow rates and efficiency for DHED with respect to MR and NG flow rates

4.6. Rapid system response

In addition to maintaining optimal efficiency and meeting set points through transients, this innovation allows the system to move much more rapidly through these transients. This is a significant benefit to several processes. Unlike THED, which experiences thermal stresses and

other temperature-profile-related performance concerns through transients, DHED has no such issues. This allows the process to move through transients, change loads, and follow set points at much more rapid speeds than is otherwise the case. One important comparison would be to compare LNG production and NG consumption for two models. For THED with (a) manually tuned PID controller, it usually takes 10-20 minutes (Figure 4-10) for THED with (b) auto tuned PID controller to adjust to the new conditions (Figure 4-11).

These results lead to several observations:

a) The two methanol streams have zero flow rates in the balanced case but for ER and ES flow rates have been optimized using MPC.

b) As the natural gas flow rate changes, there is no change in temperature in the heat exchanger for DHED. Also the efficiency does not considerably change. By contrast, the THED temperature profiles and efficiency change with changing flows.

c) All units in HYSYS include dynamic responses. For example, coolers and heaters maintain specified product temperatures. The coolers use water and the heaters use steam.

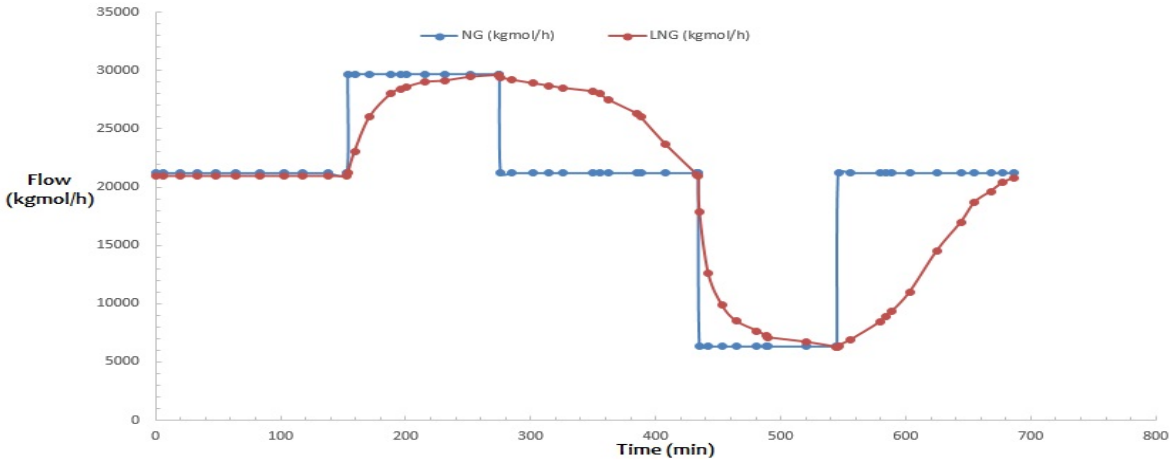

Figure 4-10. LNG (red line), kgmol/h; NG (blue line), kgmol/h; for THED with manually tuned PID controller

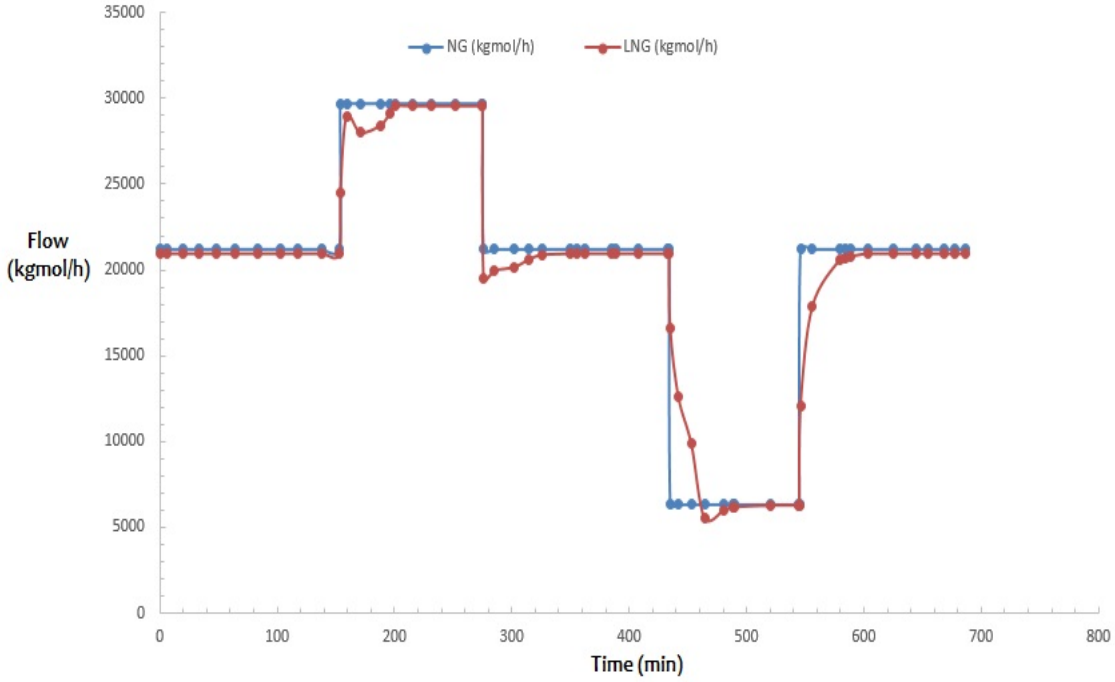

Figure 4-11. LNG (red line), kgmol/h; NG (blue line), kgmol/h; for THED with auto tuned PID controller

By contrast, it takes 2-7 minutes and for DHED (c) to adjust. As these figures indicate, the DHED process is more stable (Figure 4-12).

All units including compressors, heat exchangers and expanders, experience smaller transients with the DHED than the THED.

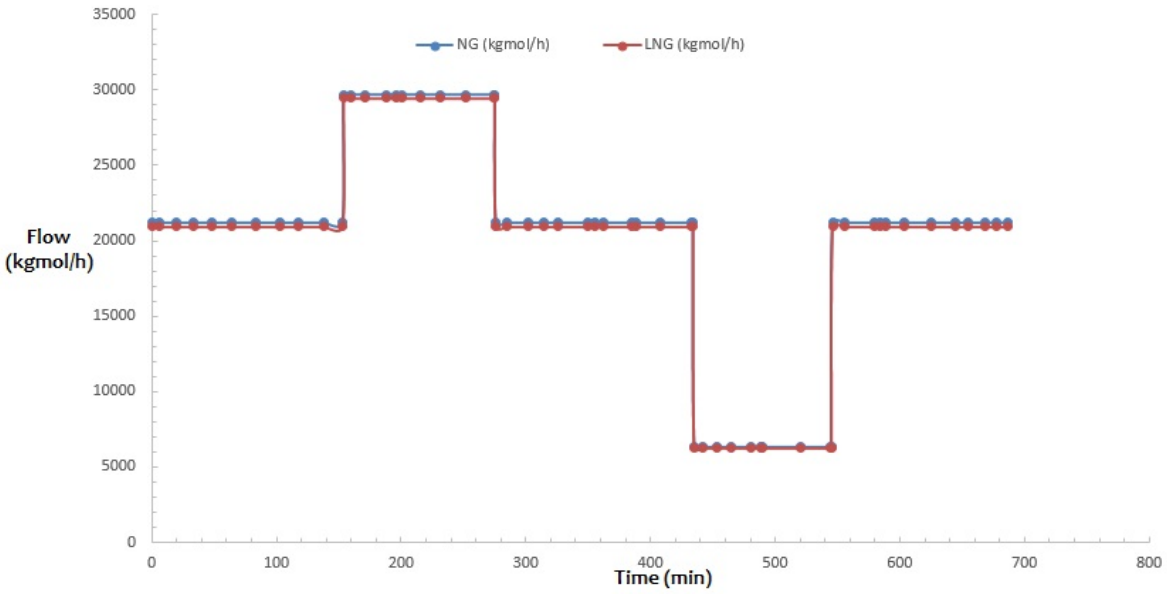

Figure 4-12. LNG (red line), kgmol/h; NG (blue line), kgmol/h; for DHED

Chapter 5. CO_2 removal from NG

5.1. Background

In an effort to satisfy the rising global demand for energy and at the same time to combat the environmental impacts such as global greenhouse gas emissions, it is worth searching for potential energy alternatives. The objective is to produce sufficient energy to meet demand at affordable prices using environmentally friendly technologies. Recent decades have seen a shift away from coal to natural gas, especially in the US [46-48, 55] driven mostly by low gas prices. The climate concerns are likely to continue to drive this shift. In addition to its primary importance as a fuel, natural gas is also a source of hydrocarbons for petrochemical feed stocks. Although many consider natural gas cleaner than coal or oil, the natural gas found in reservoir deposits contains many impurities and byproducts. Established commercial processes exist to remove the high molecular weight hydrocarbons as value-added byproducts and to remove contaminants, including both inert and toxic species. The contaminants include CO_2, N_2, Hg, He, and H_2S. The heavy hydrocarbons generate the greatest profit, in most cases more than the NG, and both the hydrocarbons and the contaminants must be removed both for operational reasons and to meet specifications. CO_2 removal figures prominently in these specifications, with separate standards for pipeline applications compared to liquefied natural gas (LNG) or similar applications. CO_2 forms weak carbonic acid when it condenses with moisture and its removal, together with sulfur and chemically active nitrogen compounds, constitutes acid gas removal.

There are many acid gas treating processes available for CO_2 in natural gas. Indeed, most of the CO_2 removal processes currently under development for flue gases trace their origins to CO_2 removal from natural gas. Each of the processes has advantages relative to others for certain applications and the decision on which technology to utilize for CO_2 removal depends on the process conditions and natural gas composition as well as the plant location. For example, high CO_2 partial pressure in the feed gas enhances the possibilities of employing a physical solvent, while the presence of significant amount of heavy hydrocarbon discourages the use of physical solvent. Low CO_2 partial pressures and low outlet pressure of the product stream may favor application of chemical solvents [56]. The major processes available can be grouped as follows [57]:

1) Absorption Processes (Chemical and Physical absorption): This process uses solvents that selectively absorb CO_2 and is the most common technology used for acid gas removal. The solubility of CO_2 depends on its partial pressure and on the temperature. Higher CO_2 partial pressure and lower temperatures favor CO_2 solubility. There are generally two categories of absorbents: potassium carbonate, which causes stress corrosion and erosion, and amine-based solvents. Due to the high capital demand of potassium carbonate methods, the amine absorption process is by far the most common [58]. This process can meet common pipeline specifications of no more than 2% CO_2, but struggles to meet the 50 ppm specification of LNG.
2) Adsorption Process: This process is based on exothermic reaction of solvent with the gas stream to remove the CO_2 present. Most chemical reactions are reversible; in this case, the reactive solvent removes CO_2 in the contactor at high pressure and preferably at low

temperature. The reaction then is reversed by endothermic stripping at high temperature and low pressure. In these processes, the gas flows through the fixed bed while the acid gases adsorb on solid particles. The beds need to be replaced or regenerated by heating once the bed saturates with acid gases. More details on process can be found elsewhere [59-61].

3) Physical Separation (Membrane, Cryogenic Separation): Membranes are an emerging process for CO_2 separation from natural gas and find increasing use in gas field operations for reducing carbon dioxide and water vapor to meet pipeline and LNG specifications. For a gas to permeate through a membrane, the gas must enter the high-pressure side of the membrane, diffuse across the membrane wall, and exit from the low-pressure side. Usually membranes are good for bulk removal of acid gases. At low concentrations of acid gases, membrane technology is inferior to other processes. This is because at low concentrations the partial pressures of the components are small and the pressure driving force of the process decreases. In such situations, membrane technology is sometimes combined with chemical solvent systems. This combined process has high adaptability to variation of CO_2 content in the feed gas, and membranes have good weight and space efficiency, which make it more applicable to an offshore environment. However, the separated CO_2 is at low pressure and requires additional compression to meet pipeline pressure requirements so the hydrocarbon loss is high.

Cryogenic separation is a commercial process commonly used to liquefy and purify carbon dioxide from relatively high purity (>90%) sources. It involves cooling the gases to a very

low temperature (lower than -73 °C) so that the carbon dioxide can freeze-out or liquefy. While it is suitable for feed gases with high concentration of CO_2, the energy for regeneration is very high, which increases the operating cost.

4) Hybrid Solution (Mixed Physical and Chemical Solvent): The hybrid separation processes combine the properties of physical and chemical solvents for effective and selective removal of acid gas from natural gas. In a physical solvent process, the acid gases are solved in instead of reacting with the solvent. The solubility of CO_2 varies with pressure and temperature and hence these processes are sensitive to changes in these operating conditions. Most physical solvent processes require licenses, such as the Selexol, Sulfinol and Fluor processes. Physical solvent processes should be avoided for gases with a high heavier hydrocarbon fractions and they usually are used when the partial pressure of the acid gases are above 3.5 bar. By combining physical and chemical solvent processes, success has been achieved [59, 62].

There is an increasing need for processing of natural gas to meet composition standards and separate high-value products, such as natural gas liquids, with increasing natural gas production both domestically and globally. Typical pipeline specifications limit CO_2 to 2-4 %, with CO_2 concentration in some fields starting as high as 70 %. Removal of CO_2 in natural gas is an industry driven practice rather than regulation driven, providing an opportunity for more immediate adoption of promising new technologies. Liquefaction processes that transform natural gas to liquid form involve operation at a very low temperature (-161 °C) and as low as atmospheric pressure. At these conditions, CO_2 freezes on exchanger surfaces, plugs lines and reduces plant

efficiency. Therefore, CO_2 must be removed before liquefaction, typically to levels of about 50 ppm. This not just avoids process failures but also prevents corrosion of process equipment.

In addition to its environmental impact, CO_2 reduces the heating value of the CH_4 gas streams in power plants [63]. NG quality requirements are 2 and 2.5 % CO_2 in Canada and the EU, respectively [64]. The US does not currently have federal LNG quality requirements, but re-vaporized LNG must meet natural gas pipeline standards of 2-4 % CO_2. Industrial natural gas specifications require 50 ppm CO_2 or less for streams that form LNG. The reason for CO_2 removal down to 50 ppm stems from concerns with degradation of operability due to potential CO_2 freezing during natural gas liquefaction. The solubility of CO_2 in the final LNG product at normal conditions is higher than 50 ppm [21]. Thus it is important to consider CCC LNG applied to the practice of achieving 50 ppm CO_2 and the potential for CO_2 tolerant liquefaction. This makes the removal of CO_2 from natural gas of crucial importance.

CCC processing of natural gas forms solids and in this aspect distinguishes itself from all but one of the alternative processes. The amine absorption processes discussed earlier are the most common and operate at temperatures and pressures well above the melting point of CO_2. The one process that does form solid CO_2 is ExxonMobil's Controlled Freeze Zone process, in which solids form in the middle of a distillation column but dissolve at the top of the column and melt in the bottom of the column. CCC removes solid CO_2 in desublimating heat exchangers and in this regard is distinct from even the controlled freeze zone technology.

The process described here removes excess CO_2 from natural gas streams prior to traditional NG processing. The process produces three streams: an essentially pure CO_2 stream that originates as solid CO_2 formed in this process, a liquid NG stream that contains small amounts of dissolved CO_2, and a vapor stream that is dominantly CH_4. The liquid NG stream is suitable for traditional, low-CO_2 level processing. The vapor stream joins NG produced downstream as a purified methane product.

The remainder of this section discusses process design and compares measured performance data with theoretical predictions. No commercial process simulation software known to the author is capable of predicting solids formation or destruction in heat exchangers or in other process equipment other than equilibrium reactors. This simulation works around these limitations using Gibbs reactors in series to approximate heat exchangers.

Even then, the multi-component, solid-liquid-vapor equilibrium calculations over a broad temperature and pressure range present computational and theoretical challenges. For example, solid dissolution in liquids normally is considered pressure independent, but it will not be if the dissolving species is also present in the vapor phase. In this application, solid CO_2 partially dissolves in liquid hydrocarbons and simultaneously is a component of the methane-rich vapor phase. This creates a pressure dependence in the amount of solid that forms in the liquid phase that is quite complex. The amount of solid CO_2 formed initially increases with pressure as increasing pressure causes CO_2 vapor to condense or desublimate.

The fraction of CO_2 in the solid then decreases with further pressure increases as the hydrocarbon vapors increasingly condense, diluting the liquid phase and dissolving additional fractions of solid CO_2. Eventually, the solid CO_2 fraction becomes insensitive to pressure as the vapor fraction drops to zero.

This and similar complex behaviors depend on thermodynamic subtleties. An experimental component of this work provides confirmation of the thermodynamic predictions. The discussion also includes a financial analysis of the process.

5.2. Process design

5.2.1. Feed gas parameters

Aspen plus has been used to simulate the NG pre-treatment system (Figure 5-1).

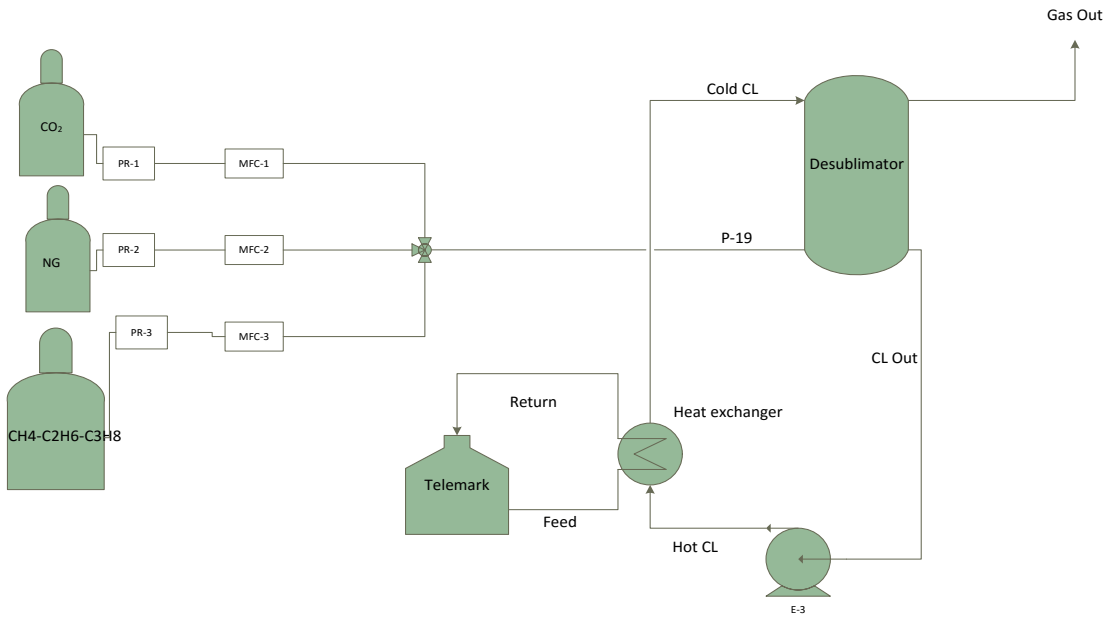

Figure 5-1. Aspen simulation of CO_2 removal system

The experimental CCC natural gas treatment system uses 8 mol/h feed stream of 84% methane, 6% ethane, 4% propane, 1% isobutane and 5 % carbon dioxide. The power plant simulations use natural gas flow rate of 1000 kmol/h of feed with the same composition. All other operating conditions are the same. Operating conditions and compositions are given in Table 5-1:

Table 5-1. Process parameters for the lab scale

Parameters	Value		Notes
Feed gas pressure	68.95 kPa		
Contact liquid pump pressure	68-2758 kPa		
Feed gas temperature	20 °C		
Feed natural gas mole fraction composition	CH_4	0.84	
	C_2H_6	0.06	
	C_3H_8	0.04	
	C_4H_{10}	0.01	
	CO_2	0.05	It varies up to 22% for economic analysis
Pressure drop in heat exchanger	5 kPa		To simplify the process
Pressure drop in cooler	1 kPa		
Ambient temperature	25 °C		
Pump adiabatic efficiency	92%		[47]

5.2.2. Contact Liquid

The contact liquid forms a nearly closed loop, with some minor losses into the solid CO_2. In general, contact liquids should have low vapor pressures to decrease losses through evaporation and otherwise be environmentally and physically benign. The contact liquid is primarily used to

prevent CO_2 solids from forming on surfaces, thus preventing process freeze up. A pump pressurizes the slurry prior to entering a solid-liquid separator. The separator consists of an auger driven continuous filter press. The bulk contact liquid, now free of solids, re-cools against a closed loop refrigeration system in preparation to reenter the desublimating column. Contact liquid recovered from the CO_2-rich stream returns to the process.

5.2.3. Solid separation

The CO_2 solids separator reduces contact liquid content of the slurry to about 6.7 % in the solid. The press filter captures 100 % of the solid CO_2 in the simulation. This does not take solubility into account, which may increase the concentration of CO_2 in the recycled contact liquid. However, this CO_2 returns to the heat exchanger in a contact liquid and therefore does not leave the process.

5.2.4. Phase equilibrium equations

Phase equilibrium provides the quantitative basis for much of the process simulation. The Peng-Robinson equation is used in this investigation [48].

5.3. Apparatus for natural gas processing experimentation

An apparatus was designed and built for natural gas experiments with an operating pressure up to 4 MPa for realistic natural gas processing conditions, see Figure 5-2. This apparatus includes a complete stainless steel construction to avoid deterioration and a 10 mm polycarbonate blast shield. The apparatus also includes safety considerations such as a hydrocarbon sensor with

interlock, an oxygen sensor, compliance with Class I, Division I national electric code (NEC) safety standards in the hydrocarbon-handling region, complete electrical isolation and multiple pressure relief valves.

Figure 5-2. Natural gas capable apparatus with cylinder gas cabinet (A), Sample analyzer (B), exhaust fume hood for flaring and venting (C), computer control interface (D), bubbler and separator cold box (E), reservoir cold box (F), data acquisition (G), mass flow controllers (H), heat exchange and pumping cold box (I), mass flow controller power supply (J), pump motor controller (K), pump motor (L), cryocooler (M)

In these experiments, the process pressure ranges from local pressure (86 kPa absolute) to 4 MPa with an additional mass flow controller on the exhaust gas. Cylinders contain 99.5 % pure CO_2 (Airgas), 99.0 % pure CH_4 (Airgas), 99.0 % pure C_3H_8 (Airgas), Natural Gas (88% CH_4, 7% C_2H_6, 4% C_3H_8 and 1% C_4H_{10}) (Airgas) and 99.0 % pure C_2H_6 (Praxair). The design maximum total gas flow rate is 3.7 L/min, which is measured by four mass flow controllers (Brooks 5850). A Sensidyne Gilibrator bubble chamber provides flow calibration with gas analyzers verifying the composition of mixed gases. The uncertainty of the flow measurements is not significant because experiments reach phase equilibrium.

The cryogenic portion of the process occurs inside the cold boxes with cooling by liquid nitrogen or an industrial refrigeration system (Telemark TVP-2000), see Figure 5-2. Heat exchangers are stainless-steel, brazed-plate styles (GEA-PHE). A pump (Micro pump EW-73005-06) circulates contacting liquid through the desublimating heat exchanger and brazed-plate heat exchangers. A cartridge filter removes solid CO_2 particles to extend experimental run times and to prevent CO_2 concentrations in the liquid from exceeding the solubility limit. The cartridge filter uses a stainless-steel, 30 x 30 mm mesh with 0.53 mm openings, and was regenerated by isolating, draining, and introducing warm nitrogen with manually operated valves. During the time the filter is not in operation for regeneration, particles continue to build up within the system. However, measurements are not reported during regeneration because the contacting liquid could have CO_2 concentrations greater than the liquid phase equilibrium. The process was repeated, using fresh contact liquid each time, to minimize experimental error.

Three different gas analyzers measure initial and final CO_2 concentrations as the experiment progressed. A non-dispersive infrared (NDIR) M-700 emissions analyzer (Enerac) has a limited resolution of 0.1 %. A 5975C quadrupole mass spectrometer (Agilent Technologies) provides additional gas analysis, specifically (1) verifying the adequacy of CO_2 measurements of NDIR analyzers and (2) quantifying the trace elements (i.e. contacting liquid). For portable skids, an industrial ABB EL3040 analyzer provides continuous results with an increased resolution compared to the M-700 (0.006 %). The EL3040 also uses NDIR techniques and is limited to the CO_2 concentration range of 0-3 %. Analyzers are calibrated with NIST-traceable Mesa Specialty gases and with in-house calibration gases. In-house calibration gases are volumetrically made in a 1 L syringe (SGE).

The desublimating heat exchanger comprises a single stage stainless steel column with five 3.2 mm diameter holes for gas bubbling and a 13 mm diameter tube or down comer, see Figures 5-3 and 5-4. The top of the down comer is 25 mm above the bubbling plate, causing liquid to build up on the stage. The column rests on the inside of a stainless steel pressure vessel. Liquid at the bottom of the vessel ensures that entering gas progress up through the liquid on the tray and exchanges heat rather than passing the stage. At least 6 inches of perlite in every direction insulate the cold portions of the apparatus. In high-pressure experiments with complete liquefaction of natural gas, there is no vapor stream from the desublimating column, and the natural gas enters the desublimating column as a warm gas.

Figure 5-3. Inside view of cold boxes with perlite insulation removed. From left to right: heat exchange and pumping cold box, reservoir cold box, and bubbling heat exchanger and separations cold box

Pressure and temperature strongly affect desublimating heat exchanger performance. The apparatus contains 16 K-type thermocouples (Omega) with uncertainties of ± 0.5 K in the range of 93-153 K. Four of the thermocouples measure the temperatures of the fluid streams immediately entering and exiting the desublimating heat exchanger. These thermocouples are calibrated by boiling pure nitrogen, pure methane, and pure ethane at known room pressures and comparing measured temperatures with theoretical boiling points at these pressures. The experimental apparatus also contains two pressure transducers (Transducers Direct) with uncertainties of ± 0.25 % over the range of 0-6.9 MPa. One of the pressure transducers is built into the desublimating heat exchanger, while the other monitors the contact liquid pressure drop over the CO_2 solids filter.

Figure 5-4. Stainless steel single stage columns

5.3.1. Data analysis using gas chromatography-mass spectrometry

During the past several decades, field-portable Gas chromatography-mass spectrometry (GC-MS) has gained much attention. GC-MS is used to identify compounds based on their retention parameters, and interpretation of mass spectral fragmentation patterns. The combination of GC and MS is capable of detecting a wide range of agents, providing high selectivity and sensitivity, as well as providing structural information about these compounds [65, 66].

The Agilent 5975C Series GC/MSD, with Triple-Axis HED-EM Detector measures product composition. The 5975C detector uses a new ion guide and shield to position a new long-life triple channel electron multiplier (EM) doubly off-axis from the analyzer exit. The optimized ion path increases signal and eliminates noise from energetic neutrals. The GC-MS analysis

process samples a fluid mixture, injects it into the GC, separates into its components, and detects the fragments using the MS (Figure 5-5).

Figure 5-5. The Agilent 5975C Series GC/MSD front view

5.3.2. Experimental procedure

Nitrogen purges the system prior to introducing the contact fluid, isopentane. The system then cools by circulating the contact liquid through the system while a cryogenic refrigerator and/or liquid nitrogen cools the contacting fluid in brazed-plate heat exchangers to temperatures generally between 123 and 183 K. The volume of the contact liquid in the system is typically 2-

3 L. The contact liquid circulates through the system at a rate of 2 L/min. When the contact liquid and process equipment are sufficiently cool, gas flow starts through the mass flow controllers at the desired composition. After starting the inlet gas flow, the exhaust valve or mass flow controller maintains a steady-state pressure as the system equilibrates. The visual verification of the desublimating column performance was extremely important in the first attempted experimental runs to ensure proper operation.

5.3.3. LABVIEW program to control natural gas apparatus

LabVIEW DAQ (National Instruments) provides data acquisition and process control. The LabVIEW front panel contains controls for pump flow rate and mass flow controllers. The front panel also allows a user to adjust the P&ID controller parameters dynamically. The P&ID controller adjusts the total flow rate of the mass flow controllers to achieve the set pressure.

The display also has numerical and graphical indicators of the measured actual flow, pressures and temperatures that are broken into four groups: bubbler contact liquid, bubbler gas, metal contacts, and other process areas.

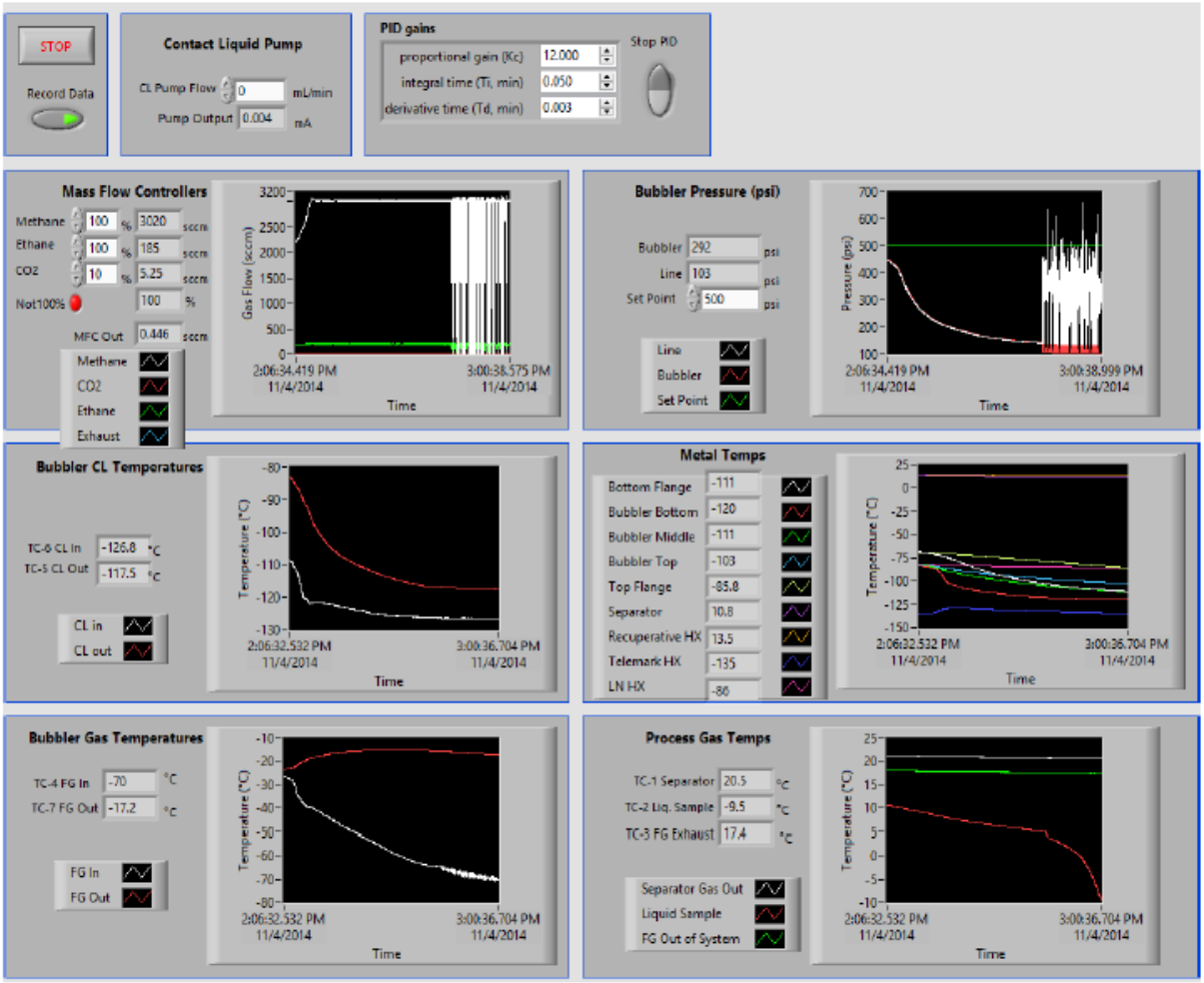

Figure 5-6. LABVIEW and computer control interface

5.4. Results and discussion

The amount of CO_2 captured equals the amount in the solid phase, which varies with temperature and pressure. This system provides reliable measurements of system temperature, pressure, and compositions of the vapor and liquid phases. The system does not provide meaningful estimates of the amounts of vapor, liquid, or solid phases. The amounts of these phases help determine the amount of CO_2 capture, which is the primary result of interest. The measured CO_2 capture as a function of pressure and temperature depend on the measured liquid and vapor phase compositions, an assumed solid phase composition of pure CO_2, and the computed amounts

of liquid and vapor phases. The assumption that the solid phase is pure CO_2 should be accurate. However, the data and the predictions are not entirely independent of each other since the data rely on the computed amounts of the liquid and vapor phases.

5.4.1. Effect of pressure

This section explores the effects of pressure on CO_2 capture and mole fraction of CO_2 and methane in the vapor. The pressure range is from 10 psi to 400 psi whilst temperature remains constant at -133 ºC. Figures 5-7a, 5-7b and 5-7c indicate how increasing pressure increases CO_2 capture and hence methane mole fraction in the vapor. Consequently, mole fraction of CO_2 in vapor decreases.

The figures contain the experimental data, simulations of the performance of the lab-scale system, and simulations of a commercial power plant using a commercial scale version of this technology. The initial increase in capture with increased pressure stems from decreasing vapor mole fractions of the condensable CO_2 with increasing pressure. However, as pressure increases, the methane in the vapor also condenses, creating more liquid in which solid CO_2 can dissolve. At a pressure of about 250 kPa, the condensing methane from the vapor more than compensates for the condensing CO_2 from the vapor, and the capture efficiency begins to decrease. At about 600 kPa, all components in the vapor phase have completely condensed. From this point on, the capture efficiency does not change with pressure because the solubility of CO_2 in the liquid mixture is insensitive to pressure.

The experimental trends are consistent with the predictions, though the 3-phase predictions require some sophistication. The Aspen simulations used here depend on some workarounds in the

software, which can only form or destroy solids in a Gibbs reactor. Neither Aspen nor any other commercial process simulation software known to us is capable of forming and destroying solids in heat exchangers, turbines, etc. Therefore, a series of Gibbs reactors represents the desublimating heat exchangers, which only approximates the actual temperature profile in a heat exchanger. SES maintains in-house process modeling software that more robustly and accurately calculates desublimating heat exchanger performance.

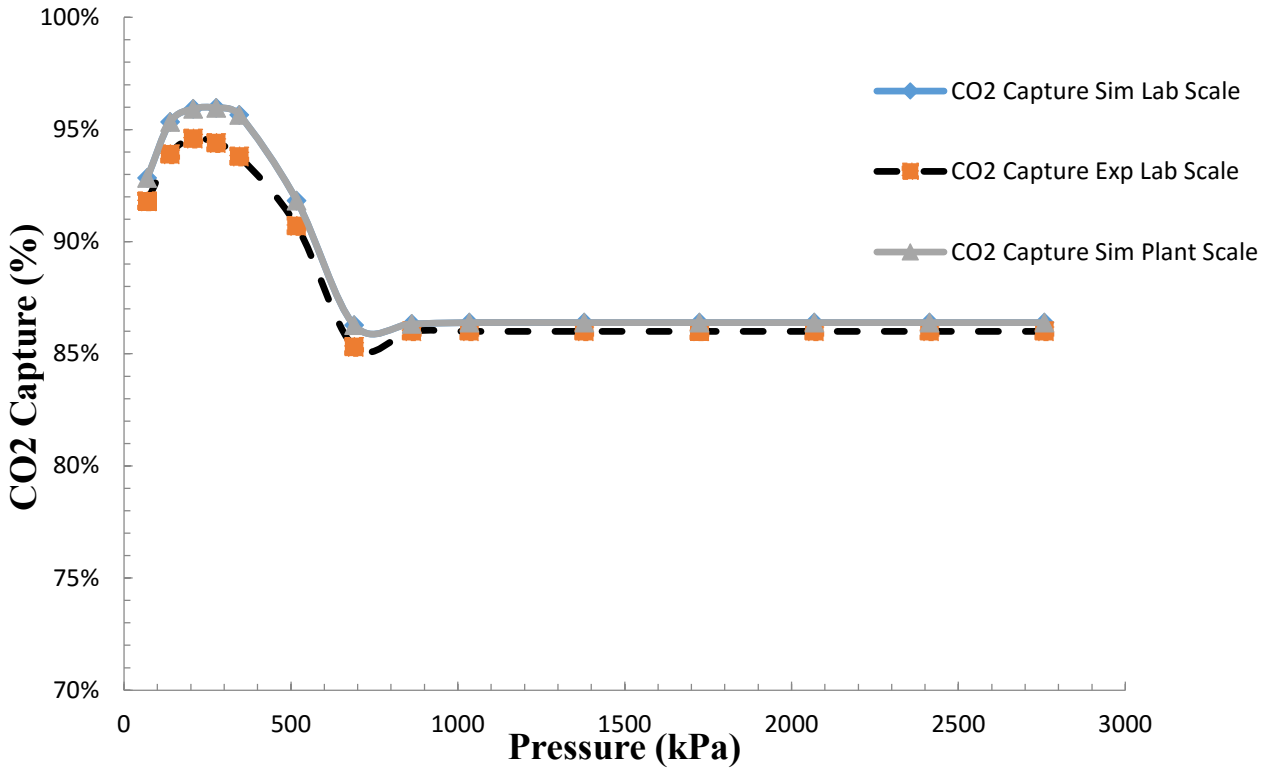

a)

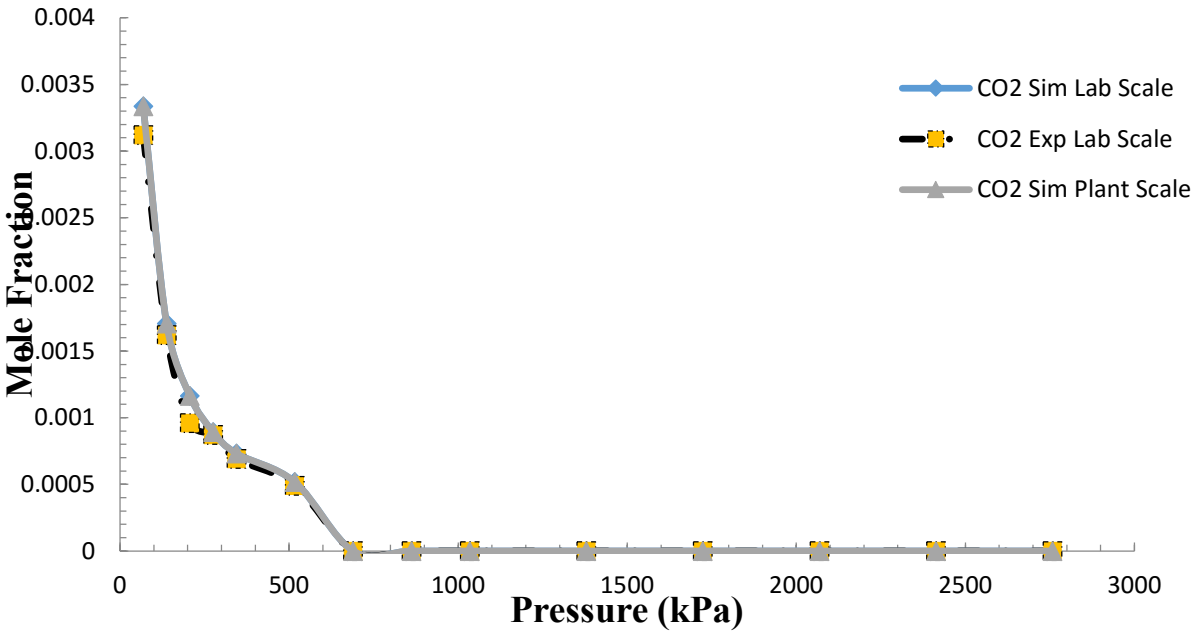

b)

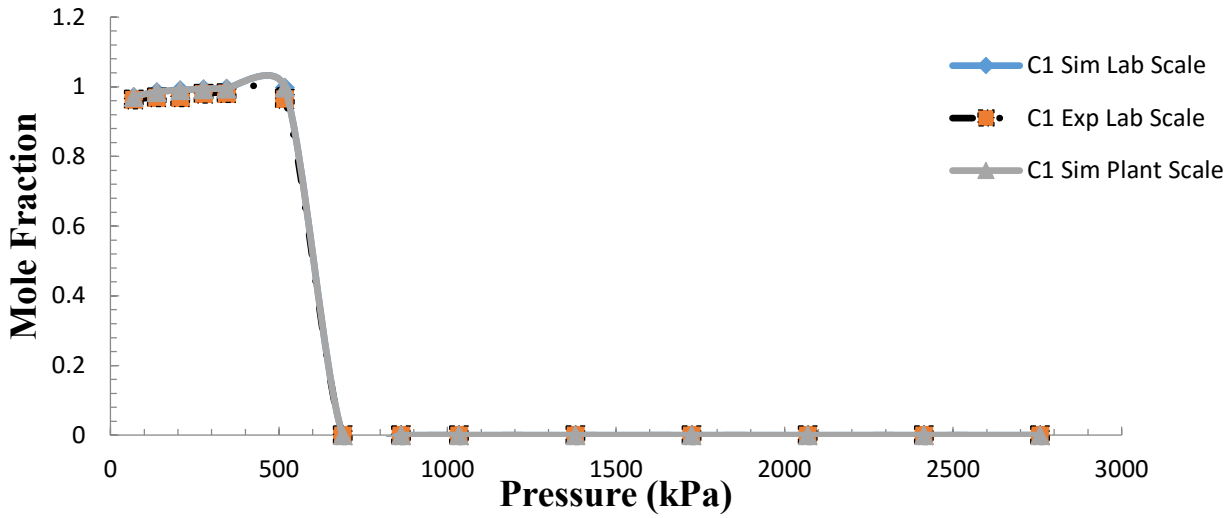

c)

Figure 5-7. Effect of pressure on a) CO_2 capture b) CO_2 mole fraction in vapor c) methane mole fraction in vapor. The simulations at lab and plant scale are essentially identical.

5.4.2. Economics

Capital and operating costs of the system depends as much or more on market demands and raw materials costs as on equipment size and type, as has been painfully obvious to the natural gas industry in the last decade. No economic analysis is capable of anticipating these market-based fluctuations. The approach used here relies on a consistent method to predict costs and to compare them across designs, with full recognition that actual costs may vary substantially based on unforeseen market shifts.

Capital and utility costs for both a skid-scale system and the experimental model are given in Table 5-2. Considering the CO_2 content in the feed stream and feed stream flow rates, these values are compared with other CO_2 removal systems, see Figure 5-8 [67].

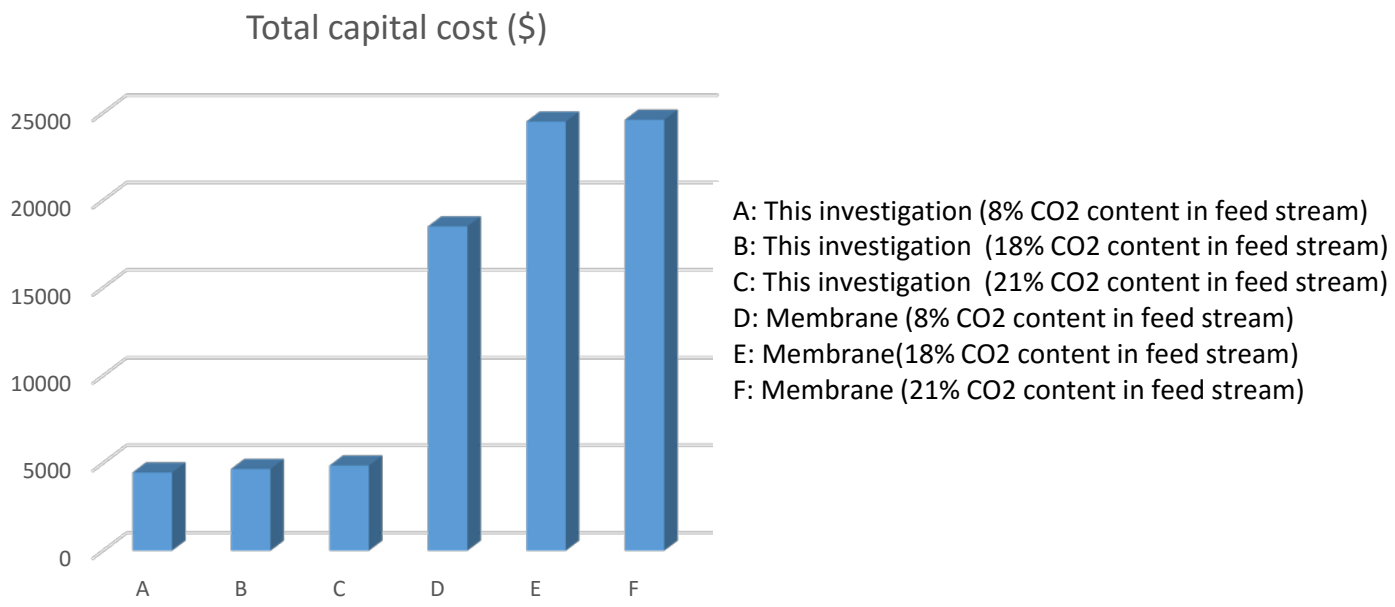

a)

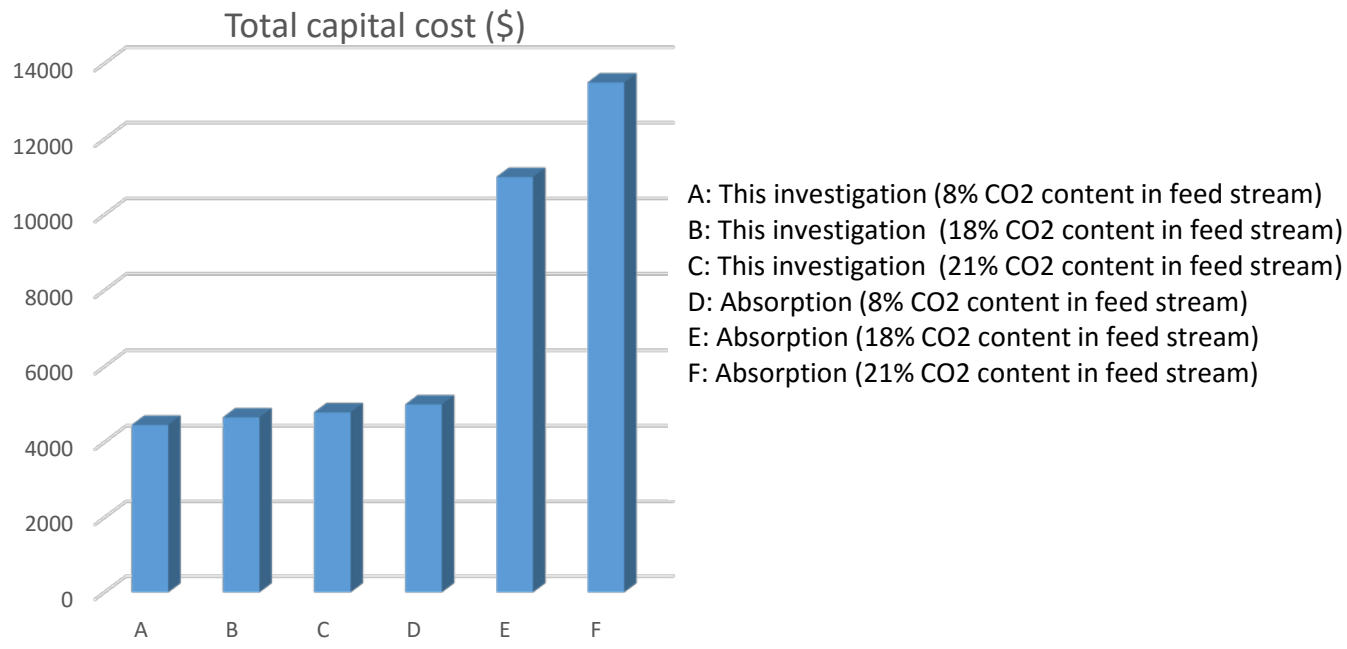

b)

Figure 5-8. Total cost comparison for different systems: a) the new system (494 cm^3/min feed stream & 8,18 and 21% CO_2 content in feed stream) versus membrane (494 cm^3/min feed stream & 8,18 and21% CO_2 content in feed stream) b) the new system (9834 cm^3/min feed stream & 8,18 and 21% CO_2 content in feed stream) versus absorption (9834 cm^3/min NG & 8,18 and 21% CO_2 content in feed stream)

Table 5-2. Total capital and operating costs for this investigation (3100 cm^3/min feed stream, 99% CO_2 capture) experimental versus simulation

Model	Total capital cost (USD)	Water cost (USD /h)	Electricity (USD /h)
Bench-Skid (Exp)	4,678	3.47821	11.823
Bench-Skid (Sim)	4,703	3.34972	11.648

An industrial model has also been simulated in Aspen and this result has been obtained:

Table 5-3. Total capital cost for the new industrial system design (1000 kmol/h feed stream, 99% CO_2 capture)

Model	Total capital cost (USD)
Industrial	657,190

5.4.3. Heat exchanger efficiency and exergy losses

This discussion defines heat exchanger efficiency. Insulated heat exchangers conserve enthalpy, so a first-law definition is problematic. That is, the enthalpy flowing out of the system equals that flowing in. Heat exchangers do not involve shaft work, so a second-law definition (work over heat) does not naturally fit the system. Nevertheless, this dissertation proposes a second-law definition for heat exchanger efficiency that is both useful and simple [48, 52, 68]. Fazlollahi et all and Li et all [48, 50] have introduced the exergy losses equations of the heat exchanger. Table 5-4 summarizes the heat exchanger's efficiency and exergy losses associated with this process.

Table 5-4. Heat exchanger efficiency and exergy loss for both simulation and experiment

Parameter	Lab scale Sim	Lab scale Exp	Plant scale Sim
Heat exchanger efficiency (%)	93.4	92.2	93.1
Exergy loss (kW/ kg treated NG)	39.57	44.81	41.42

Chapter 6. Conclusions

Several natural gas liquefaction processes that provide coolant for the energy-storing version of cryogenic carbon capture™ differ in their overall energy demand, exergy loss, heat exchanger efficiencies, capital costs, and operating costs. The processes analyzed and optimized in detail included propane and mixed-refrigerant systems (C3-MR), a modified dual mixed refrigerant system (MDMR), and two single mixed refrigerant systems (SMR 1 and SMR 2). Process simulations for three operation modes provide a basis for comparison:

- Energy storing, where LNG production increases to 40% more than is required by the CCC process, as would be used when excess energy is available on the grid,
- Balanced, where LNG production equals LNG demand from the power plant to run the CCC process, and
- Energy recovery, where LNG production decreases by 70% to decrease the parasitic loss and hence place more power on the grid when demand is low.

The optimal LNG energy demand ranges from 0.2 GJ_e/ton of LNG delivered to the CCC process or higher, depending on the specifics of the design. The SMR process has the lowest demand. During energy storage, energy demand increases significantly as excess LNG is produced. During energy recovery, energy demand decreases as stored LNG supplements the LNG produced from this process. The exergy analytical results show that the compressors and water coolers primarily contribute to total exergy loss. Results show that for SMR models energy input requirements have been reduced to 0.06 kW/kg NG for Balanced, 0.008 kW/kg NG for ER and 0.07 kW/kg NG for ES which are the minimum compared to other models. SMR models have the

highest heat exchanger's efficiencies of above 90% for Balanced, highest efficiencies for ER. For ES, MDMR has the highest efficiency. C3-MR has the exergy loss of 0.0046 kW/kg NG for ER, 0.0356 kW/kg NG for Balanced and 0.0393 kW/kg NG for ES and is lower than the other system models. MDMR is the most expensive model at 71,146,000 USD capital cost whilst C3-MR has the highest electricity cost of 3389.7 (USD/h) and 121.2 ($/h) for water.

The SMR process provides the most efficient overall design. Energy storage increases energy demand significantly compared to the other states since it requires excess LNG. This operating mode most closely resembles traditional LNG production. During energy recovery, the energy demand decreases relative to the other states since stored LNG supplements the amount produced from this process and heat integration from the excess LNG decreases energy consumption. Heat exchanger efficiencies in all three cases remain nearly constant except for short transients. Exergy analysis has been studied for major equipment in this process and indicates the importance of high efficiency for heat exchangers. Transient techniques for modeling include K-values, U-values, zone configuration and heat transfer rating. Optimum energy input requirements of 0.008 kW/kg NG for ER, 0.0613kW/kg NG for B and 0.0706 kW/kg NG for ES have been obtained. The highest efficiencies of 93.86% for B, 80.21% for ES and 74.35% for ER have been achieved. Exergy losses of 1%, 2% and 13% for the heat exchanger in the three cases confirm the high efficiency for this unit. The optimized PID controller takes 2-7 minutes for the MR flow and heat exchanger temperatures to reach the required set points. As illustrated, in moving through transitions, the internal temperatures change over a large range in a short amount of time. Depending on heat exchanger construction and operation details, these changes could exceed the allowable temperature stress limits of the heat exchangers. The heat exchanger in THED has a

constant transient efficiency of 78-82%. Transient responses during ramping and step changes indicate typical system responses to changes in load. Temperature profiles illustrate low exergy losses for the heat exchangers after their internal temperature profiles adjust to the new flow rates. Transient efficiencies of the heat exchangers indicate that heat exchanger efficiencies vary considerably as the internal temperature profiles adjust.

Aspen HYSYS simulations of two natural gas liquefaction processes, that provide coolant for the energy storing version of the CCC, indicate process performance in transient modes. During energy storage, the energy demand increases significantly since excess LNG is produced. During energy recovery, the energy demand decreases since stored LNG supplements the amount produced from the process. The THED and DHED processes differ in the construction of heat exchangers, the first being a traditional LNG design and the second being an innovative new dynamic heat exchanger design. The dynamic heat exchangers are more efficient and demand less energy in general but the versions used here (retrofit version) are slightly less efficient and demand slightly more energy under balanced conditions if they are constrained to be the same total size as the traditional heat exchangers. The balanced behavior could be made equally efficient if the heat exchanger size increases, but this analysis compares comparably sized heat exchangers.

NG pretreatment systems have been simulated to remove more than 99% of the CO_2 from NG. Steady-state simulations with Aspen plus illustrate the effects of different parameters on CO_2 capture percentage. Vapor mole fractions of CO_2 and methane also have been investigated by changing the pressure at constant temperature. An experimental bench-scale apparatus verified the simulation results. Exergy loss and heat exchange efficiency have been calculated and equipment

sizes and cost estimates are complete. A total capital cost of 4,678 USD, water cost of 3.4782 USD/h and electricity of 11.823 USD/ h have been obtained for experimental data that agree with simulation results. The results confirm the low exergy losses of 39.57 kW/ kg treated NG for simulation and 44.8 kW/ kg treated NG for bench-scale apparatus. High heat exchanger efficiency of +90% has been achieved. High pressure and low methane in NG composition results in high CO_2 capture, though the capture efficiency reaches a maximum at intermediate pressure.

It is recommended that these following areas be addressed in the future:

1. Application of CCC with energy storage to industrial-scale processes
2. Development of CO_2 separation to NG processing independent of CCC
3. Using dynamic heat exchangers to isolate process upsets in otherwise highly integrated processes
4. Applying de-sublimating processes to other separation processes.

Chapter 7. Nomenclature

Parameters and variables

a the attractive parameter [Pa(m^3/mole)^2]

A dimensionless attractive parameter

b the effective molecular volume [m^3/mole]

B dimensionless effective molecular volume in Peng-Robinson equation of state

E exergy [kW]

ΔE_x exergy losses of the equipment [kW]

E_{in} inlet exergy of the equipment [kW]

E_{out} outlet exergy of the equipment [kW]

g_i Gibbs energy of stream i [kJ/kg]

$\hat{g}_i$ specific Gibbs energy of stream i [kJ/kg]

$\hat{h}_i$ specific enthalpy of stream i [kJ/kg]

H_0 enthalpy at ambient temperature [kJ]

H_{in} inlet enthalpy of the equipment [kJ]

H_{out} outlet enthalpy of the equipment [kJ]

k pressure flow coefficient [$\frac{kg}{h}\times\sqrt{\frac{kg}{\frac{m^3}{kPa}}}$]

k_{ij} binary interaction coefficient

m_i mass flow rate of stream i [kg/h]

P pressure [kPa]

ΔP total pressure drop [kPa]

q_{LNG} mass flow of the produced LNG [kg NG]

R universal gas constant

S entropy [kJ/K]

S_i entropy of stream i in efficiency equation [kJ/K]

$\hat{s}_i$ specific entropy of stream i [[kJ/kg K]

S_0 entropy at ambient temperature [kJ/K]

S_{in} inlet entropy of the equipment [kJ/K]

S_{out} outlet entropy of the equipment [kJ/K]

T temperature [K, ° C]

T_i Temperature of stream i [K]

t time [s]

T_0 ambient temperature [K]

$T_{w,in}$ Temperature of water into the water cooler [K]

$T_{w,out}$ Temperature of water out of the water cooler [K]

UA overall heat transfer coefficient [kJ/°C h]

V volume [m^3]

v molar volume [m^3/mole]

W power [kW]

W_c power consumption of the compressor [kW]

W_e power consumption of the expander [kW]

Z compression factor

z_i mole fraction for the component of i

z_j mole fraction for the component of j

η heat exchanger's efficiency

ρ density[kg/m^3]

Acronyms

B balanced case

CCC cryogenic carbon capture™

C3MR propane-pre-cooled mixed refrigerant

ER energy recovery case

ES energy storage case

LNG liquefied natural gas

MITA minimum internal temperature approach

MDMR modified dual mixed refrigerant

MR mixed refrigerant

NG natural gas

PR Peng-Robinson equation of state

SMR single mixed refrigerant

References

[1] EIA.2005. International energy outlook 2005.http://www.eia.doe.gov/oiaf/archive/aeo05/pdf/0383, 2005.

[2] Aspelund A, Gundersen T, "A liquefied energy chain for transport and utilization of natural gas for power production with CO_2 capture and storage e part 1" *Appl. Energy*. 2009; 86: 781-792.

[3] Aspelund A, Gundersen T, "A liquefied energy chain for transport and utilization of natural gas for power production with CO_2 capture and storage e part 2: the offshore and the onshore processes" *Appl. Energy* 2009; 86: 793- 804.

[4] Aspelund A, Gundersen T, "A liquefied energy chain for transport and utilization of natural gas for power production with CO_2 capture and storage part 3: the combined carrier and onshore storage" *Appl. Energy.* 2009; 86: 805-814.

[5] Aspelund A, Gundersen T, "A liquefied energy chain for transport and utilization of natural gas for power production with CO_2 capture and storage part 4: sensitivity analysis of transport pressures and benchmarking with conventional technology for gas transport" *Appl. Energy.* 2009*;* 86: 815-825.

[6] Thomas S, Dawe RA, "Review of ways to transport natural gas energy from countries which do not need the gas for domestic use" *Energy.* 2003; 28:1461-1477.

[7] Sloan ED, "Fundamental principles and applications of natural gas hydrates" *Nature.* 2003; 426: 353-363.

[8] Javanmardi J, Nasrifar K, Najibi SH, Moshfeghian M, "Economic evaluation of natural gas hydrates as an alternative for natural gas transportation" *Appl. Therm. Eng.* 2005; 25: 1708-1723.

[9] Wood DA, Nwaoha C, Towler BF, "Gas-to-liquids (GTL): a review of an industry offering several routes for monetizing natural gas" *J. Nat. Gas Sci. Eng*. 2012; 9: 196-208.

[10]. Khalilpour R, Karimi IA, "Evaluation of utilization alternatives for stranded natural gas "*Energy.* 2012; 40: 317-328.

[11] Aspelund A, Gundersen T, "A liquefied energy chain for transport and utilization of natural gas for power production with CO_2 capture and storage part 1" *Appl. Energy*. 2009; 86: 781-792.

[12] Sakmar SL, "Energy for the 21st Century: Opportunities and Challenges for Liquefied Natural Gas (LNG)" Edward Elgar Publishing, 2013.

[13] Jensen JB, Skogestad S, "Optimal operation of a mixed fluid cascade LNG plant" *Computer Aided Chem Eng*. 2006; 21:1569-1574.

[14] Sultan P, "Semester project titled as "Natural Gas Liquefaction Process on Board an LNG-FPSO"" NTNU, January 2011.

[15] Khan MS, Lee M, "Design optimization of single mixed refrigerant natural gas liquefaction process using the particle swarm paradigm with nonlinear constraints" *Energy*. 2013; 49: 146–155.

[16] Xu Xa, Liu J , Cao L, Pang W, "Automatically varying the composition of a mixed refrigerant solution for single mixed refrigerant LNG (liquefied natural gas) process at changing working conditions" *Energy*. 2014; 64: 931-941.

[17] Alabdulkarem A, Mortazavi A, Hwang Y, Radermacher R, Rogers P, "Optimization of propane pre-cooled mixed refrigerant LNG plant" *Appl Therm Eng*. 2011; 31: 1091-1098.

[18] He T, Ju Y. A novel conceptual design of parallel nitrogen expansion liquefaction process for small-scale LNG (liquefied natural gas) plant in skid-mount packages. Energy. 2014; 75: 349-359.

[19] Remeljej CW, Hoadley AFA, "An exergy analysis of small-scale liquefied natural gas (LNG) liquefaction processes" *Energy*. 2006; 31: 2005-2019.

[20] Brendeng E, Neksa P, "Method for Liquefaction of Gas" U.S. Patent Application 12/447,978, 2007.

[21] Neksa P, Brendeng E, Drescher M, Norberg B, "Development and analysis of a natural gas reliquefaction plant for small gas carriers" *J Nat Gas Sci Eng*. 2010; 2: 143-149.

[22] Li QY, Ju YL, "Design and analysis of liquefaction process for offshore associated gas resources" *Appl Therm Eng*. 2010; 30: 2518-2525.

[23] Gu A, Lu X, Wang R, Shi Y, Lin W, "Liquefied Natural Gas Technology" China Machine Press, 2004.

[24] Kirillov NG, "Analysis modern natural gas liquefaction technologies" *Chem. Pet. Eng.* 2004; 40: 401-406.

[25] Remeljej CW, Hoadley AFA, "An exergy analysis of small-scale liquefied Natural gas (LNG) liquefaction processes, a BHP Billiton",180 Lonsdale Street, Melbourne, Vic. 3000, Australia Department of Chemical Engineering, Building 36, Clayton Campus, Monash University, Vic. 3800, Australia, 2004.

[26] Chang HM, Chung MJ, Lee S, Choe KH , "An efficient multi-stage Brayton–JT cycle for liquefaction of natural gas" Hong Ik University, Seoul 121-791, Republic of Korea ,b Korea Gas Corporation, Incheon 406-130, Republic of Korea Journal homepage: www.elsevier.com/locate/cryogenics.

[27] Barclay M, "Selecting offshore LNG processes," *LNG J* 2005; 10: 34-36.

[28] Gao T, Lin W, Gu A, Gu M, "Coalbed methane liquefaction adopting a nitrogen expansion process with propane pre-cooling". *Appl. Energy.* 2010; 87: 2142- 2147.

[29] Mahabadipour H, Ghaebi H, "Development and comparison of two expander cycles used in refrigeration system of olefin plant based on exergy analysis" *Appl. Therm. Eng.* 2013; 50: 771-780.

[30] Li Y, Pan W, "Offshore adaptability of the CO_2 pre-cooling dual nitrogen expander natural gas liquefaction process" *Adv. Mater. Res.* 2013; 608: 1369- 1374.

[31] Terry L, "Comparison of liquefaction process" *LNG J.* 1998; 21: 28–33.

[32] Yoshitugi K, Moritaka N, "Development of liquefaction process for natural gas" *J of Chem Eng of Japan.* 1997; 30: 626–630.

[33] Lun LY, Xie YB, Yang XL, "LNG peak-shaving proposal based on pressure energy recovery of pipe gas" *Nat. Gas Ind.* 2006; 26: 114-116.

[34] Huang ZG, Wang RS, Shi YM, Gu AZ, "Review of mini-natural gas liquefier" *Cryogenics.* 2002; 6: 59-62.

[35] Shirazi MMH, Mowla D, "Energy optimization for liquefaction process of natural gas in peak shaving plant" *Energy.* 2010; 35: 2878-2885.

[36] Cao WS, Lu XS, Lin WS, Gu AZ, "Parameter comparison of two small-scale natural gas liquefaction processes in skid-mounted packages" *Appl. Therm. Eng.* 2006; 26:898-904.

[37] Maunder AD, Skinner GF, "Method for Liquefying Methane-rich Gas" The United States, 0255616A1, 2004.

[38] Alabdulkarem A, Mortazavi A, Hwang Y, Radermacher R, Rogers P, "Optimization of propane pre-cooled mixed refrigerant LNG plant" *Appl. Therm. Eng.* 2011; 31: 1091-1098.

[39] Shen DM, Feranades F, Moreir JRS, "Using gas pipeline pressure to liquefy natural gas or generate electricity" *Hydrocarb. Process.* 2006; 85: 47-50.

[40] Xiong YQ, Hua B, Luo DX, "Pipeline gas liquefaction flow for gas peak shaving and light hydrocarbons recovery" *Nat Gas Ind* . 2006; 26:130-132.

[41] Gao T, Lin WS, Gu AZ, Gu M, Coalbed methane liquefaction adopting a nitrogen expansion process with propane pre-cooling. *Appl. Energy* 2010; 87: 2142-2147.

[42] He TB, Ju YL, "A novel process for small-scale pipeline natural gas liquefaction" *Applied Energy.* 2014; 115: 17–24.

[43] Yuan Z, Cui M, Xie Y, Li C, "Design and analysis of a small-scale natural gas liquefaction process adopting single nitrogen expansion with carbon dioxide pre-cooling" *Appl Therm Eng.* 2014; 64: 139-146.

[44] Baxter LL, "Carbon Dioxide Capture from Flue Gas" Patent US 20110226010 A1, 2011.

[45] Baxter LL, "System and Methods for Integrated Energy and Cryogenic Carbon Capture" Patent WO 2013062922 A1, 2013.

[46] Safdarnejad SM, Hedengren JD, Baxter LL, "Plant-level dynamic optimization of Cryogenic Carbon Capture with conventional and renewable power sources" *Applied energy*. 2015; 149: 354-466.

[47] Jensen MJ, Russel CS, Bergeson D, Hoeger CD, Frankman DJ, Bence CS, Baxter LL, "Prediction and validation of external cooling loop cryogenic carbon capture (CCC-ECL) for full-scale coal-fired power plant retrofit" *Int J of Greenhouse Gas Control*. 2015; 42: 200-212.

[48] Fazlollahi F, Bown A, Ebrahimzadeh E, Baxter LL, "Design and analysis of the natural gas liquefaction optimization process- Energy Storage of Cryogenic Carbon Capture (CCC ES)" *Energy*. 2015; 90: 244-257.

[49] Jensen MJ, Energy Processes Enabled by Cryogenic Carbon Capture, a PhD dissertation in Brigham Young University February 2014.

[50] Li QY, Ju YL, "Design and analysis of liquefaction process for offshore associated gas resources" *Appl Therm Eng*. 2010; 30: 2518-2525.

[51] Yuan Z, Cui M, Xie Y, Li C, "Design and analysis of a small-scale natural gas liquefaction process adopting single nitrogen expansion with carbon dioxide pre-cooling" *Appl Therm Eng*. 2014; 64: 139-146.

[52] Ebrahimzadeh E, Wilding P, Frankman D, Fazlollahi F, Baxter LL, "Theoretical and experimental analysis of dynamic plate heat exchanger: non-retrofit configuration" *Applied Thermal Eng.* 2015; 93: 1006-1019.

[53] Fazlollahi F, Bown A, Ebrahimzadeh E, Baxter LL, "Transient natural gas liquefaction and its application to CCC-ES (energy storage with cryogenic carbon capture™)" *Energy*. 2016; 103: 369-384.

[54] Kemp IC, "Pinch Analysis and Process Integration" Second ed. Elsevier: Oxford, 2007.

[55] Wei L, Geng P, "A review on natural gas/diesel dual fuel combustion, emissions and performance" *Fuel Processing Technology.* 2016; 142: 264-278.

[56] Tennyson RN, Schaaf RP, "Guideline can help choose Proper Process for Gas Treating Plants," *Oil and Gas Journal*, 1977; 10: 78-85.

[57] He X, Hagg MB, "Hybrid FSC membrane for CO_2 removal from natural gas: experimental. Process simulation, and economic feasibility analysis" *AIChE J*. 2014; 60, 4174–4184.

[58] Sohbi B, Meakaff M, Emtir M, "The using of mixing amines in an industrial gas sweetening plant" *World Acad. Sci. Eng. Technol*. 2007; 31: 301– 305.

[59] Yingjie Li, Wang W, Cheng X, Su M, Ma X, Xie X, "Simultaneous CO_2/HCl removal using carbide slag in repetitive adsorption/desorption cycles" *Fuel.* 2015; 142:21-27.

[60] Dou B, Wang C, Song Y, Chen H, Jianga B, Yang M, Xu Y, "Solid sorbents for in-situ CO_2 removal during sorption-enhanced steam reforming process: A review" *Renewable and Sustainable Energy Reviews.* 2016; 53: 536-546.

[61] Álvarez-Gutiérrez N, Gil MV, Rubiera F, Pevida C, "Adsorption performance indicators for the CO_2/CH_4 separation" *Application to biomass-based activated carbons*. 2016; 142: 361-369.

[62] He X, Kim TJ, Hägg MB, "Hybrid fixed-site-carrier membranes for CO_2 removal from high pressure natural gas: Membrane optimization and process condition investigation" *Journal of Membrane Science.* 2014; 470:266-274.

[63] Staudt-Bickel C, Koros WJ, "Improvement of CO_2/CH_4 separation characteristics of polyimides by chemical crosslinking" *Journal of Membrane Science.* 155 (1999) 145-154.

[64] Trends in global CO_2 emissions, 2013 reports published by PBL Netherlands environmental assessment agency.

[65] Mesilaakso M, Ratio M, Encyclopedia of analytical chemistry; Wiley: New York, 2000; PP. 899.

[66] Rautio M, Recommended Operating Procedures for Sampling and Analysis in the Verification of Chemical Disarmament, 1993.

[67] Gadelhaa TS, Guimarãesa ARS, Nakaoa A, Araújoa OQF, Medeirosa JLD, A Comparative Economical Analysis of Technologies for CO_2 Removal from Offshore Natural Gas, I.A. Karimi and Rajagopalan Srinivasan (Editors), Proceedings of the 11th International Symposium on Process Systems Engineering, 15-19 July 2012, Singapore.

[68] Ebrahimzadeh E, Wilding P, Frankman D, Fazlollahi F, Baxter LL, "Theoretical and experimental analysis of dynamic heat exchanger: Retrofit configuration" *Energy.* 2016; 96: 545-560.

Appendix

A. VBA optimization codes for the SMR

```
Option Explicit

'This is a function that changes variables to minimize the energy usage
    Function EnergyMin(FlowMR As Double, TempMR As Double, Temp2 As Double, Temp6 As Double)

'Connect VBA to Active HYSYS Document
    Set HysApp = CreateObject("HYSYS.Application")
    HysApp.Visible = True
    Set SimCase = HysApp.ActiveDocument

'Assign appropriate HYSYS objects to variables
    Set StreamMR = SimCase.Flowsheet.Streams.Item("MR")
    Set Stream2 = SimCase.Flowsheet.Streams.Item("2")
    Set QTotal = SimCase.Flowsheet.EnergyStreams.Item("Q-Total")
    Set Stream6 = SimCase.Flowsheet.Streams.Item("6")
    Set LNG = SimCase.Flowsheet.Operations.Item("LNG")

'Turn off solver
    SimCase.Solver.CanSolve = False

'Send Stream 5 temperature to HYSYS
    StreamMR.Temperature.SetValue TempMR, "C"
    Stream2.Temperature.SetValue Temp2, "C"
    Stream6.Temperature.SetValue Temp6, "C"

'Send other variables to HYSYS
    StreamMR.MolarFlow.SetValue FlowMR, "kgmole/h"

'turn on solver
    SimCase.Solver.CanSolve = True

'Get objective function from HYSYS
    netEnergy = QTotal.Power.GetValue("kW")
    MinApproachConstraint = LNG.MinApproach.GetValue("C")
```

```
'Return the work value
      Off = 0
   If MinApproachConstraint < 1 Then
      Off = (1 - MinApproachConstraint) * 100000
   End If

   EnergyMin = netEnergy + Off

'Record Value in macroHistory.csv
   Dim Data As String, myFile As String

'Build string
   Data = EnergyMin & "," & netEnergy & "," & TempMR & "," & Temp2 & "," & FlowMR & "," &
MinApproachConstraint & "," & Temp6

'Add string
   myFile = "C:\Users\ke7kto\Desktop\Optimizer\macroHistory.csv"
   Open myFile For Append As #1
   Print #1, Data
   Close #1
End Function
```

B. VBA optimization codes for the MDMR

```
Option Explicit
Public HysApp As HYSYS.Application
Public SimCase As SimulationCase

'Stream Varibles
Public StreamHot As ProcessStream
Public Stream5 As ProcessStream
Public Stream2 As ProcessStream
Public StreamCold As ProcessStream
Public Stream14 As ProcessStream
Public StreamMet As ProcessStream
Public Stream20 As ProcessStream

'Operation Unit Varibles
Public LNG As LngOp
Public LNGM As LngOp
Public K_Hot As ExpandOp
Public K_Hot2 As CompressOp
Public K_Cold As CompressOp
Public P_Cold As PumpOp
Public K_Met As CompressOp
Public K_Met2 As ExpandOp
Public P_NG As PumpOp

'Other Varibles
Public compEnergy As Double
```

```
Public turbEnergy As Double
Public netEnergy As Double
Public MinApproachConstraint1 As Double
Public MinApproachConstraint2 As Double
Public VaporFraction1 As Double
Public LiqueFraction As Double
Public VaporFraction2 As Double
Public VaporFraction3 As Double
Public Off1 As Double
Public Off2 As Double
Public Off3 As Double
Public Off4 As Double
Public Off5 As Double
Public Off6 As Double
Public Off As Double

'This is a function that takes the varibles from excel and uses them in the function
   Function EnergyMin(Temp5 As Double, TempHot As Double, FlowHot As Double, Temp14 As Double,
_
   FlowCold As Double, FlowMet As Double)

'Connect VBA to Active HYSYS Document
   Set HysApp = CreateObject("HYSYS.Application")
   HysApp.Visible = True
   Set SimCase = HysApp.ActiveDocument

'Assign appropriate HYSYS objects to variables
     Set StreamHot = SimCase.Flowsheet.Streams.Item("Hot")
   Set Stream5 = SimCase.Flowsheet.Streams.Item("5")
   Set Stream2 = SimCase.Flowsheet.Streams.Item("2")
   Set StreamCold = SimCase.Flowsheet.Streams.Item("Cold")
   Set Stream14 = SimCase.Flowsheet.Streams.Item("14")
   Set StreamMet = SimCase.Flowsheet.Streams.Item("Met")
   Set Stream20 = SimCase.Flowsheet.Streams.Item("20")
   Set LNG = SimCase.Flowsheet.Operations.Item("LNG")
   Set LNGM = SimCase.Flowsheet.Operations.Item("LNG-Met")
   Set K_Hot = SimCase.Flowsheet.Operations.Item("K-Hot")
   Set K_Hot2 = SimCase.Flowsheet.Operations.Item("K-Hot2")
   Set K_Cold = SimCase.Flowsheet.Operations.Item("K-Cold")
   Set P_Cold = SimCase.Flowsheet.Operations.Item("P-Cold")
   Set K_Met = SimCase.Flowsheet.Operations.Item("K-Met")
   Set K_Met2 = SimCase.Flowsheet.Operations.Item("K-Met2")
   Set P_NG = SimCase.Flowsheet.Operations.Item("P-NG")

'Turn off solver
   SimCase.Solver.CanSolve = False

'Send Stream temperatures to HYSYS
   Stream5.Temperature.SetValue Temp5, "C"
   StreamHot.Temperature.SetValue TempHot, "C"
   Stream14.Temperature.SetValue Temp14, "C"
```

```
'Send Stream Pressures and Flow Rates to HYSYS
   StreamHot.MolarFlow.SetValue FlowHot, "kgmole/h"
   StreamCold.MolarFlow.SetValue FlowCold, "kgmole/h"
   StreamMet.MolarFlow.SetValue FlowMet, "kgmole/h"

'turn on solver
   SimCase.Solver.CanSolve = True

'Gets values from HYSYS for Calculations and Contraints
   compEnergy = K_Hot2.Energy.GetValue("kW") + K_Cold.Energy.GetValue("kW") +
K_Met.Energy.GetValue("kW")
   turbEnergy = -K_Hot.Energy.GetValue("kW") + P_Cold.EnergyStream.Power.GetValue("kW") -
K_Met2.Energy.GetValue("kW") _
   + P_NG.EnergyStream.Power.GetValue("kW")
   netEnergy = compEnergy + turbEnergy
   MinApproachConstraint1 = LNG.MinApproach.GetValue("C")
   MinApproachConstraint2 = LNGM.MinApproach.GetValue("C")
   VaporFraction1 = Stream2.VapourFraction.GetValue()
   LiqueFraction = Stream14.LiquidFraction.GetValue()
   VaporFraction2 = Stream20.VapourFraction.GetValue()
   VaporFraction3 = Stream5.VapourFraction.GetValue()

'These if statements prevent the solver from letting temperature crosses happen and control vap and liq
fractions
        Off1 = 0
        Off2 = 0
        Off3 = 0
        Off4 = 0
        Off5 = 0
        Off6 = 0
        Off = 0

   If MinApproachConstraint1 < 1 Then
      Off1 = (1 - MinApproachConstraint1) * 1000000
   End If

   If MinApproachConstraint2 < 1 Then
      Off2 = (1 - MinApproachConstraint2) * 100000
   End If

   If VaporFraction1 < 1 Then
      Off3 = 30000
   End If

   If VaporFraction2 < 1 Then
      Off4 = 30000
   End If

   If LiqueFraction < 1 Then
      Off5 = 30000
```

```
    End If

    If VaporFraction3 < 1 Then
       Off6 = 30000
    End If

    Off = Off1 + Off2 + Off3 + Off4 + Off5 + Off6

    EnergyMin = netEnergy + Off

'Record Value in macroHistory.csv
    Dim Data As String, myFile As String

'Build string
    Data = EnergyMin & "," & netEnergy & "," & Temp5 & "," & TempHot & "," & FlowHot & "," &
Temp14 & "," & _
    FlowCold & "," & FlowMet & "," & MinApproachConstraint1 & "," & MinApproachConstraint2 _
    & "," & VaporFraction1 & "," & LiqueFraction & "," & VaporFraction2 & "," & VaporFraction3

'Add string
    myFile = "C:\Users\ke7kto\Desktop\Optimizer\macroHistory.csv"
    Open myFile For Append As #1
    Print #1, Data
    Close #1
End Function
```

C. VBA optimization codes for the C3-MR

```
Option Explicit
Public HysApp As HYSYS.Application
Public SimCase As SimulationCase

'Stream Varibles
Public StreamMR As ProcessStream
Public Stream2 As ProcessStream
Public QTotal As ProcessStream
Public Stream6 As ProcessStream

'Operation Unit Varibles
Public LNG As LngOp

'Other Varibles
Public compVec As Variant
Public netEnergy As Double
Public MinApproachConstraint As Double
Public Off As Double


'This is a function that takes the variables and changes them to minimize the energy usage
```

```
    Function EnergyMin(FlowMR As Double, TempMR As Double, Temp2 As Double)

'Connect VBA to Active HYSYS Document
    Set HysApp = CreateObject("HYSYS.Application")
    HysApp.Visible = True
    Set SimCase = HysApp.ActiveDocument

'Assign appropriate HYSYS objects to variables
    Set StreamMR = SimCase.Flowsheet.Streams.Item("MR")
    Set Stream2 = SimCase.Flowsheet.Streams.Item("2")
    Set QTotal = SimCase.Flowsheet.EnergyStreams.Item("Q-Total")
    Set LNG = SimCase.Flowsheet.Operations.Item("LNG")

'Turn off solver
    SimCase.Solver.CanSolve = False

'Send Stream 5 temperature to HYSYS
    StreamMR.Temperature.SetValue TempMR, "C"
    Stream2.Temperature.SetValue Temp2, "C"

'Send other variables to HYSYS
    StreamMR.MolarFlow.SetValue FlowMR, "kgmole/h"

'turn on solver
    SimCase.Solver.CanSolve = True

'Get objective function from HYSYS
    netEnergy = QTotal.Power.GetValue("kW")
    MinApproachConstraint = LNG.MinApproach.GetValue("C")

'Return the work value
        Off = 0
    If MinApproachConstraint < 1 Then
        Off = (1 - MinApproachConstraint) * 100000
    End If

    EnergyMin = netEnergy + Off

'Record Value in macroHistory.csv
    Dim Data As String, myFile As String

'Build string
    Data = EnergyMin & "," & netEnergy & "," & TempMR & "," & Temp2 & "," & FlowMR & "," &
MinApproachConstraint

'Add string
    myFile = "C:\Users\ke7kto\Desktop\Optimizer\macroHistory.csv"
    Open myFile For Append As #1
    Print #1, Data
    Close #1
End Function
```

D. VBA optimization codes for MPC

MPC has three sets of code. The first one calculates temperature difference and it is as follows:

```
Option Explicit
Public HysApp As HYSYS.Application
Public SimCase As SimulationCase

'Stream Varibles
Public Stream3 As ProcessStream
Public Stream1 As ProcessStream
Public Stream7 As ProcessStream
Public Stream8 As ProcessStream
Public Stream11 As ProcessStream
Public Stream13 As ProcessStream
Public Stream12 As ProcessStream
Public Stream10 As ProcessStream
Public Stream9 As ProcessStream
Public Stream6 As ProcessStream
Public Stream5 As ProcessStream
Public Stream4 As ProcessStream

'Operations
Public LNG As LngOp

'Enthalpy Values
Public H3 As Double
Public H1 As Double
Public H7 As Double
Public H8 As Double
Public H11 As Double
Public H13 As Double
Public H12 As Double
Public H10 As Double
Public H9 As Double
Public H6 As Double
Public H5 As Double
Public H4 As Double

'Heat Capacity Values
Public Cp3 As Double
Public Cp1 As Double
Public Cp7 As Double
Public Cp8 As Double
Public Cp11 As Double
Public Cp13 As Double
Public Cp12 As Double
Public Cp10 As Double
```

```
Public Cp9 As Double
Public Cp6 As Double
Public Cp5 As Double
Public Cp4 As Double

'Other
Public MinApproach As Double
Public DeltaT As Double

Function deltaTemp(Flow3 As Double, Flow7 As Double, Flow9 As Double)

Set HysApp = CreateObject("HYSYS.Application")
HysApp.Visible = True
Set SimCase = HysApp.ActiveDocument

Set Stream3 = SimCase.Flowsheet.Streams.Item("3")
Set Stream1 = SimCase.Flowsheet.Streams.Item("1")
Set Stream7 = SimCase.Flowsheet.Streams.Item("7")
Set Stream8 = SimCase.Flowsheet.Streams.Item("8")
Set Stream11 = SimCase.Flowsheet.Streams.Item("11")
Set Stream13 = SimCase.Flowsheet.Streams.Item("13")
Set Stream12 = SimCase.Flowsheet.Streams.Item("12")
Set Stream10 = SimCase.Flowsheet.Streams.Item("10")
Set Stream9 = SimCase.Flowsheet.Streams.Item("9")
Set Stream6 = SimCase.Flowsheet.Streams.Item("6")
Set Stream5 = SimCase.Flowsheet.Streams.Item("5")
Set Stream4 = SimCase.Flowsheet.Streams.Item("4")
Set LNG = SimCase.Flowsheet.Operations.Item("LNG")

SimCase.Solver.CanSolve = False

Stream3.MolarFlow.SetValue Flow3, "kgmole/h"
Stream7.MolarFlow.SetValue Flow7, "kgmole/h"
Stream9.MolarFlow.SetValue Flow9, "kgmole/h"

SimCase.Solver.CanSolve = True

H3 = Stream3.MolarEnthalpy.GetValue("kJ/kgmole")
H1 = Stream1.MolarEnthalpy.GetValue("kJ/kgmole")
H7 = Stream7.MolarEnthalpy.GetValue("kJ/kgmole")
H8 = Stream8.MolarEnthalpy.GetValue("kJ/kgmole")
H11 = Stream11.MolarEnthalpy.GetValue("kJ/kgmole")
H13 = Stream13.MolarEnthalpy.GetValue("kJ/kgmole")
H12 = Stream12.MolarEnthalpy.GetValue("kJ/kgmole")
H10 = Stream10.MolarEnthalpy.GetValue("kJ/kgmole")
H9 = Stream9.MolarEnthalpy.GetValue("kJ/kgmole")
H6 = Stream6.MolarEnthalpy.GetValue("kJ/kgmole")
H5 = Stream5.MolarEnthalpy.GetValue("kJ/kgmole")
H4 = Stream4.MolarEnthalpy.GetValue("kJ/kgmole")

Cp3 = Stream3.MolarHeatCapacity.GetValue("kJ/kgmole-C")
```

```
Cp1 = Stream1.MolarHeatCapacity.GetValue("kJ/kgmole-C")
Cp7 = Stream7.MolarHeatCapacity.GetValue("kJ/kgmole-C")
Cp8 = Stream8.MolarHeatCapacity.GetValue("kJ/kgmole-C")
Cp11 = Stream11.MolarHeatCapacity.GetValue("kJ/kgmole-C")
Cp13 = Stream13.MolarHeatCapacity.GetValue("kJ/kgmole-C")
Cp12 = Stream12.MolarHeatCapacity.GetValue("kJ/kgmole-C")
Cp10 = Stream10.MolarHeatCapacity.GetValue("kJ/kgmole-C")
Cp9 = Stream9.MolarHeatCapacity.GetValue("kJ/kgmole-C")
Cp6 = Stream6.MolarHeatCapacity.GetValue("kJ/kgmole-C")
Cp5 = Stream5.MolarHeatCapacity.GetValue("kJ/kgmole-C")
Cp4 = Stream4.MolarHeatCapacity.GetValue("kJ/kgmole-C")

DeltaT = 0

DeltaT = ((H13 + H11 + H8 + H6 + H5 + H4) / (Cp13 + Cp11 + Cp8 + Cp6 + Cp5 + Cp4) _
- (H12 + H10 + H9 + H7 + H1 + H3) / (Cp12 + Cp10 + Cp9 + Cp7 + Cp1 + Cp3)) * -1

MinApproach = LNG.MinApproach.GetValue("C")
If MinApproach < 1 Then
   DeltaT = (1 - MinApproach) * 1000
End If

deltaTemp = DeltaT

End Function
```

The second one minimizes the temperature difference by adjusting MR and two methanol streams' flow rates and is as follows:

```
Option Explicit
Public HysApp As HYSYS.Application
Public SimCase As SimulationCase
Public Stream1 As ProcessStream
Public Flow1 As Double
Public Stream3 As Double
Public Stream7 As Double
Public Stream9 As Double
Public SE As Double
Public mmr As Double
Public bmr As Double
Public mtankh As Double
Public btankh As Double
Public MRflow As Double
Public TankHflow As Double


Sub Solver()
'Link HYSYS to VBA
Set HysApp = CreateObject("HYSYS.Application")
HysApp.Visible = True
```

```
Set SimCase = HysApp.ActiveDocument

'Sets Stream1 variables to the following code
Set Stream1 = SimCase.Flowsheet.Streams.Item("1")

'This is where the recursion will happen
Flow1 = 11000
Do
   Flow1 = Flow1 - 100
If Flow1 <= 3000 Then Exit Do

'turns solver off
SimCase.Solver.CanSolve = False

'Add slope values
mmr = 0.161498537
bmr = 4729.433806
mtankh = -0.656231135
btankh = 14006.05453

'Calcuates MR and Tank flow
MRflow = mmr * Flow1 + bmr
TankHflow = mtankh * Flow1 + btankh

'Enters slope values into excel
Sheets("Optimizer").Select
Range("C9").Select
ActiveCell.Value = MRflow
Range("C10").Select
ActiveCell.Value = TankHflow

'Assigns Stream1 a value of flow rate
Stream1.MolarFlow.SetValue Flow1, "kgmole/h"

'turns solver on
SimCase.Solver.CanSolve = True

' Solver Macro
   Range("E5").Select
   SolverOk SetCell:="$E$5", MaxMinVal:=3, ValueOf:=0, ByChange:="$C$9,$C$10", _
      Engine:=1, EngineDesc:="GRG Nonlinear"
   SolverSolve True

'Takes values and stores them.
Stream3 = Range("C9")
Stream7 = Range("C10")
Stream9 = Range("C11")
SE = Range("E5")

'Record Value in macroHistory.csv
   Dim Data As String, myFile As String
```

```
'Build string
    Data = Stream3 & "," & Stream7 & "," & Stream9 & "," & Flow1 & "," & SE

'Add string
    myFile = "C:\Users\ke7kto\Desktop\3000-21200.csv"
    Open myFile For Append As #1
    Print #1, Data
    Close #1

'Loop it to the next value
Loop

End Sub
```

And finally, the third one is to test the fit line:

```
Option Explicit
Public HysApp As HYSYS.Application
Public SimCase As SimulationCase
Public Stream1 As ProcessStream
Public Flow1 As Double
Public mmr As Double
Public bmr As Double
Public mtankh As Double
Public btankh As Double
Public MRflow As Double
Public TankHflow As Double
Public SE As Double

Sub testSE()
'This is to test the line fit

'Link HYSYS to VBA
Set HysApp = CreateObject("HYSYS.Application")
HysApp.Visible = True
Set SimCase = HysApp.ActiveDocument

'Sets Stream1 variables to the following code
Set Stream1 = SimCase.Flowsheet.Streams.Item("1")

'Set slope and intercept from equation
mmr = 0.158678382
bmr = 4796.018302
mtankh = -0.658923534
btankh = 14069.17892

'This is where the recursion will happen
```

```
Flow1 = 21300
Do
   Flow1 = Flow1 - 100
If Flow1 <= 6100 Then Exit Do

'turns solver off
SimCase.Solver.CanSolve = False

'Assigns Stream1 a value of flow rate
Stream1.MolarFlow.SetValue Flow1, "kgmole/h"

'Calcuates MR and Tank flow
MRflow = mmr * Flow1 + bmr
TankHflow = mtankh * Flow1 + btankh

'Enters slope values into excel
Sheets("Optimizer").Select
Range("C9").Select
ActiveCell.Value = MRflow
Range("C10").Select
ActiveCell.Value = TankHflow

'turns solver on
SimCase.Solver.CanSolve = True

'Collects SE Data
SE = Range("E5")

'Record Value in macroHistory.csv
   Dim Data As String, myFile As String

'Build string
   Data = Flow1 & "," & SE & "," & MRflow & "," & TankHflow

'Add string
   myFile = "C:\Users\ke7kto\Desktop\SEdata.csv"
   Open myFile For Append As #1
   Print #1, Data
   Close #1

'Loop it to the next value
Loop

End Sub
```

Figure 9-1 illustrates results from two methanol streams (streams 9 and 7), one MR stream and one NG stream from the pipeline. The NG flow rate is changing and hence will affect heat exchanger efficiency. The code determines flow rates for two methanol streams and the MR to maintain high heat exchanger efficiency as this fluctuation occurs in NG flow rates. The MR and methanol streams regulate the flow rates and temperatures in heat exchanger. This scheme minimizes energy consumption and temperature differences around the heat exchanger as the objective functions.

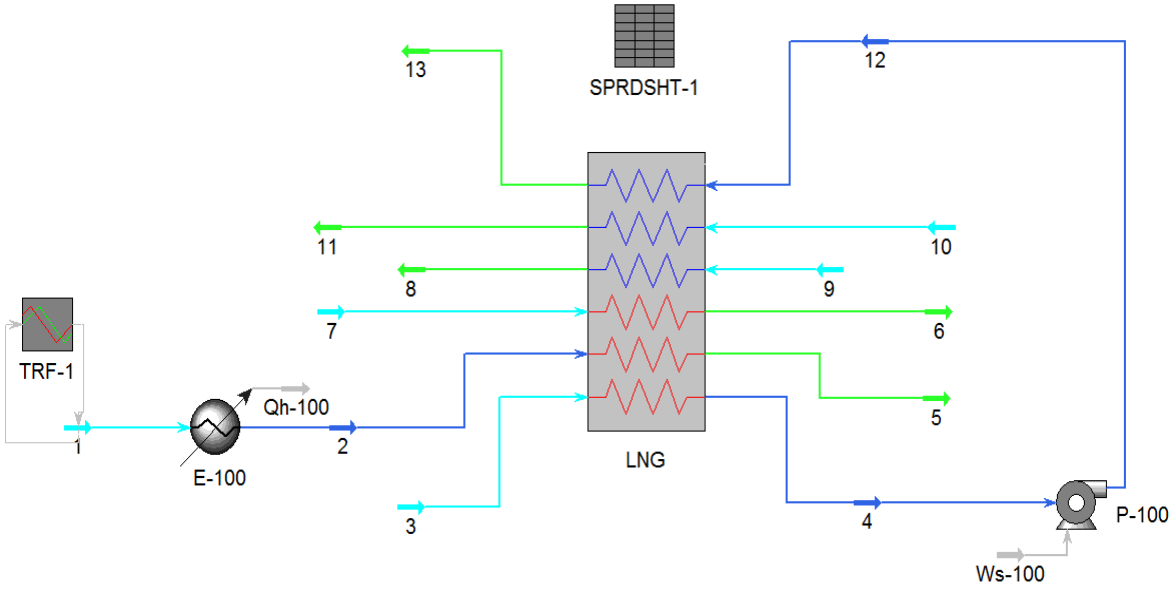

Figure A-1. Simplified HYSYS simulation for MPC

The optimum NG flow rate is the balanced one (21200 kgmol/h). An enthalpy balance determines the ΔT for this flow. This is the optimum ΔT. When NG flow changes, it determines the real ΔT. The objective function minimizes the difference between these two. As Figure 52 indicates, this spreadsheet calculates both ΔTs. (The bold blue values are the set points, the black

ones are calculated and imported by HYSYS, the thinner blue ones are calculated by optimizer which will be exported to the software and streams 7 and 9 are the two methanol streams)

The ER cases involve flow rates of less than 21200 and higher than 6360 kgmol/h and the ES cases involve flows higher than 21200 and less than 29680 kgmol/h. The following discussion considers these cases.

Two sets of correlations exist for ER and ES cases. Each set has three correlations. Optimization in VBA determines those correlations ($y = mx + b$) and inserts them in a HYSYS spreadsheet. Once NG flow changes, the spreadsheet checks if this flow is for ER or ES. Then it uses the proper correlations to minimize ΔT. There is another spreadsheet, as shown, for energy consumption. All these spreadsheets interact with each other. This determines the best flow rates for the MR and the methanol streams; those that produce a minimum ΔT and minimum energy consumption.

The predicted heat exchanger temperature profile continuously updated during the simulation. These dynamic solution and optimization codes determined the temperature profiles for B, ER and ES cases, all of which are essentially equal.

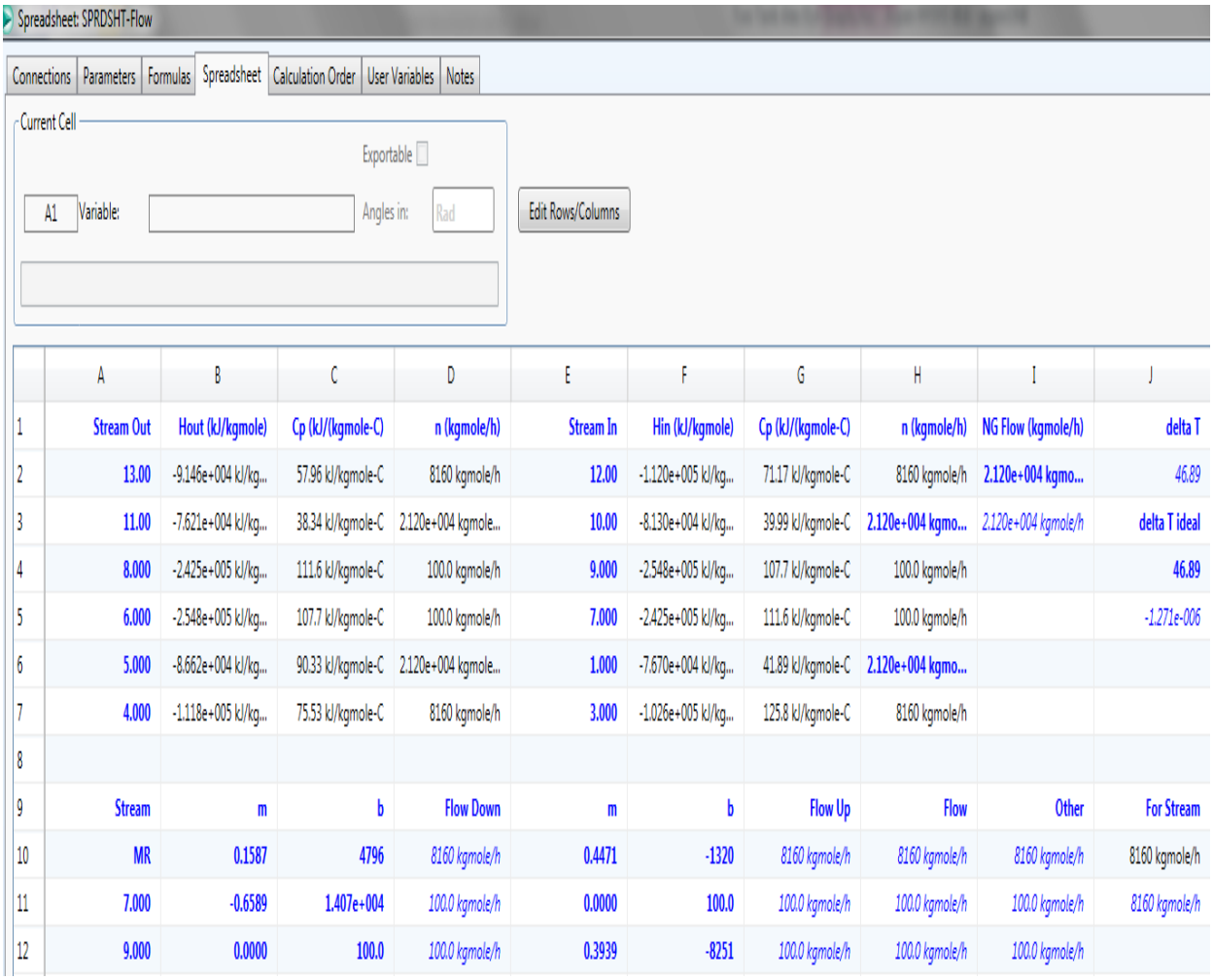

	A	B	C	D	E	F	G	H	I	J
1	Stream Out	Hout (kJ/kgmole)	Cp (kJ/(kgmole-C)	n (kgmole/h)	Stream In	Hin (kJ/kgmole)	Cp (kJ/(kgmole-C)	n (kgmole/h)	NG Flow (kgmole/h)	delta T
2	13.00	-9.146e+004 kJ/kg...	57.96 kJ/kgmole-C	8160 kgmole/h	12.00	-1.120e+005 kJ/kg...	71.17 kJ/kgmole-C	8160 kgmole/h	2.120e+004 kgmo...	46.89
3	11.00	-7.621e+004 kJ/kg...	38.34 kJ/kgmole-C	2.120e+004 kgmole...	10.00	-8.130e+004 kJ/kg...	39.99 kJ/kgmole-C	2.120e+004 kgmo...	2.120e+004 kgmole/h	delta T ideal
4	8.000	-2.425e+005 kJ/kg...	111.6 kJ/kgmole-C	100.0 kgmole/h	9.000	-2.548e+005 kJ/kg...	107.7 kJ/kgmole-C	100.0 kgmole/h		46.89
5	6.000	-2.548e+005 kJ/kg...	107.7 kJ/kgmole-C	100.0 kgmole/h	7.000	-2.425e+005 kJ/kg...	111.6 kJ/kgmole-C	100.0 kgmole/h		-1.271e-006
6	5.000	-8.662e+004 kJ/kg...	90.33 kJ/kgmole-C	2.120e+004 kgmole...	1.000	-7.670e+004 kJ/kg...	41.89 kJ/kgmole-C	2.120e+004 kgmo...		
7	4.000	-1.118e+005 kJ/kg...	75.53 kJ/kgmole-C	8160 kgmole/h	3.000	-1.026e+005 kJ/kg...	125.8 kJ/kgmole-C	8160 kgmole/h		
8										
9	Stream	m	b	Flow Down	m	b	Flow Up	Flow	Other	For Stream
10	MR	0.1587	4796	8160 kgmole/h	0.4471	-1320	8160 kgmole/h	8160 kgmole/h	8160 kgmole/h	8160 kgmole/h
11	7.000	-0.6589	1.407e+004	100.0 kgmole/h	0.0000	100.0	100.0 kgmole/h	100.0 kgmole/h	100.0 kgmole/h	8160 kgmole/h
12	9.000	0.0000	100.0	100.0 kgmole/h	0.3939	-8251	100.0 kgmole/h	100.0 kgmole/h	100.0 kgmole/h	

Figure A-2. Dynamic solution for B case illustrating small temperature differences, approaching zero

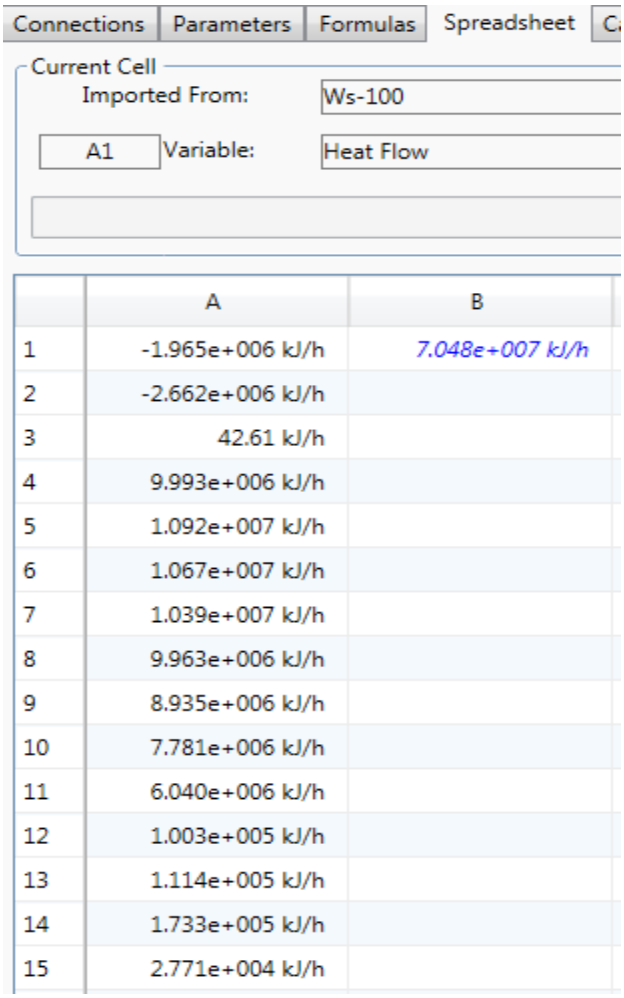

	A	B
1	-1.965e+006 kJ/h	7.048e+007 kJ/h
2	-2.662e+006 kJ/h	
3	42.61 kJ/h	
4	9.993e+006 kJ/h	
5	1.092e+007 kJ/h	
6	1.067e+007 kJ/h	
7	1.039e+007 kJ/h	
8	9.963e+006 kJ/h	
9	8.935e+006 kJ/h	
10	7.781e+006 kJ/h	
11	6.040e+006 kJ/h	
12	1.003e+005 kJ/h	
13	1.114e+005 kJ/h	
14	1.733e+005 kJ/h	
15	2.771e+004 kJ/h	

FigureA-3. Energy consumption calculated by optimizer

Several flow rates provided here serve as examples to show the differences between B, ER and ES cases in dynamic solution. NG flow rates change quickly in these simulations, and the MPC controller responds rapidly to maintain essentially constant temperature profiles. The thinner blue values are the ones calculated by optimizer and exported to HYSYS and HYSYS uses them in the simulation.

For flow rates 24000 kgmol/h (ES case):

Spreadsheet: SPRDSHT-Flow

Connections | Parameters | Formulas | Spreadsheet | Calculation Order | User Variables | Notes

Current Cell

Exportable

A1 Variable: Angles in: Rad Edit Rows/Columns

	A	B	C	D	E	F	G	H	I	J
1	Stream Out	Hout (kJ/kgmole)	Cp (kJ/(kgmole-C)	n (kgmole/h)	Stream In	Hin (kJ/kgmole)	Cp (kJ/(kgmole-C)	n (kgmole/h)	NG Flow (kgmole/h)	delta T
2	13.00	-9.147e+004 kJ/kg...	57.95 kJ/kgmole-C	9412 kgmole/h	12.00	-1.120e+005 kJ/kg...	71.17 kJ/kgmole-C	9412 kgmole/h	2.400e+004 kgmo...	46.96
3	11.00	-7.621e+004 kJ/kg...	38.34 kJ/kgmole-C	2.120e+004 kgmole...	10.00	-8.130e+004 kJ/kg...	39.99 kJ/kgmole-C	2.120e+004 kgmo...	2.400e+004 kgmole/h	delta T ideal
4	8.000	-2.425e+005 kJ/kg...	111.6 kJ/kgmole-C	1203 kgmole/h	9.000	-2.548e+005 kJ/kg...	107.7 kJ/kgmole-C	1203 kgmole/h		46.89
5	6.000	-2.548e+005 kJ/kg...	107.7 kJ/kgmole-C	100.0 kgmole/h	7.000	-2.425e+005 kJ/kg...	111.6 kJ/kgmole-C	100.0 kgmole/h		-6.850e-002
6	5.000	-8.662e+004 kJ/kg...	90.33 kJ/kgmole-C	2.400e+004 kgmole...	1.000	-7.670e+004 kJ/kg...	41.89 kJ/kgmole-C	2.400e+004 kgmo...		
7	4.000	-1.118e+005 kJ/kg...	75.53 kJ/kgmole-C	9412 kgmole/h	3.000	-1.026e+005 kJ/kg...	125.8 kJ/kgmole-C	9412 kgmole/h		
8										
9	Stream	m	b	Flow Down	m	b	Flow Up	Flow	Other	For Stream
10	MR	0.1587	4796	8604 kgmole/h	0.4471	-1320	9412 kgmole/h	9412 kgmole/h	9412 kgmole/h	9412 kgmole/h
11	7.000	-0.6589	1.407e+004	-1745 kgmole/h	0.0000	100.0	100.0 kgmole/h	100.0 kgmole/h	100.0 kgmole/h	9412 kgmole/h
12	9.000	0.0000	100.0	100.0 kgmole/h	0.3939	-8251	1203 kgmole/h	1203 kgmole/h	1203 kgmole/h	

Figure A-4. Random example for ES case

This means that, according to the dynamic solution, the second set of correlations is used and MR flow is 9412, methanol 1 is 100 and methanol 2 is 1203 kgmol/h. These values automatically export to HYSYS and HYSYS shows the results for energy and temperature profile.

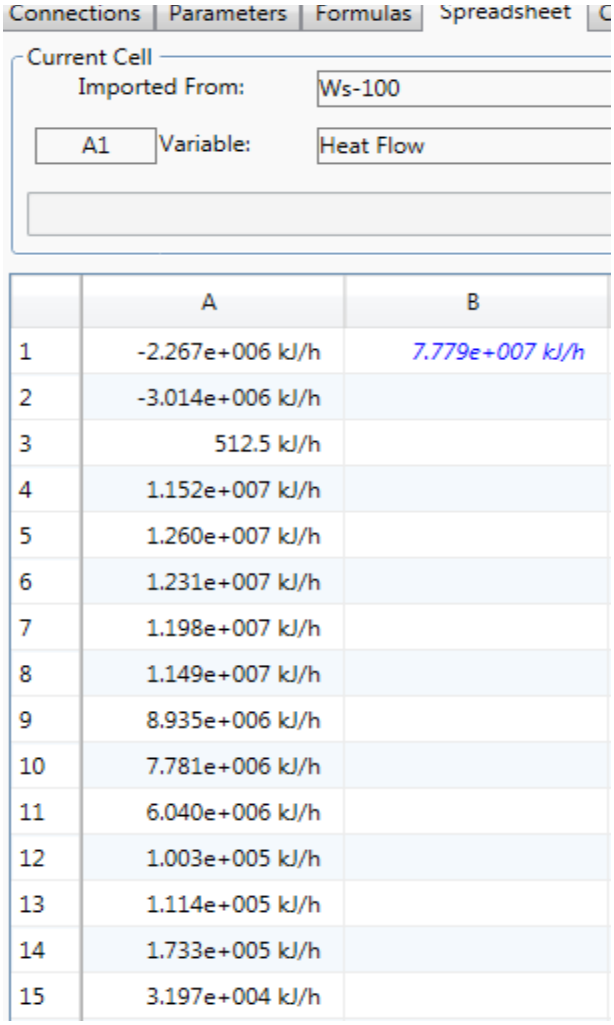

	A	B
1	-2.267e+006 kJ/h	7.779e+007 kJ/h
2	-3.014e+006 kJ/h	
3	512.5 kJ/h	
4	1.152e+007 kJ/h	
5	1.260e+007 kJ/h	
6	1.231e+007 kJ/h	
7	1.198e+007 kJ/h	
8	1.149e+007 kJ/h	
9	8.935e+006 kJ/h	
10	7.781e+006 kJ/h	
11	6.040e+006 kJ/h	
12	1.003e+005 kJ/h	
13	1.114e+005 kJ/h	
14	1.733e+005 kJ/h	
15	3.197e+004 kJ/h	

Figure A-5. Energy calculated for random ES flow rate in optimizer

For flow rate 8234 kgmol/h (ER):

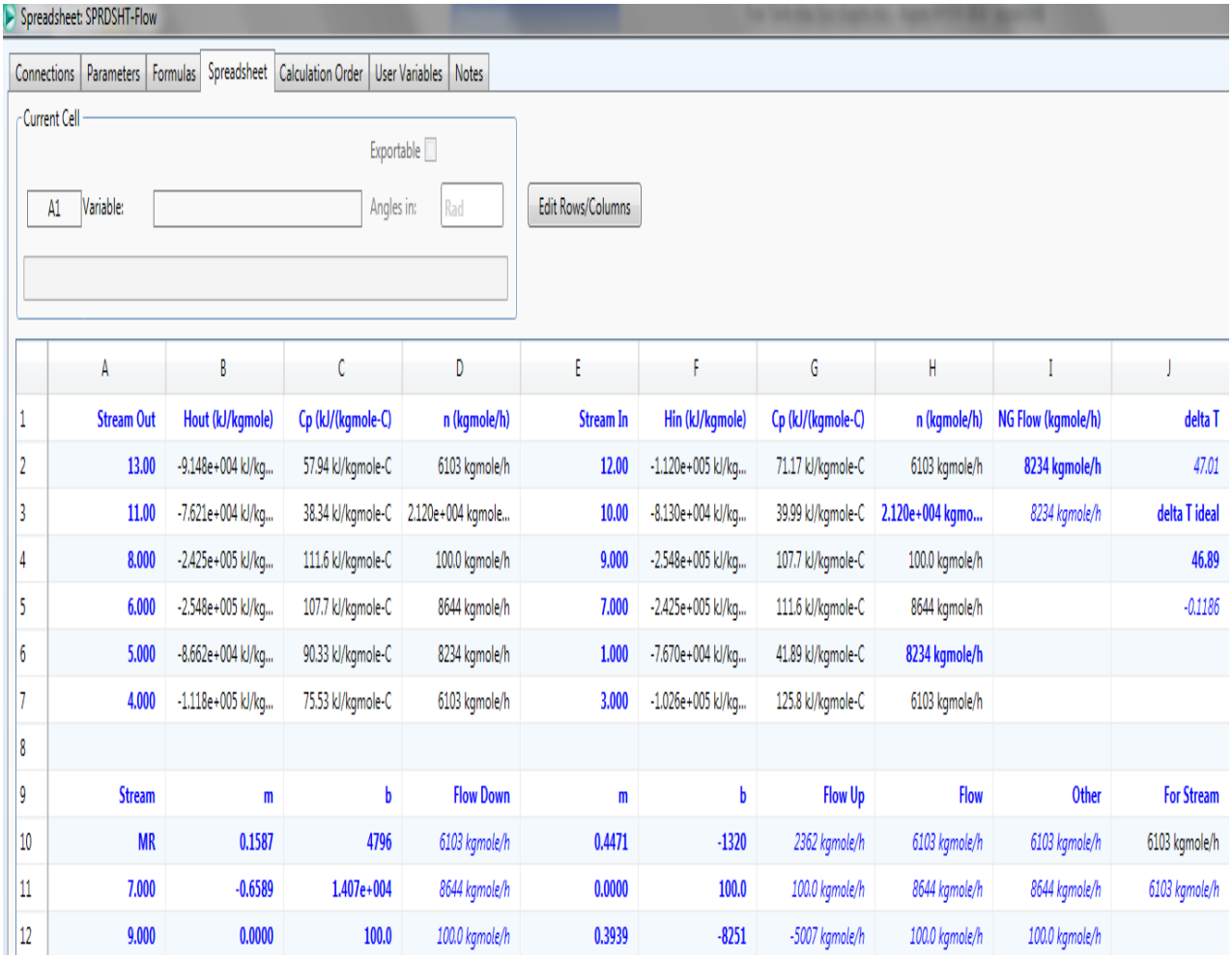

	A	B	C	D	E	F	G	H	I	J
1	Stream Out	Hout (kJ/kgmole)	Cp (kJ/(kgmole-C)	n (kgmole/h)	Stream In	Hin (kJ/kgmole)	Cp (kJ/(kgmole-C)	n (kgmole/h)	NG Flow (kgmole/h)	delta T
2	13.00	-9.148e+004 kJ/kg...	57.94 kJ/kgmole-C	6103 kgmole/h	12.00	-1.120e+005 kJ/kg...	71.17 kJ/kgmole-C	6103 kgmole/h	8234 kgmole/h	47.01
3	11.00	-7.621e+004 kJ/kg...	38.34 kJ/kgmole-C	2.120e+004 kgmole...	10.00	-8.130e+004 kJ/kg...	39.99 kJ/kgmole-C	2.120e+004 kgmo...	8234 kgmole/h	delta T ideal
4	8.000	-2.425e+005 kJ/kg...	111.6 kJ/kgmole-C	100.0 kgmole/h	9.000	-2.548e+005 kJ/kg...	107.7 kJ/kgmole-C	100.0 kgmole/h		46.89
5	6.000	-2.548e+005 kJ/kg...	107.7 kJ/kgmole-C	8644 kgmole/h	7.000	-2.425e+005 kJ/kg...	111.6 kJ/kgmole-C	8644 kgmole/h		-0.1186
6	5.000	-8.662e+004 kJ/kg...	90.33 kJ/kgmole-C	8234 kgmole/h	1.000	-7.670e+004 kJ/kg...	41.89 kJ/kgmole-C	8234 kgmole/h		
7	4.000	-1.118e+005 kJ/kg...	75.53 kJ/kgmole-C	6103 kgmole/h	3.000	-1.026e+005 kJ/kg...	125.8 kJ/kgmole-C	6103 kgmole/h		
8										
9	Stream	m	b	Flow Down	m	b	Flow Up	Flow	Other	For Stream
10	MR	0.1587	4796	6103 kgmole/h	0.4471	-1320	2362 kgmole/h	6103 kgmole/h	6103 kgmole/h	6103 kgmole/h
11	7.000	-0.6589	1.407e+004	8644 kgmole/h	0.0000	100.0	100.0 kgmole/h	8644 kgmole/h	8644 kgmole/h	6103 kgmole/h
12	9.000	0.0000	100.0	100.0 kgmole/h	0.3939	-8251	-5007 kgmole/h	100.0 kgmole/h	100.0 kgmole/h	

Figure A-6. Random example for ER case

Again here, according to dynamic solution, the first correlation is used, and MR flow is 6103, methanol 1 is 8644 and methanol 2 is 100 kgmol/h.

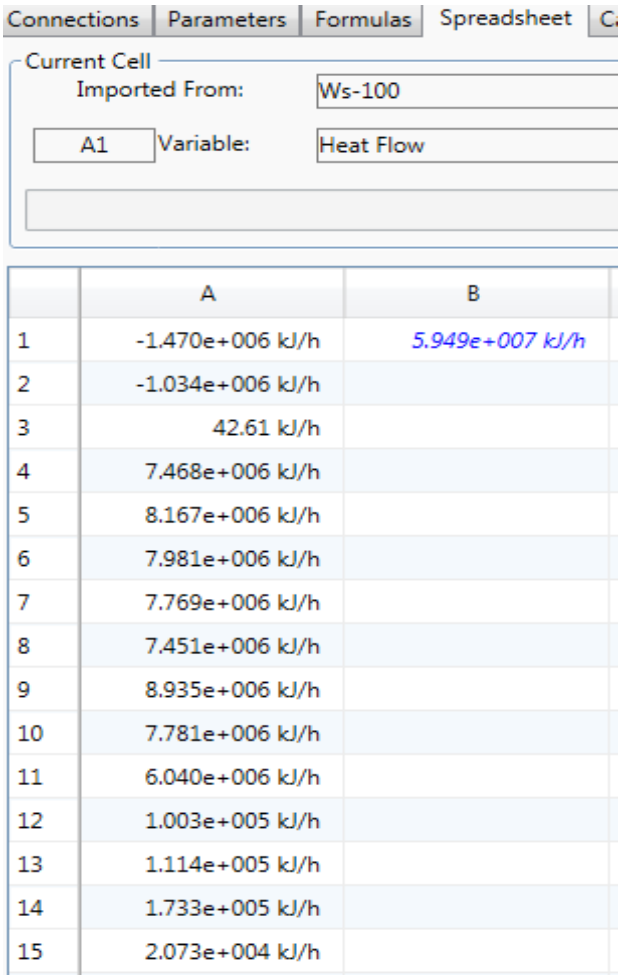

	A	B
1	-1.470e+006 kJ/h	*5.949e+007 kJ/h*
2	-1.034e+006 kJ/h	
3	42.61 kJ/h	
4	7.468e+006 kJ/h	
5	8.167e+006 kJ/h	
6	7.981e+006 kJ/h	
7	7.769e+006 kJ/h	
8	7.451e+006 kJ/h	
9	8.935e+006 kJ/h	
10	7.781e+006 kJ/h	
11	6.040e+006 kJ/h	
12	1.003e+005 kJ/h	
13	1.114e+005 kJ/h	
14	1.733e+005 kJ/h	
15	2.073e+004 kJ/h	

Figure A-7. Energy calculated for ER random flow rate in optimizer